Westerduinweg 3
1755 LE Petten
P.O. Box 15
1755 ZG Petten
The Netherlands

www.tno.nl

T +31 88 866 50 65

TNO report | TNO 2018 R11592

Understanding of the Offshore Wind Resource up to High Altitudes (≤ 315 m)

Date	14 January 2019
Author(s)	J.B. Duncan, P.A. van der Werff and E.T.G. Bot
Copy no	
No. of copies	
Number of pages	76 (incl. appendices)
Number of appendices	7
Sponsor	Supported with Topsector Energy Subsidy from the Ministry of Economic Affairs and Climate Policy
Project name	Dutch Offshore Wind Atlas (DOWA)
Project number	060.33810

Summary

In order to better understand North Sea wind conditions, analyses were performed on wind speed and direction measurements by light-detection and ranging (lidar) at eight offshore measurement locations distributed throughout the North Sea. Lidar enabled measurement of the North Sea wind conditions at relatively high altitudes (i.e. $\leq$ 315 m) and therefore was used to examine vertical profiles of wind shear and veer. The greatest wind shear was observed with south-westerly wind directions and high wind speeds, and in general wind direction veered (i.e. increased in magnitude) with height. The wind speed distribution as defined by the Weibull probability distribution was also determined at each measurement location and height. Measurement-site wind speed distributions exhibited inter-annual variability and varied as a function of height and proximity to the coast. The Weibull scale parameter on average increased with height, while the Weibull shape parameter decreased with height. Vertical tendencies in the Weibull scale parameter were expected (i.e. wind speed on average increases with height); however, vertical tendencies in the Weibull shape parameter were nontrivial. This reduction in the Weibull shape parameter with height indicates that although the winds become less turbulent with height, the range of possible wind speeds is greater at higher altitudes (i.e. wider distribution). Further, correlation in wind speed and direction between lidar measurement locations was determined in order to examine the potential applicability of measurement-correlate predict methods within the North Sea.

Analyses conclude with a comparison of the lidar wind speed measurements to wind data produced by the KNW-atlas. KNW atlas wind speed comparisons were made to lidar measurements at LEG, HKZA, and HKZB and overall, the KNW atlas compares well with these measurements. The analyses are not meant as validation of KNW – this is already done elsewhere – but to deepen the understanding of high altitude offshore wind resource.

Contents

1 Introduction

The Dutch Part of the North Sea is expected to see significant growth in offshore wind energy over the coming decades. By 2023, the Dutch Part of the North Sea should have a total installed capacity of 4.5 GW, and by 2030 an installed capacity of 11.5 GW. As part of this offshore wind development, wind energy will be extracted at increasingly higher altitudes due to trends in wind turbine size and innovations to wind power technologies (e.g. kite power). Efficient development of North Sea wind energy therefore requires a comprehensive understanding of the offshore winds across large depths of the atmospheric boundary layer (ABL).

Measurements that are needed to thoroughly understand offshore wind behavior are historically limited. However, advancements in remote sensing technologies in recent years have enabled enhanced measurement of the offshore wind environment. These systems typically measure atmospheric boundary layer (ABL) winds across larger depths and at greater spatial frequencies than traditional meteorological masts. As part of a meteorological campaign commissioned by the Dutch Ministry of Economic Affairs, multiple measurement platforms distributed across the North Sea were equipped with remote sensing instruments. Using these measurements, this report seeks to provide improved characterization of the North Sea wind environment. Wind speed distributions, wind shear and veer profiles, and correlation between measurement locations are examined herein.

This report is structured as follows: section two details the available measurement platforms, section three provides a summary of the ECN part of TNO North Sea wind resource assessment, and section four provides a comparison of the offshore lidar measurements with the KNMI North Sea Wind (KNW) atlas (more information found here: http://projects.knmi.nl/knw/). Here, KNMI is the Royal Netherlands Meteorological Institute. Appendices are also included that detail the site-specific wind conditions.

2 Measurement platform overview

An increasing number of measurement sites were established across the Dutch Part of the North Sea within the last decade in an attempt to provide improved characterization of the offshore wind environment. For a complete overview we refer to www.windopzee.net. Eight of these measurement locations (Figure 1) were used in this study to provide enhanced characterization of the offshore wind resource. Each station chosen was equipped with light detection and ranging (lidar) – previously validated by ECN part of TNO in [1], [2], and [3] – and at one location a meteorological mast was also installed. Measurement site specifics are detailed in the following sections. Ten-minute average wind data were provided at each of the measurement locations. Because wind conditions can vary as a function of proximity to the coast, a table is provided (Table 1) that defines measurement site distance to the coast.

Figure 1 Location of the eight measurement sites used to examined North Sea wind behaviour.

Table 1 Measurement site distance to the coast

Measurement site	Distance to the coast (km)
K13_A	101
MMIJ	82
HKZA	28
HKZB	27
LEG	18
EPL	45
BWFZ_L1	33
BWFZ_L2	36

2.1 Measurement locations

2.1.1 IJmuiden

Measurements at IJmuiden (MMIJ) were carried out using a platform-mounted Zephir 300s continuous-wave light detection and ranging (lidar) instrument (Figure 2). The lidar, which was mounted approximately 20.9 m above the height of the lowest astronomical tide (LAT [~ 1.06 m below the mean sea level (MSL)]), recorded wind speed and direction at 25-m height intervals between 90 m and 315 m (10 total levels) above LAT. Wind data were collected at this site between November 2011 and March 2016. Further information regarding instrumentation and measurements can be found in [4], [5], [6], [7], [8], and [9].

Figure 2 Measurement platform MMIJ.

2.1.2 Lichteiland Goeree

Southwest of Hoek van Holland is a platform serving as a beacon for ships on the North Sea. This platform, referred to as Lichteiland Goeree (LEG), was equipped with a WINDCUBE v2 pulsed lidar to examine offshore wind conditions (Figure 3). The wind lidar was mounted 23 m above MSL and provided both wind speed and direction measurements at 10 different elevations between 63 m and 240 m above MSL. Wind data were collected since November 2014. Further information regarding instrumentation and measurements can be found in [10].

Figure 3 Measurement platform LEG.

2.1.3 Europlatform

Also serving as a beacon for ships on the North Sea is the Europlatform that is situated west of Hoek van Holland (Figure 4). A ZephIR 300S lidar was mounted atop this platform, about 18.8 m above MSL, in order to document wind speed and direction at 10 different heights between 63 m and 291 m. Wind data were collected since June 2016. Further information regarding instrumentation and measurements can be found in [11].

Figure 4 Measurement platform EPL.

2.1.4 K13a

The K13a offshore platform is located northwest of Den Helder (Figure 5). The platform serves as a production platform for natural gas, but since November 2016 also makes wind measurements using a platform-mounted (~35 m above MSL)

ZephIR 300s wind lidar. Similar to at EPL and K13a, wind measurements occur at 10 different levels between 63 m and 291 m above MSL. Further information regarding instrumentation and measurements can be found in [12].

Figure 5 Measurement platform K13a.

2.1.5 *Hollandse Kust Zuid*

Hollandse Kust Zuid (HKZ) is a wind farm development zone located northwest of Scheveningen. On behalf of Rijksdienst voor Ondernemend (RVO) Nederland, Fugro Oceanor has performed wind measurements using their ZephIR 300s lidar-equipped Seawatch buoy (Figure 6). The Seawatch systems were calibrated before deployment (https://offshorewind.rvo.nl/windwaterzh), and after were analyzed to identify any potential system degradation that may have occurred during data collection. Two Seawatch buoys (HKZA and HKZB) were deployed for the experiment, which lasted between June 2016 and June 2018. The two buoys were separated by a distance of 2 km along a north-south bearing and provided wind speed and direction measurements at 10 different elevations between 30 m and 200 m.

2.1.6 *Borssele Wind Farm Zone*

The Borssele Wind Farm Zone (BWFZ) is a wind farm development zone located northwest of Vlissingen. Similar to at the HKZ wind farm zone, a measurement campaign was carried out by Fugro Oceanor to document offshore wind conditions within the respective wind farm development region. A single Seawatch buoy (BWFZ_L1) was deployed in June 2015 and a second (BWFZ_L2) in February 2017. The second buoy was situated approximately 9 km southwest of BWFZ_L1 and was deployed with the primary objective of documenting wind farm wake effects. Because of these measurement objectives, the deployment of BWFZ_L2 was temporary with data collection ceasing in February 2016. Measurements by BWFZ_L1 continued until February of 2017. Wind speed and direction measurements were made using these lidar-equipped buoys at 10 different elevations between 30 m and 200 m.

Figure 6 Seawatch wind lidar buoy (photo provided by Fugro).

2.2 Data availability

Data collection periods varied between sites. Contributing to these variations were not only differences in measurement campaign start and end times, but also instrument downtime. Measurement site data availability is shown in Figure 7.

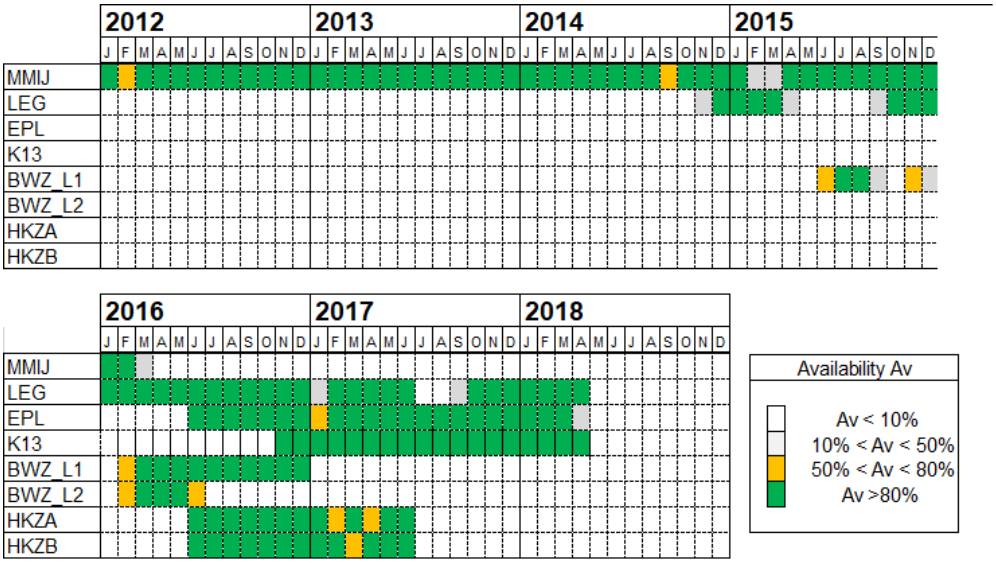

Figure 7 Site-specific monthly average data availability (per May 2018)

Wind resource assessment requires data sets of at least one year in order to reduce the impact of seasonality on the derived wind statistics. A total of 12 datasets were identified from Figure 7 that satisfy the criteria for wind resource assessment analysis. The 'Dataset ID' depicts the measurement station acronym, the data collection year, and whether the data represents a full calendar year (no suffix), an annual period that does not start on 1 January (suffix A), or an annual period of measurements that was developed using data reconstruction methods (suffix C). Datasets that exhibited significant data gaps (i.e. suffix C datasets) were reconstructed using either data from the same season but a different year, or alternatively by double counting the

neighbouring periods of data. For instance, data between 10 February 2015 and 18 March 2015 were missing, and therefore were replaced with data measured between 10 February 2014 and 18 March 2014. Alternatively, at BWFZ_L1, wherein data was missing for the beginning periods of 2016, data was reconstructed using three weeks of data on either side of the gap.

Table 2 Identified data sets with a length of one year

Data Set	Measurement Location	Dataset ID	Data Collection Start	Data Collection End
1	**MMIJ**	MMIJ_2012	2012-01-01	2013-01-01
2	**MMIJ**	MMIJ_2013A	2012-10-01	2013-10-01
3	**MMIJ**	MMIJ_2014	2014-01-01	2015-01-01
4	**MMIJ**	MMIJ_2015C	2015-01-01	2015-02-10
			2014-02-10	2014-03-18
			2015-03-18	2016-01-01
5	**LEG**	LEG_2015C	2015-01-01	2015-04-09
			2016-04-09	2016-09-21
			2015-09-21	2016-01-01
6	**LEG**	LEG_2016	2016-01-01	2017-01-01
7	**LEG**	LEG_2017C	2017-02-01	2017-05-01
			2016-05-01	2016-10-01
			2017-10-01	2018-02-01
8	**EPL**	EPL_2017	2017-01-01	2018-01-01
9	**K13a**	K13A_2017	2017-01-01	2018-01-01
10	**HKZA**	HKZA_2016A	2016-06-15	2017-06-15
11	**HKZB**	HKZB_2016A	2016-06-15	2017-06-15
12	**BWFZ_L1**	BWFZ_L1_2016C	2016-02-01	2016-02-14
			2016-02-01	2017-01-01
			2016-12-15	2017-01-01

3 North Sea wind resource assessment

3.1 Wind speed distributions

Knowledge of wind variability is paramount for the success of wind energy. Not only is it important for accurate estimates of wind energy potential, but it is also enables improved wind turbine siting. Intra-annual wind variability has been found to be reasonably explained using a two-parameter Weibull distribution [13], [14], [15]. It is for this reason that commercial wind energy applications and software, such as the Wind Atlas Analysis and Applications Program (WASP), use the Weibull distribution to model the wind speed frequency distribution.

The two-parameter (*A* and *k*) Weibull distribution used herein to depict the wind speed frequency distribution is defined as:

$$f(x;A,k) = \frac{k}{A}\left(\frac{x}{A}\right)^{k-1} e^{-(x/A)^k}; \mathrm{x} \geq 0.$$

The parameter *A* is the Weibull scale factor and is proportional to the mean wind speed of the distribution. The parameter *k* is the Weibull shape factor and depicts the shape of the distribution. The value of *k* is inversely proportional to wind variability, i.e. large *k* values indicate less wind variability. The parameter *x* represents wind speed.

In order to estimate the Weibull shape and scale factors, the values μ and σ are first estimated from:

$$\mu = \frac{\sum_{i=1}^{N} V_i}{N}, \qquad \sigma = \sqrt{\frac{\sum_{i=1}^{N}(V_i - \mu)}{N}},$$

where V_i are the individually measured 10-min average wind speeds. A Gamma function table is then used to find the value of *k* that satisfies the 'measured value' of σ/μ. The scale factor was then determined using

$$A = \frac{\mu}{\Gamma\left(1+\frac{1}{k}\right)}.$$

As wind turbine technologies advance and wind energy extraction occurs at progressively higher altitudes, how Weibull parameters vary with height is of increasing importance. Therefore, for each of identified datasets (i.e. Table 2), a Weibull distribution was fit to the measured wind data to examine vertical variability in *A* and *k* (Figure 8). Because *A* is proportional to the mean of the wind speed distribution, the magnitude of *A* increased with height at each measurement location. Further, except for at LEG, the rates with which *A* increased with height were similar. In addition to the sensitivity of *A* to measurement height, the magnitude of *A* varied heavily depending upon the North-Sea-relative measurement location. Measurements made further offshore, such as those made at MMIJ and K13a, observed higher annual average wind speeds. This explains why the wind speed distribution at these two stations exhibited a larger Weibull scale parameter than neighbouring locations. At the other measurement locations (i.e. EPL and HKZ), the value of *A* roughly decreased as a function of distance from the coast. The wind speed distribution at BWFZ appeared to be heavily impacted by the presence of neighbouring wind farms (Table 3), which explains the reduced value of the Weibull scale parameter for the year examined. Winds at HKZ were also impacted by wind

farm wake effects; albeit, the impact appeared to be less severe than at BWFZ. Also, as demonstrated by the winds at MMIJ, interannual variability in the offshore wind resource cannot be neglected. The value of *A* at MMIJ varied by over 0.5 m s^{-1} at 90 m between 2012 and 2015, with this variability increasing with height.

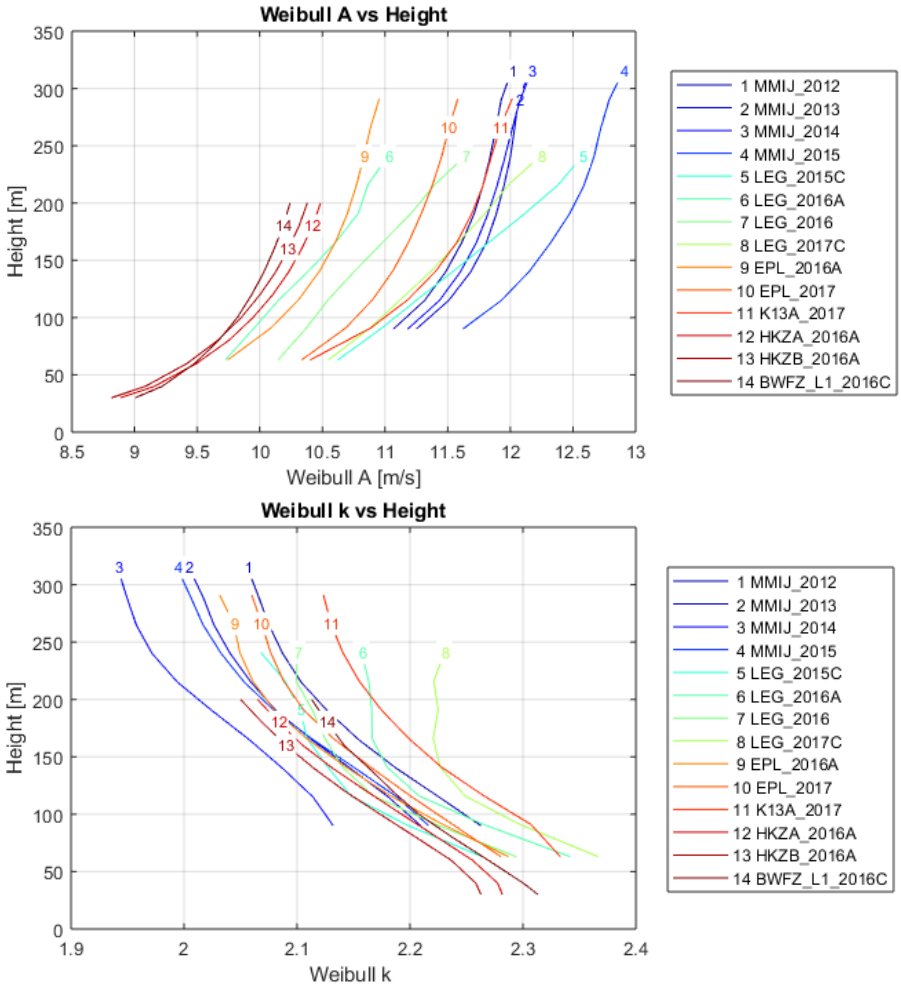

Figure 8 Weibull scale (*A*) (top) and shape (*k*) (bottom) factors as a function of measurement height for the identified datasets in Table 1. Vertical profiles of *A* and *k* at BWFZ and HKZ might have been impacted by the presence of neighbouring wind farms.

Many of the results presented thus far were expected – i.e. wind speed generally increases with height and distance from the coast and therefore it makes sense that the value of *A* would follow these trends. The same cannot be said regarding vertical tendencies in *k*. Wind conditions are typically assumed to be steadier (i.e. less turbulent) at higher altitudes, which suggests that the value of *k* should increase with height (i.e. less spread). However, measurements demonstrate an opposite trend wherein *k* steadily decreases with height. Although winds become less turbulent at higher altitudes, the range of possible wind speeds is greater at higher altitudes. This enhanced wind speed variability can be attributed, in part, to the correlation between sea surface roughness and wind speed. Within most wind speed regimes, sea surface roughness increases directly with wind speed, which has the impact of lessening wind speeds near the surface. The effect of sea surface roughness on the mean wind speed reduces with height [16], [17] such that there will be a higher frequency of strong wind events aloft. The enhanced range of wind speeds

experienced at higher altitudes explains the vertical tendencies in *k*. Similar to the Weibull scale parameter, *k* exhibits notable interannual variability; at MMIJ, *k* ranged between 2.13 and 2.26 at 90 m.

Table 3 Wind farms that were located within 30 km of measurement platforms BWFZ and HKZ.

Measurement Platform Name	Neighbouring Wind Farm Name	Distance to Wind Farm Center (km)
BWFZ	Belwind	13.12
	Nobelwind	12.22
	Northwind	8.97
	Thornton Bank Phase I	15.23
	Thornton Bank Phase II	13.51
	Thornton Bank Phase III	15.96
HKZ	Eneco Luchterduinen	15.87

3.2 Wind shear

Wind speed variation with height (i.e. wind shear) is typically modeled within the wind energy community using either one of two models. The logarithmic model, or log law, is based on a combination of theory (e.g. mixing length theory, eddy viscosity theory, similarity theory) and empirical research. However, theoretical support of this model breaks down outside of the surface layer (i.e. roughly less than 10 % of the boundary layer height) and also requires knowledge of several other meteorological variables outside of wind speed (e.g. surface roughness, friction velocity, zero-displacement height). A simpler model, the power law, defines the relationship between wind speed and height with a single power-law coefficient (α). This relationship,

$$\frac{U_h}{U_{ref}} = \left(\frac{H}{H_{ref}}\right)^{\alpha},$$

requires wind speed measurements at two levels: (1) a reference level (i.e. $U_{ref}\ and\ H_{ref}$) and (2) at any other height. Due to the simplicity in determining α, and because there are no height limitations for which it can be applied, the power law model was used to examine variations in offshore wind shear. In the presented analysis, 90 m was used as the reference height.

The mean wind profile at each measurement site are provided in Figure 9 to give a visual depiction of the site-specific wind shear.

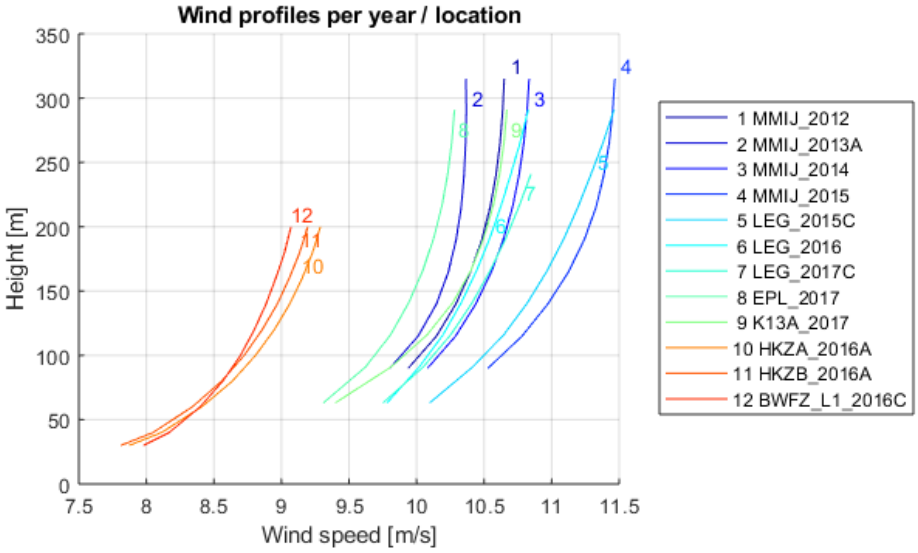

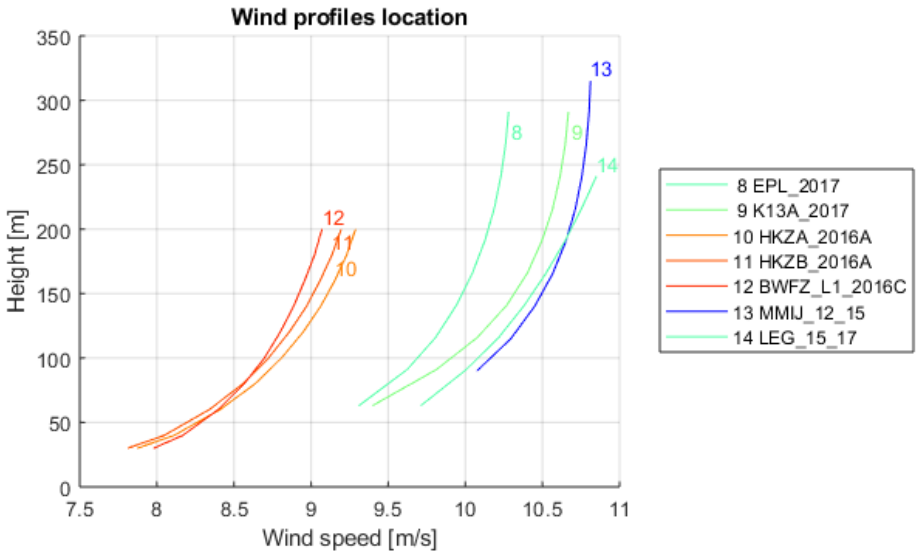

Figure 9 (Top) Measurement site mean wind profiles for the datasets identified in Table 1, and (Bottom) the measurement site average mean wind profile.

For a more quantitative analysis of wind shear, the behavior of the power law fit was examined as a function of wind direction. The values of both $U_{ref,90m}$ and α – derived from the mean wind profiles (i.e. not 10-min average data) – significantly varied as a function of wind direction (Figure 10). The magnitude of $U_{ref,90m}$ was greatest with winds emanating from the south-southwest (~ 210º), and was weakest with north-northeast winds (~ 30º). Using 90 m as the reference measurement level, α was directly proportional to the magnitude of $U_{ref,90m}$. This suggests that offshore wind shear increases as near-hub-height (i.e. ~ 90 m) wind velocities increase. However, these results are only valid for the site-dependent layers examined. The value of α will vary depending upon U_{ref} and the measurement level examined. Prior research [19] indicates that α is largest near the surface, but similar to the research presented here, maximum α values were consistent with high wind speeds and southwesterly winds. Although strong variations in ABL stability are not as present offshore as they are onshore, the relationship between α and U_{ref} might also vary relative to whether the offshore boundary layer is stable, neutral, or convective.

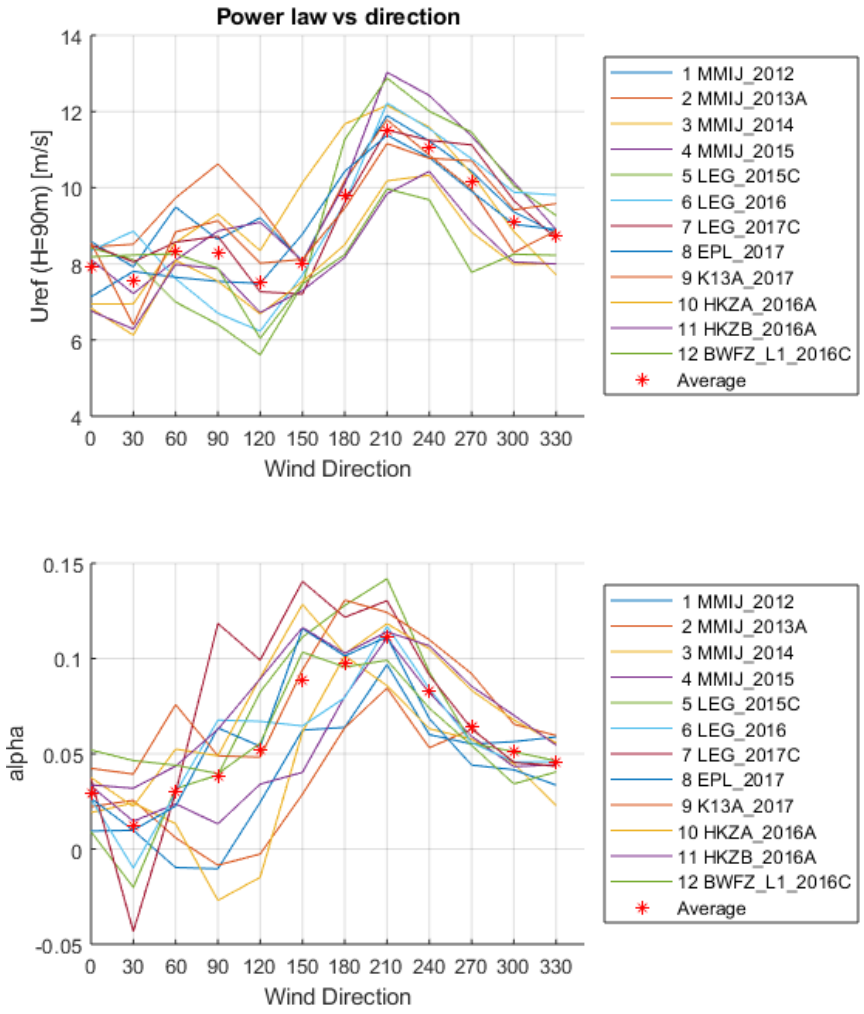

Figure 10 The (Top) reference velocity ($U_{ref,90m}$) and (Bottom) power-law coefficient (α) for each of the datasets identified in Table 1 as a function of wind direction. The mean $U_{ref,90m}$ and α values for all the datasets is shown in red.

3.3 Wind veer

Wind veer quantifies how wind direction varies with height, which can occur due to a variety of mechanisms [20]. Quantifying wind veer is important because the wind turbine rotor must remain normal to the inflow wind direction in order to ensure optimal performance. Wind veer is defined here as the difference in wind direction between some measurement height (H) and the lowest available measurement height. Positive wind veer values indicate clockwise rotation (i.e. veering) with height, whereas negative values indicate counter-clockwise (i.e. backing) vertical rotation. For each of the identified datasets (Figure 11), wind direction on average veered (i.e. increased in magnitude) with height. The rate of this veering appeared to be relatively consistent between sites, except at BWFZ (Lot 1) where the wind direction steadily increased. Noisy wind veer signals at higher elevations, such as that observed K13a, were more than likely due to reduced lidar data quality (or reduced availability) at these heights.

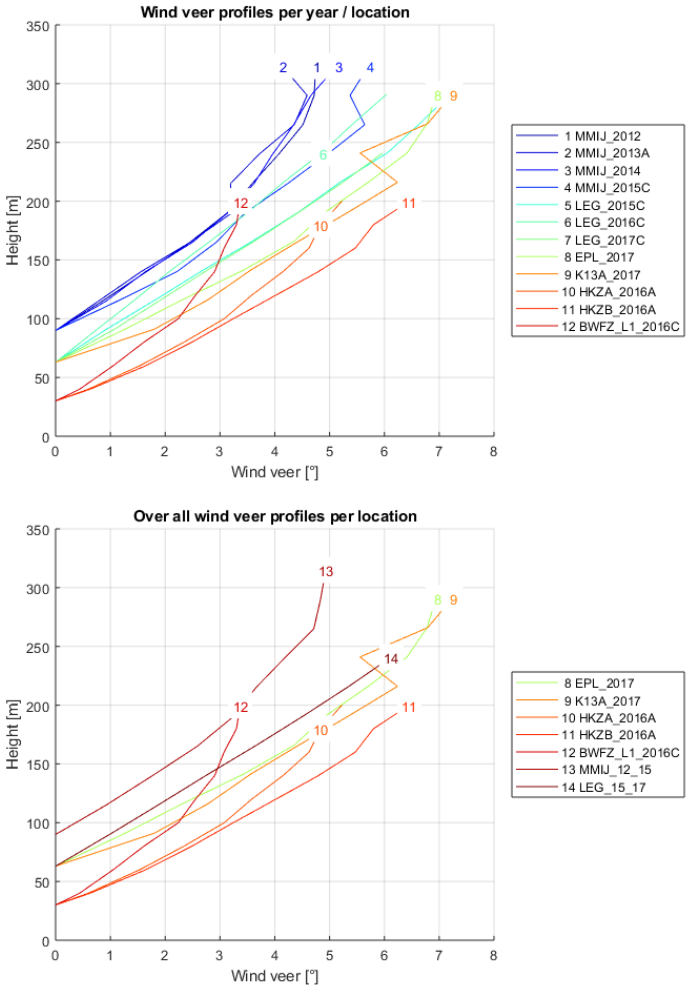

Figure 11 Same as Figure 9 except for wind veer.

3.4 Correlation between measurement locations

Measure-correlate-predict (MCP) is a method used to forecast long-term wind conditions at a site that has only a limited record of wind observations. These methods leverage long-term wind conditions at a neighboring site(s) to reconstruct the long-term data record at the site of interest. Therefore, imperative to the efficacy of MCP methods is the ability to quantify the relationship between wind data at the site of interest and that at the reference location(s). In order to examine MCP method potential for sites distributed throughout the North Sea, correlation in wind data between measurement locations was examined.

A Pearson correlation coefficient (ρ) was used to quantify the relationship in wind speed at 90 m between two sites (i.e. A and B), and a circular coefficient (ρ_c) was used to quantify the relationship in wind direction at 90 m. Correlation in wind direction is only examined if the 90-m wind speed was greater than three meters per second. The resulting correlation coefficients (Pearson [wind speed] and circular [wind direction]) as a function of distance between measurement sites – summarized in Table 4 – are provided in Figure 12.

Table 4 Distance between measurement locations [km]

	MMIJ	LEG	EPL	K13A	HKZA	HKZB	BWFZ_L1	BWFZ_L2
MMIJ		105	95	44	72	73	130	138
LEG			28	148	49	48	49	58
EPL				136	61	60	36	45
K13A					115	116	168	176
HKZA						2	94	103
HKZB							93	102
BWFZ_L1								9
BWFZ_L2								

Correlation in both wind speed and direction was inversely proportional to distance between measurement sites. The greatest wind speed correlation (0.99) was measured between HKZA and HKZB, which were separated by only 2 km . On average, wind speed correlation between measurement locations decreased at a rate of -1.37 per km. This inverse relationship between wind speed correlation and distance between measurement sites was strong as evidenced by an R^2 value of 0.91. Although, wind direction correlation also exhibited an inverse relationship to measurement platform separation distance, its linear relationship (-0.87 per km) was not as strong (R^2 ~ 0.41). The best correlation in wind direction (0.98) was measured between BWFZ (Lot 1) and BWFZ (Lot 2), which were separated by 9 km. Correlation in α between measurement locations as a function of measurement platform separation distance was also examined (Figure 13). In general, correlation in α was quite poor, only two of the measurement site pairs – HKZA and HKZB and BWFZ (Lot 1) and BWFZ (Lot 2) – exhibited correlation coefficients in excess of 0.5. The inverse relationship in α correlation between sites as a function of measurement platform separation distance (-0.33 per km) was less than that for either wind speed or direction, albeit the strength of this relationship (R^2 ~ 0.70) was greater than that for wind direction and less than that of wind speed.

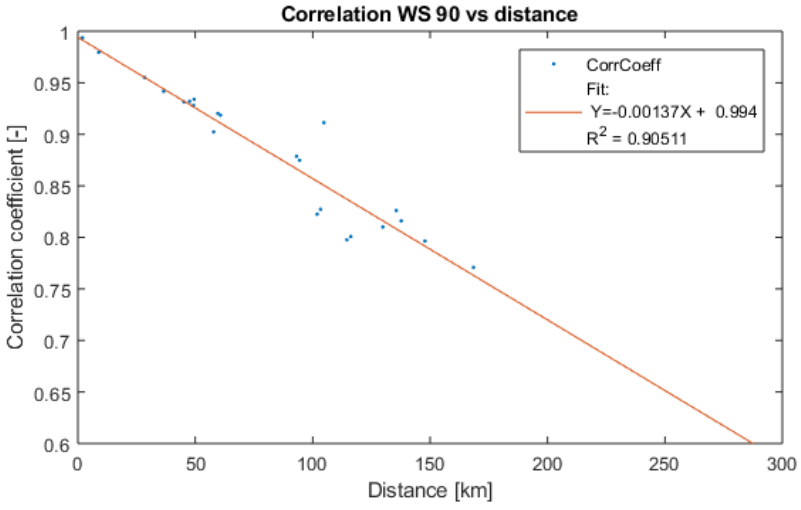

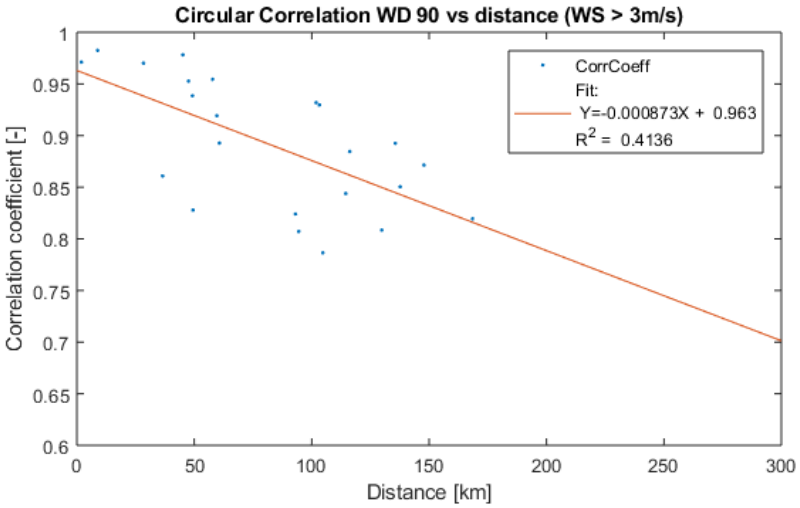

Figure 12 Correlation in (Top) wind speed and (Bottom) direction as function of distance between measurement sites A and B (Table 4).

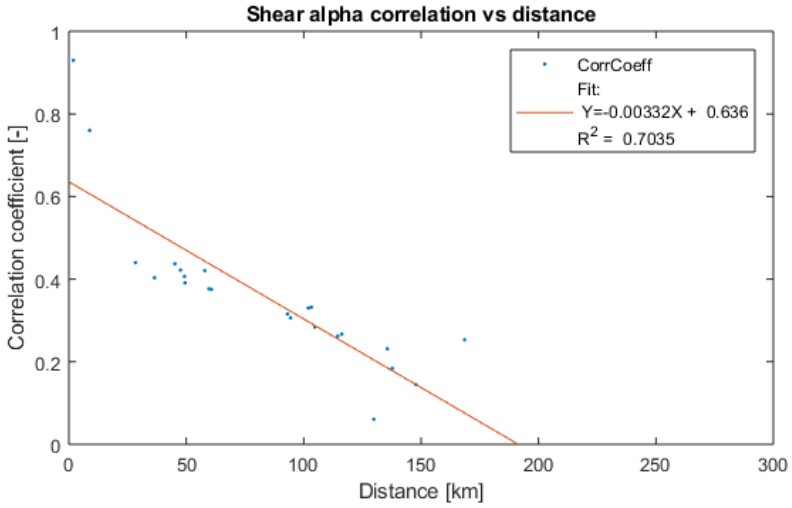

Figure 13 Correlation in α as a function of distance between measurement sites A and B (Table 4).

4 Comparison of measured wind data with KNW data

Offshore wind measurements suffer from both space and time limitations., i.e. measurements only exist for the measurement location and the data collection period. Model output in the sense of a wind atlas can overcover these spatial and temporal data gaps.

The KNW atlas is a 4D wind atlas based on the ERA-Interim reanalyses dataset. The atlas provides meteorological measurements including wind speed and direction from 1979 to now across an 80-km grid with a horizontal grid spacing of 2.5 km [20]. This atlas was previously validated both onshore and offshore using meteorological masts at MMIJ, OWEZ, and Cabauw [21] and 10-m scatterometer wind data [22].

As depicted in chapter 2, over the recent years various offshore measurement stations have become available comprising measurements ranging up to altitudes of 300 m. This gives the opportunity to compare these measurements with KNW particularly for offshore locations and at higher altitudes. A good comparison of the KNW atlas with measurements at higher heights will strengthen its use for future wind resource analysis. So, in the sections below, the KNW atlas is compared with lidar measurements at LEG, HKZA, and HKZB in terms of vertical wind profile and wind speed distributions.

4.1 Vertical wind profile comparisons

The mean wind profile measured, the corresponding power law and logarithmic fits, and the KNW-atlas mean wind profile are provided for the measurement locations LEG (Figure 14), HKZA (Figure 15), and HKZB (Figure 16). Overall, the KNW wind profiles compare well with the measurements and the fitted profiles. More specifically, at LEG, KNW overestimated the mean wind speed by approximately 1.7 %. However, at both HKZA and HKZB, the KNW atlas slightly overestimated the mean wind speed up to heights of about 160m. Above this altitude the spread in various profiles is too big to be conclusive.

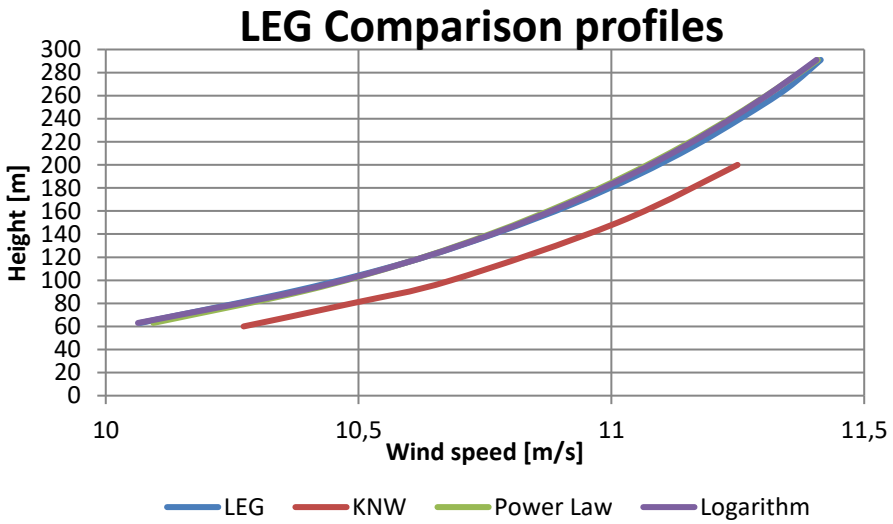

Figure 14 Comparison between the measured wind profile, power law and logarithmic fits, with KNW data for LEG.

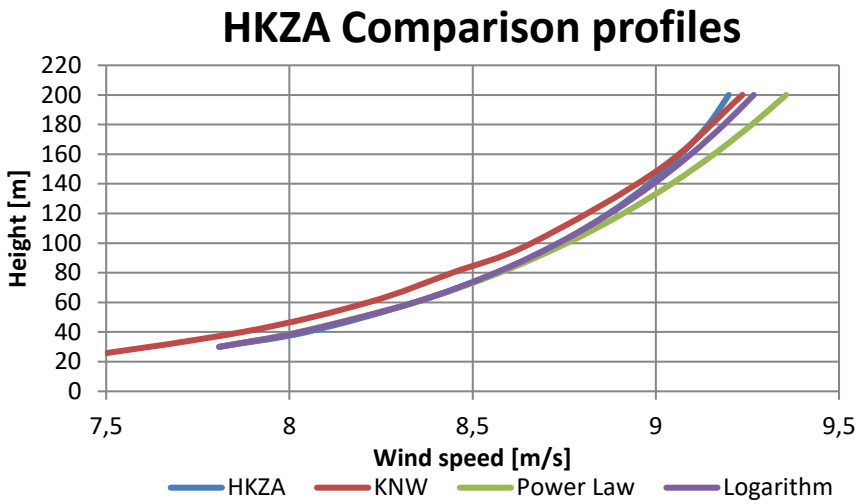

Figure 15 Comparison between the measured wind profile, power law and logarithmic fits, with KNW data for HKZA.

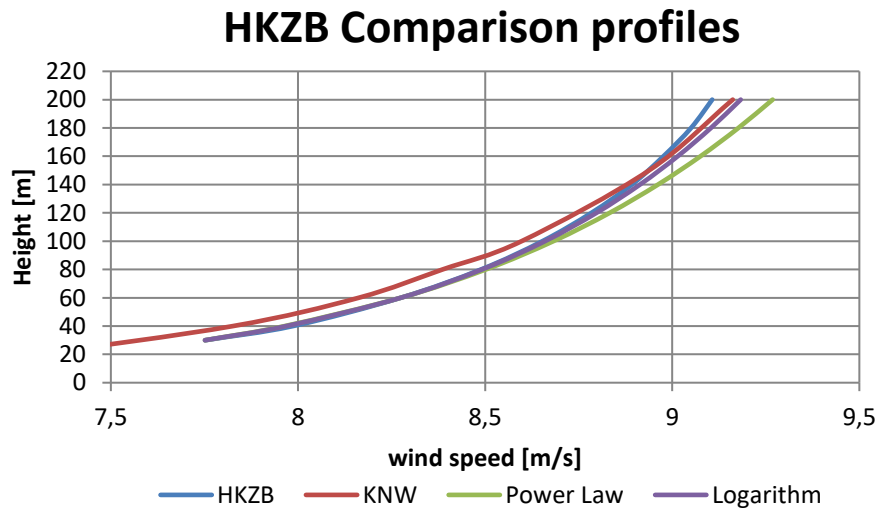

Figure 16 Comparison between the measured wind profile, power law and logarithmic fits, with KNW data for HKZB.

4.2 Wind speed distribution comparisons

The Weibull parameters were also extracted at each available measurement level and location for both the lidar and KNW atlas wind data. Vertical tendencies in *A* and *k*, along with wind speed, was examined at LEG (Figure 17), HKZA (Figure 18) and HKZB (Figure 19). Overall, the KNW atlas Weibull parameters compare well with the ones obtained from the measurements. Particularly, we see that at each location, the KNW atlas underestimates the Weibull shape parameter *k*, meaning that the KNW atlas predicts more wind variability than observed. This overestimation is amplified at lower elevations, with the KNW wind atlas better depicting the Weibull *k* factor as elevation increased.

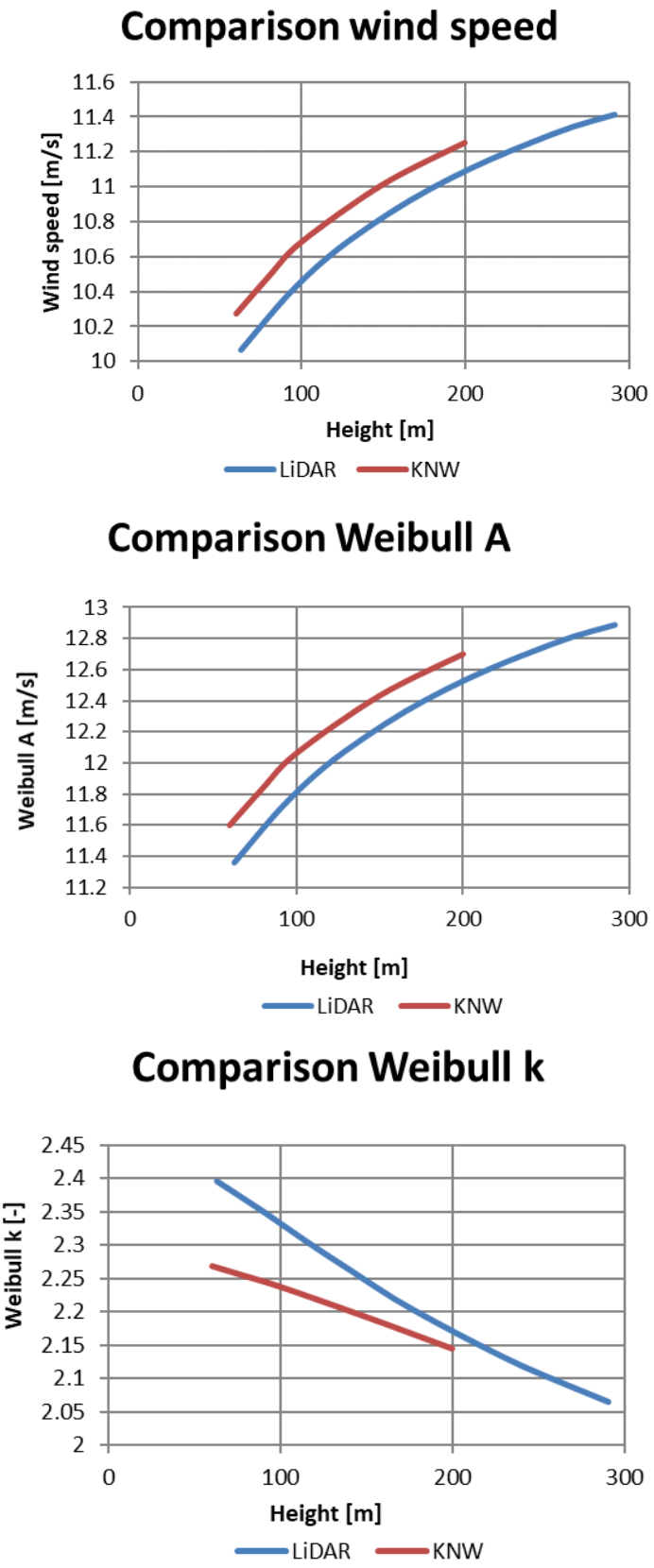

Figure 17 Comparison at LEG between the measured wind data and KNW for the (Top) mean wind speed, and the Weibull shape parameters (Middle) *A*, and (Bottom) *k*.

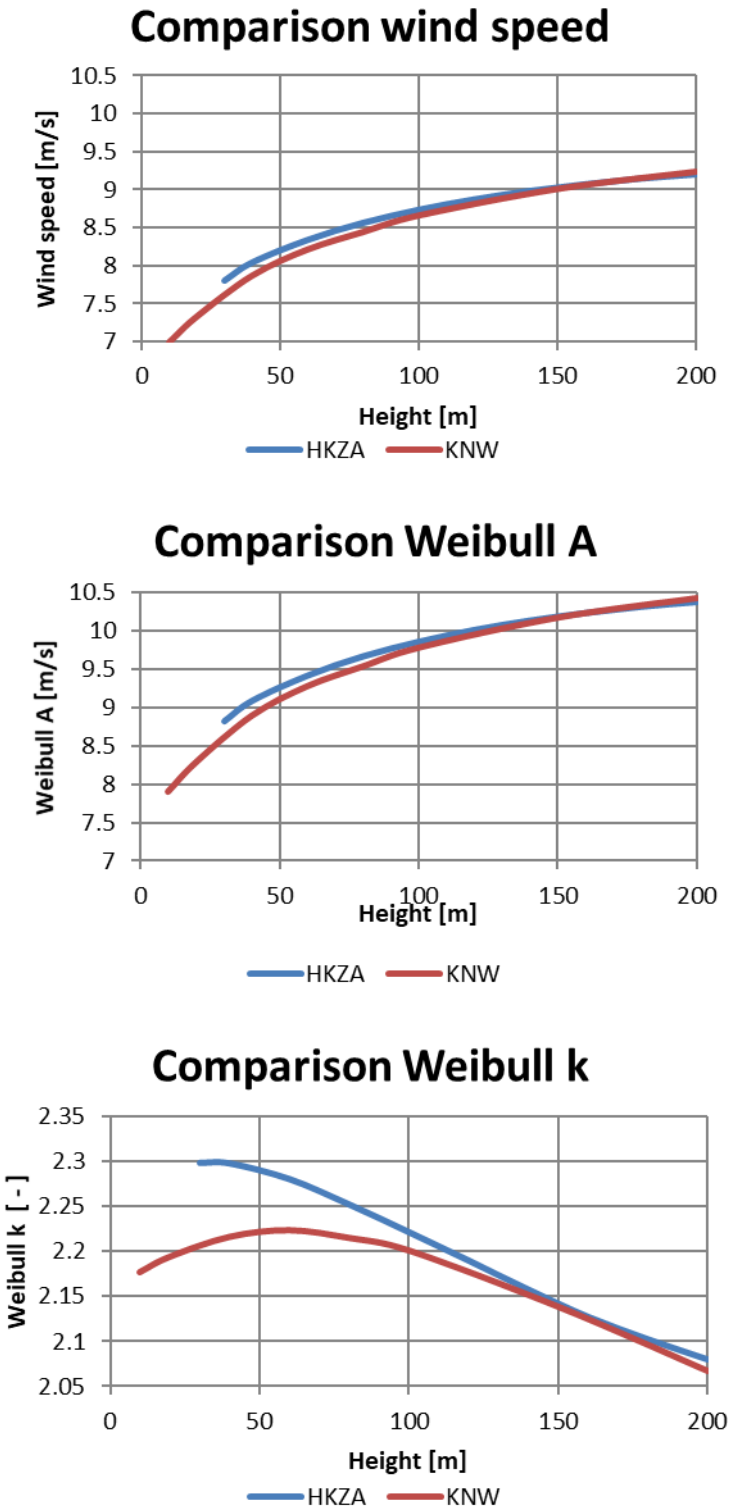

Figure 18 Comparison at HKZB between the measured wind data and KNW for the (Top) mean wind speed, and the Weibull shape parameters (Middle) *A*, and (Bottom) *k*.

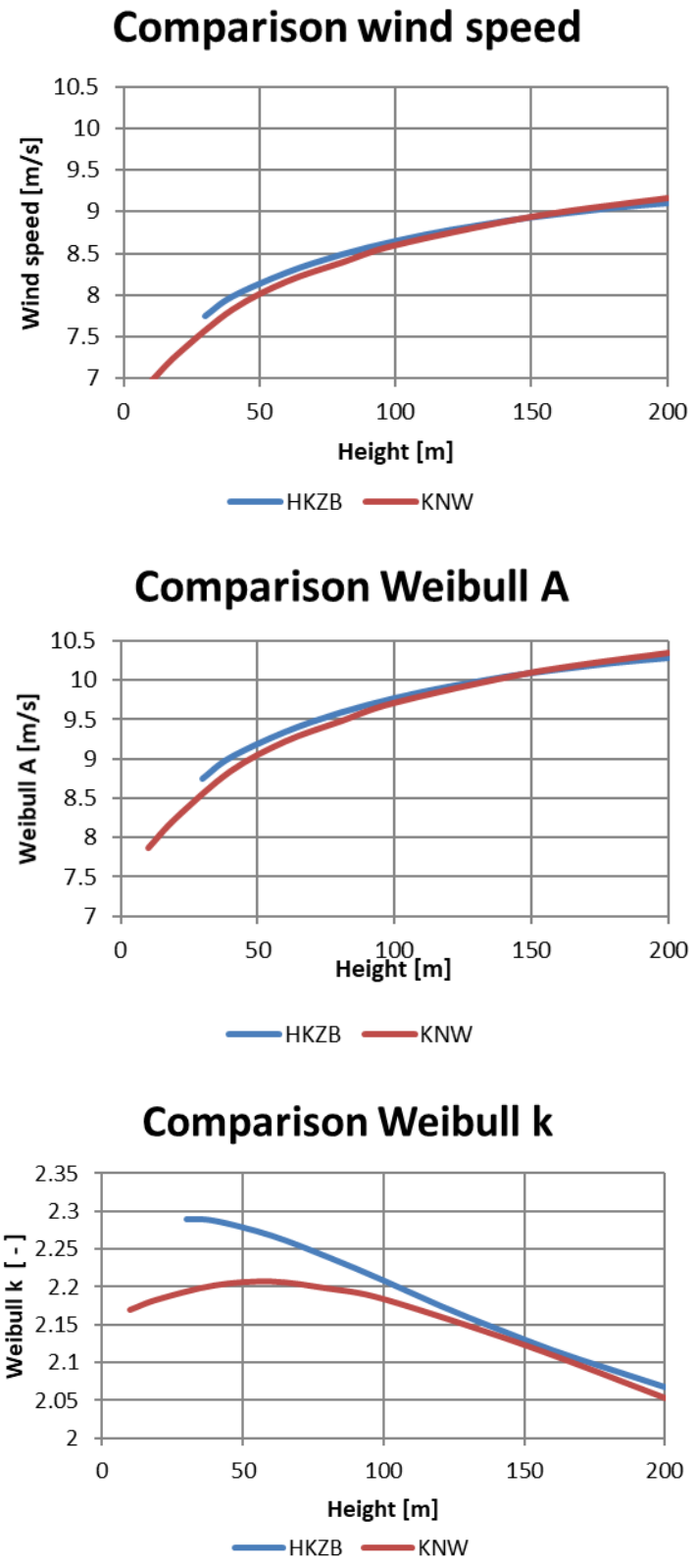

Figure 19 Comparison at HKZB between the measured wind data and KNW for the (Top) mean wind speed, and the Weibull shape parameters (Middle) *A*, and (Bottom) *k*.

5 Concluding remarks and discussion

As wind turbines continue to grow in size, and new technologies emerge that seek to exploit wind at high altitudes, a proper characterization of the offshore wind environment across a large depth of the ABL is of paramount importance. Therefore, within this study, wind conditions were analysed at eight different offshore measurement sites that were equipped lidar in order to better understand wind conditions relevant for the future development of North Sea wind. Wind distributions (i.e. Weibull fits), wind shear and veer profiles, and correlation between measurement locations were all examined as part of this study.

In general, wind conditions varied with height and as a function of proximity to the coast. Those stations further from the coast (i.e. MMIJ and K13a) exhibited stronger wind profiles; albeit, the wind profiles at both HKZ and BWFZ were probably significantly impacted by the presence of neighbouring wind farms. While these results might be expected, knowledge of the vertical tendencies in *k* require further thought. Although winds become less turbulent with height, the range of possible wind speeds is greater at higher altitudes because of the relationship between sea surface and wind speed. Therefore, there will be a higher frequency of anomalous wind events aloft than near the surface (i.e. wider distribution), which means that the value of *k* will decrease with height. Vertical wind shear was also examined at each measurement location where it was found that the greatest shear was associated with high wind speeds and south-westerly wind directions. Analyses of wind veer demonstrated a steady increase in wind direction with height at each measurement location examined. Correlation in wind speed, wind direction, and α were all inversely proportional to distance between measurement sites. On average, wind speed correlation between measurement locations decreased at a rate of -1.37 per km, wind direction correlation between sites decreased at a rate of -0.87 per km, and α correlation between sites decreased at a rate of -0.33 per km.

Measured wind data were also compared to the KNW atlas. Although previously validated against instrumented tower and scatterometer wind data, comparison with high altitude wind data made by lidar has yet to be performed. KNW atlas wind speed comparisons were made to lidar data at LEG, HKZA, and HKZB and overall, the KNW atlas compares well with these measurements. Particularly, we see that at each location, the KNW atlas predicts more wind variability than observed, specifically at lower elevations. Also, at LEG, KNW overestimated the mean wind speed by approximately 1.7 %.

5.1 Acknowledgements

The authors acknowledge KNMI for their support in providing the KNW data and for valuable discussions on the evaluation of Weibull parameters over height.

This report was supported with Topsector Energy subsidy from the Ministry of Economic Affairs and Climate Policy.

6 References

[1] Verification of WC577 at ECN LiDAR Calibration Facility for LEG campaign
D.A.J. Wouters and J.P.Verhoef
2017, ECN
ECN-E—17-080

[2] Validation of Z315 at ECN LiDAR Calibration Facility for EPL Campaign
D.A.J. Wouters
2018. ECN
TNO 2018 R10761

[3] Validation of Z563 at ECN LiDAR Calibration Facility for K13a Campaign
D.A.J. Wouters en J.P.Verhoef,
2018, ECN
TNO 2018 R10849

[4] Instrumentation report for Offshore Meteorogical Mast IJmuiden MMIJ campaign
J.P. Verhoef and E.J. Werkhoven
2018, ECN
TNO 2018 R10910

[5] Offshore Meteorogical Mast IJmuiden MMIJ Measurements Report 01-11-2011 - 31-12-2012
J.P. Verhoef and F. Papathanasiou
2018, ECN
TNO 2018 R10911

[6] Offshore Meteorogical Mast IJmuiden MMIJ Measurements Report 01-01-2013 - 31-12-2013
J.P. Verhoef and F. Papathanasiou
2018, ECN
TNO 2018 R10912

[7] Offshore Meteorogical Mast IJmuiden MMIJ Measurements Report 01-01-2014 - 31-12-2014
J.P. Verhoef and F. Papathanasiou
2018, ECN
TNO 2018 R10913

[8] Offshore Meteorogical Mast IJmuiden MMIJ Measurements Report 01-01-2015 - 31-12-2015
J.P. Verhoef and F. Papathanasiou
2018, ECN
TNO 2018 R10914

[9] Offshore Meteorogical Mast IJmuiden MMIJ Measurements Report 01-11-2011 - 31-12-2015
J.P. Verhoef and F. Papathanasiou

2018, ECN
TNO 2018 R10915

[10] Instrumentation Report for Lichteiland Goeree LiDAR Measurement Campaign
J.P.Verhoef, G.Bergman and E.J. Werkhoven
2018, ECN
TNO 2018 R10907

[11] Instrumentation Report for Europlatform LiDAR Measurement Campaign
J.P.Verhoef, G.Bergman and E.J. Werkhoven
2018, ECN
TNO 2018 R10908

[12] Instrumentation Report for K13a LiDAR Measurement Campaign
J.P.Verhoef, G.Bergman, C.A. van Diggelen and E.J. Werkhoven
2018, 2018
TNO 2018 R10909

[13] Wind Energy Handbook: Second Edition
T. Burton, N. Jenkins, D. Sharpe and E. Bossanyi
2011, John Wiley & Sons, Ltd. (Chichester, U.K.)

[14] Wind Speed Characteristics and Resource Assessment using Weibull Parameters
S. Rehman, A. M. Mahbub Alam, J. P. Meyer and L. M. Al-Hadhrami
2012, International Journal of Green Energy, 9: 800-814

[15] Estimation of Wind Power Potential Using Weibull Distribution
A. Genc, M. Erisoglu, A. Pekgor, G. Oturanc, A. Hepbasli and K. Ulgen
2005, Energy Sources, 9: 809-822

[16] Sea Surface Roughness and Drag Coefficients as Functions of Neutral Wind Speed
H. Hersbach
2011, Journal of Physical Oceanography, 41: 247-251

[17] Aerodynamic Roughness of the Sea Surface at High Winds
V. N. Kudryavstev and V. K. Makin
2007, Boundary-Layer Meteorology, 125: 289-303

[18] Boundary Layer Theory: Sixth Edition
H. Schlichting
1968, McGraw-Hill (New York, USA)

[19] An observational climatology of anomalous wind events at offshore meteomast IJmuiden
P. C. Kalverla, G. J. Steeneveld, R. J. Ronda and A. A. M. Holtslag
2017, Journal of Wind Engineering and Industrial Aerodynamics, 165: 86-99

[19] Wind turbine across the marine atmospheric boundary layer
A. R. Brown, A. C. M. Hersbach, H. Hollingsworth, A. Miller and M. Vasiljevic
2005, Quarterly Journal Royal Meteorological Society, 131: 1233-1250

[20] User manual of the (KNMI North Sea Wind) KNW-atlas
I. L. Wijnant, A. Stepek, M. Savenije and H. W. van den Brink
2016, KNMI
User manual

[21] Validation of KNW atlas with publicly available mast observations (Phase 3 of KNW project)
A. Stepek, M. Savenije, H. W. van den Brink and I. L. Wijnant
2015, KNMI
TR-352

[22] Validation of KNW atlas with scatterometer winds (Phase 3 of KNW project)
I. L. Wijnant, G. J. Marseille, A. Stoffelen, H. W. van den Brink and A. Stepek
2015, KNMI
TR-353

A Measurement site wind resource summary

In order to examine mean wind state and variability, a Weibull distribution was fit to the measured wind data (using 1 m s^{-1} histogram bins) and a wind rose (using 30º wind direction bins) was defined. This analysis was performed on the datasets identified in Table 1 at each available measurement level. Wind shear and veer were also examined at each measurement site for the entire data record. The results of this first-order wind resource assessment are provided below for each measurement site.

B MMIJ wind resource summary

MMIJ_2012 Dataset

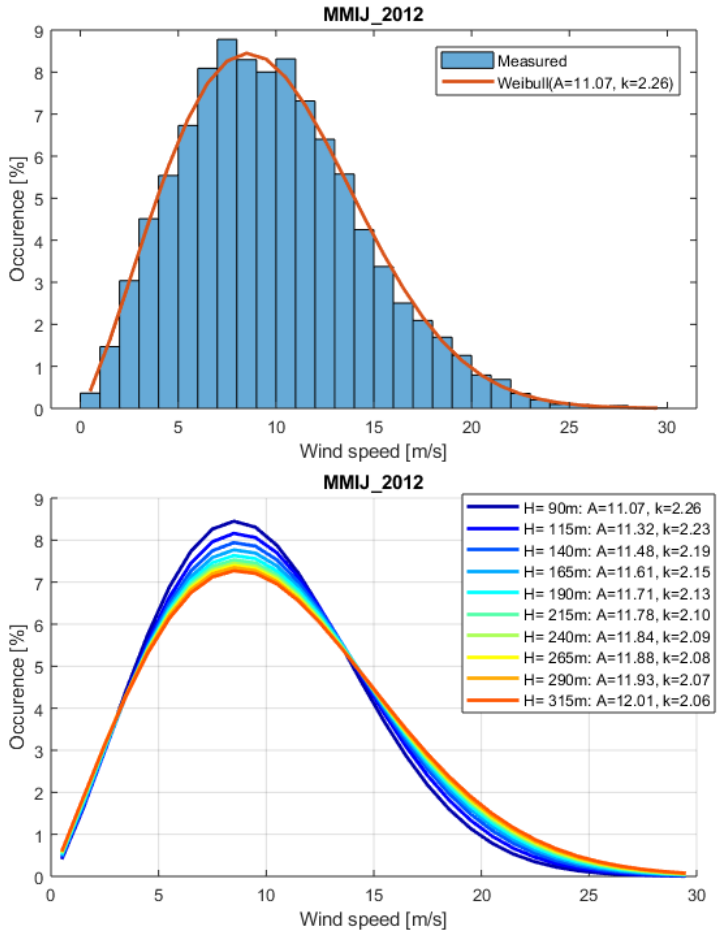

Figure B.1 (Top) Histogram (1 m s^{-1} bins) of the 10-min mean wind speeds at 90 m overlaid by the fitted Weibull distribution. (Bottom) The fitted Weibull distribution at each available measurement level from 90 m through 315 m.

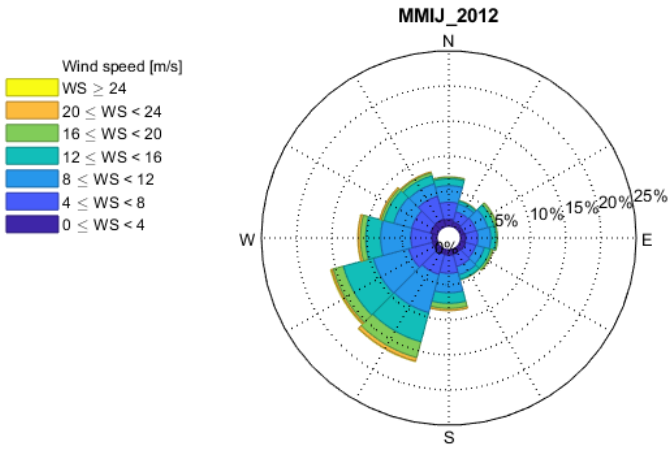

Figure B.2 Wind rose (30º wind direction bins) at 90 m.

MMIJ_2013 Dataset

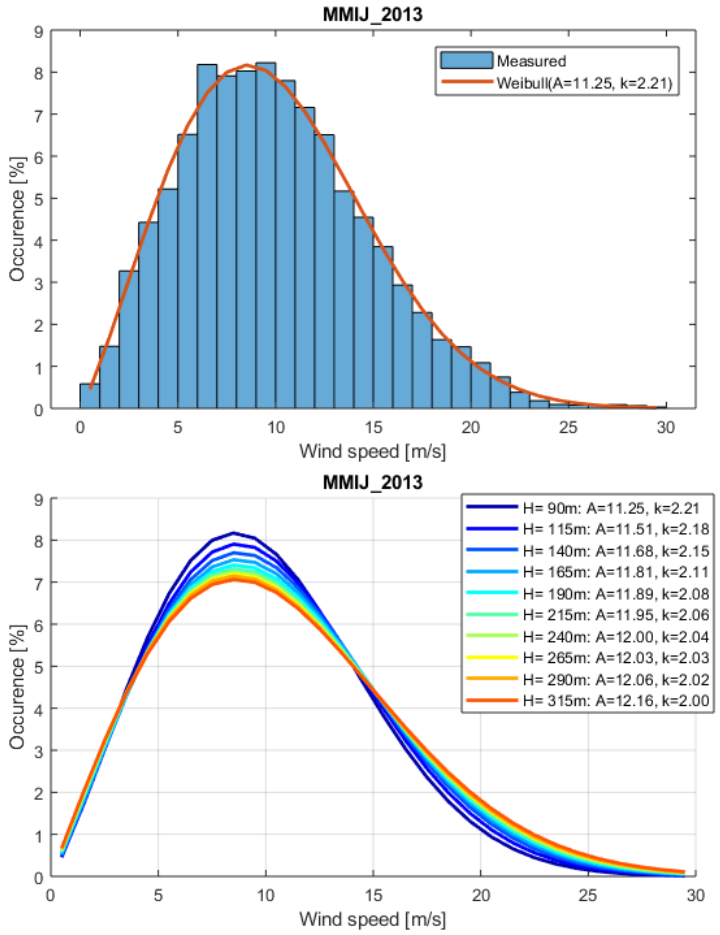

Figure C.3 (Top) Histogram (1 m s^{-1} bins) of the 10-min mean wind speeds at 90 m overlaid by the fitted Weibull distribution. (Bottom) The fitted Weibull distribution at each available measurement level from 90 m through 315 m.

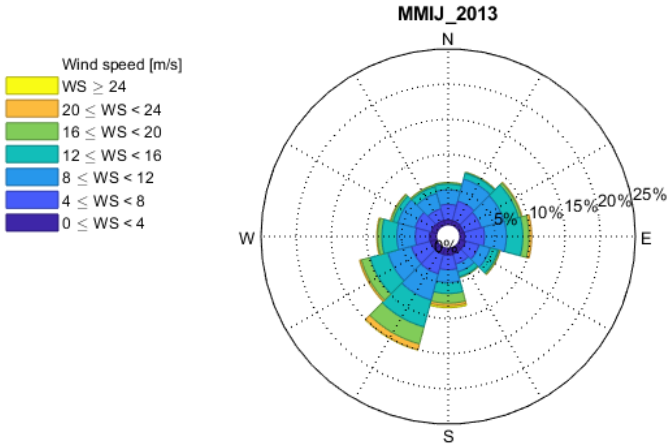

Figure C.4 Wind rose (30º wind direction bins) at 90 m.

MMIJ_2014 Dataset

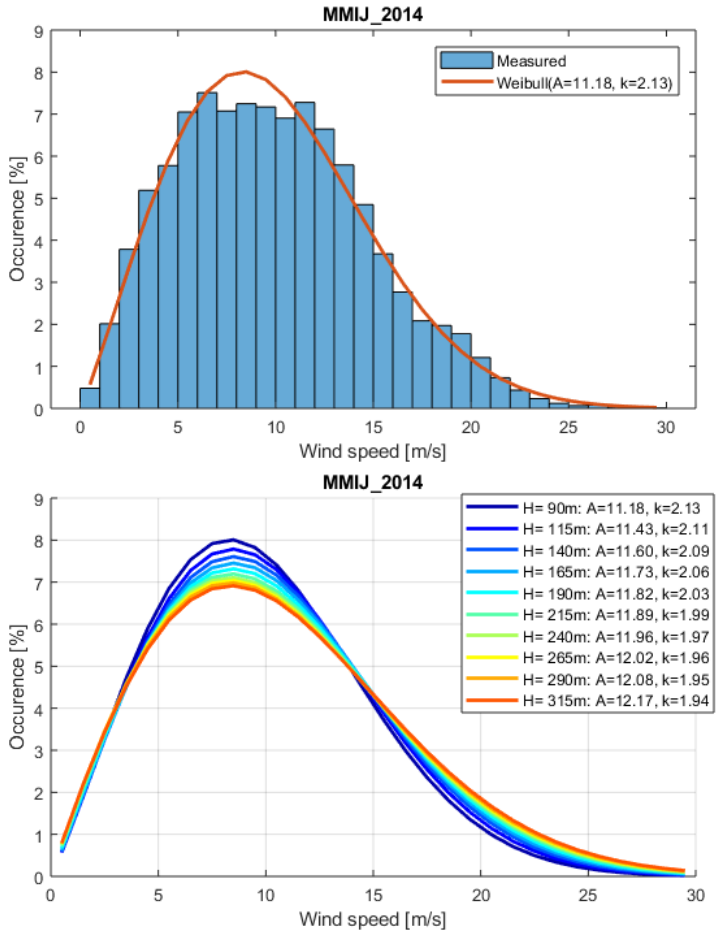

Figure C.5 (Top) Histogram (1 m s^{-1} bins) of the 10-min mean wind speeds at 90 m overlaid by the fitted Weibull distribution. (Bottom) The fitted Weibull distribution at each available measurement level from 90 m through 315 m.

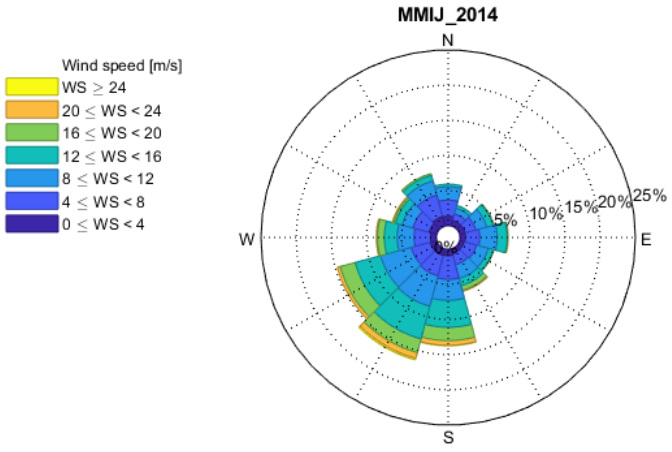

Figure C.6 Wind rose (30º wind direction bins) at 91 m.

MMIJ_2015 Dataset

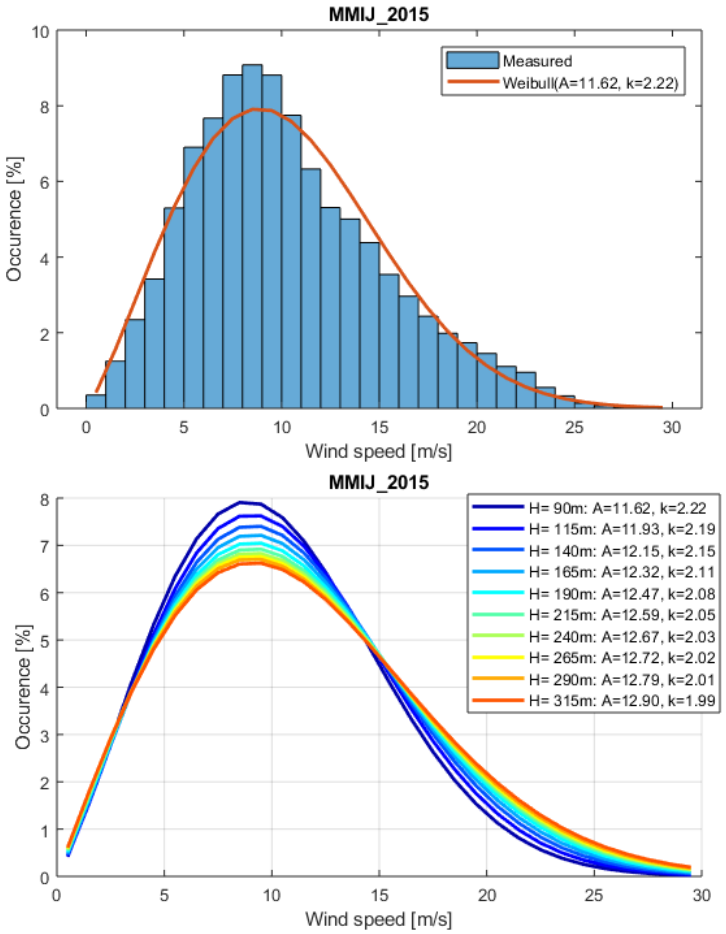

Figure C.7 (Top) Histogram (1 m s^{-1} bins) of the 10-min mean wind speeds at 90 m overlaid by the fitted Weibull distribution. (Bottom) The fitted Weibull distribution at each available measurement level from 90 m through 315 m.

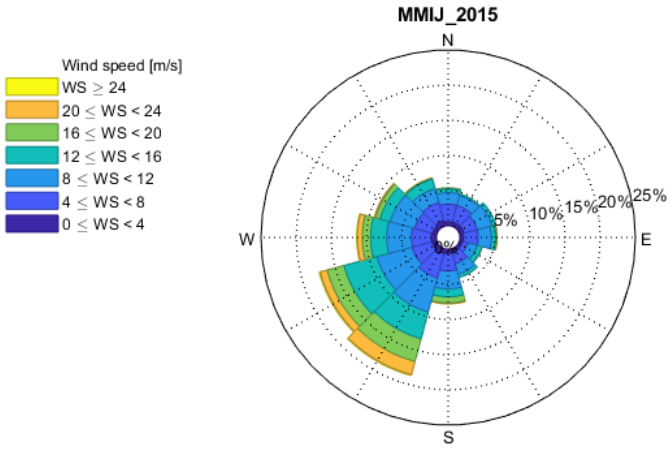

Figure C.8 Wind rose (30º wind direction bins) at 90 m.

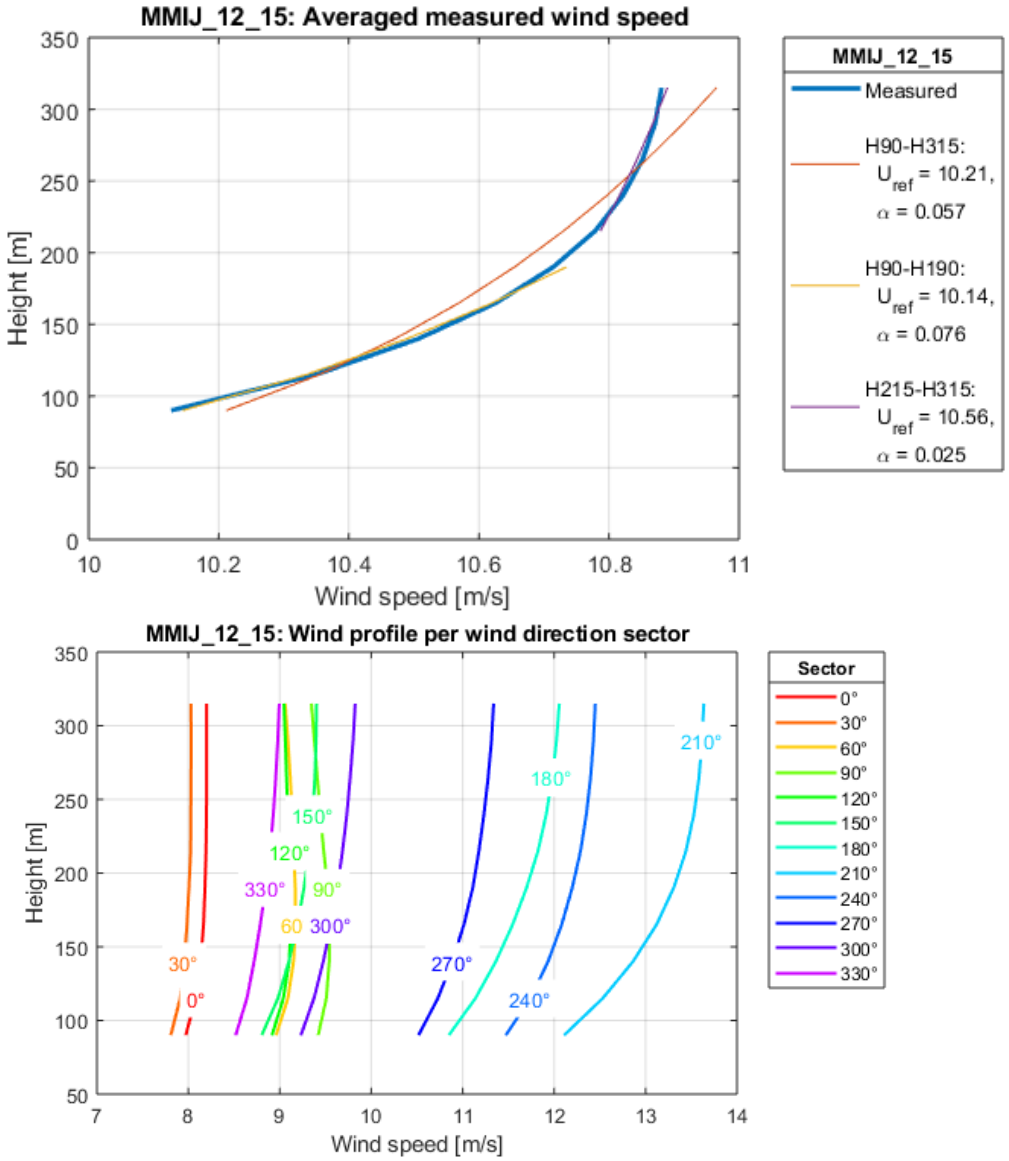

Figure B.9 (Top) Mean wind profile overlaid by varying power-law fits that depend upon which measurements levels (or layers) were considered. (Bottom) Mean wind profile as a function of wind direction.

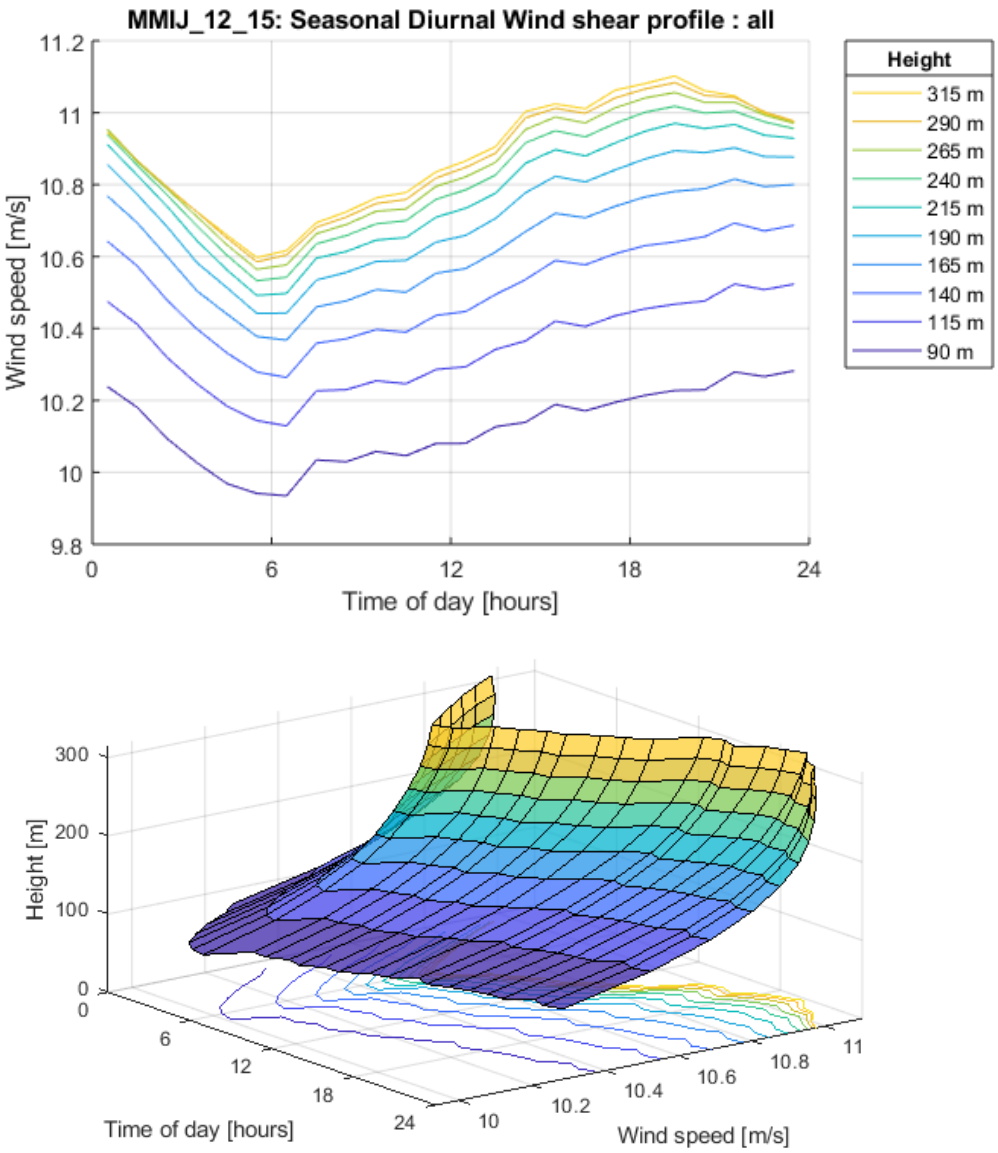

Figure B.10 (Top/Bottom) Different visual representations of variability in mean wind speed with height and the diurnal cycle.

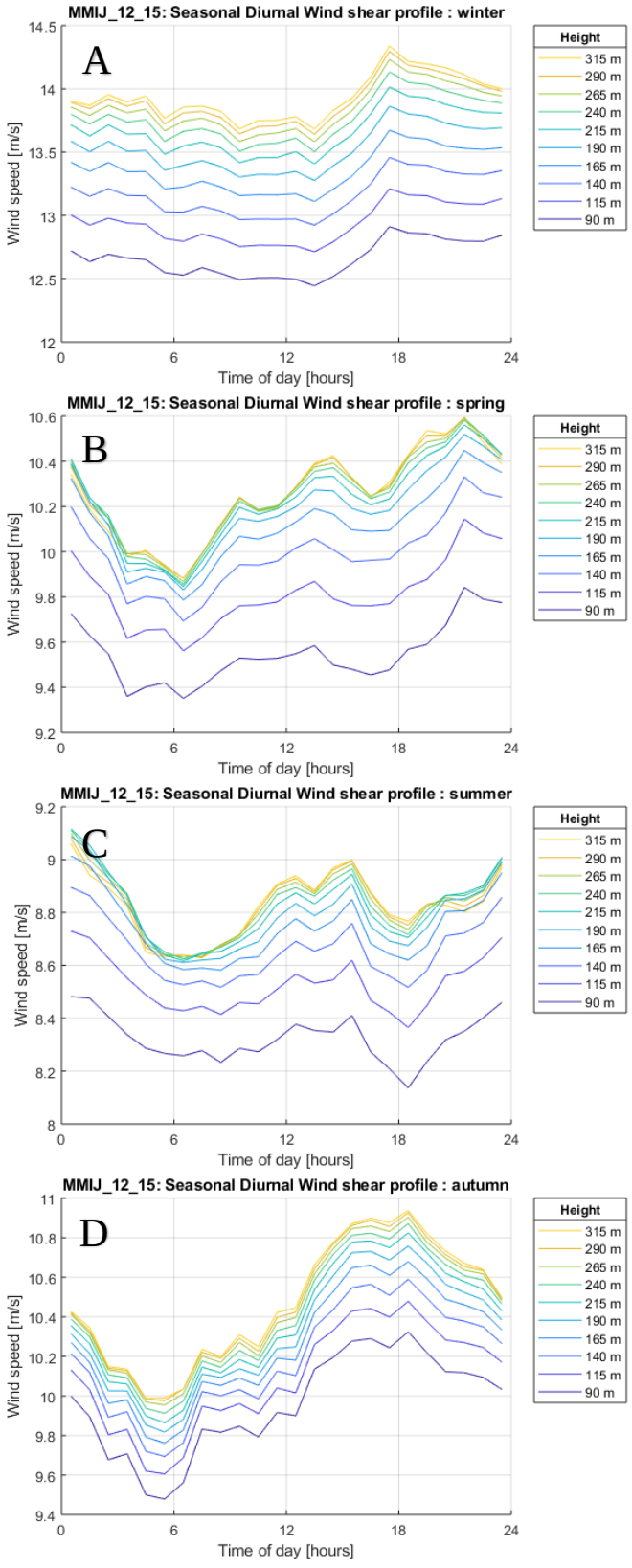

Figure B.11 Same as B.10 (Top) except that the mean wind speed data is parsed according to seasonal cycle – i.e. Winter (A), Spring (B), Summer (C), Autumn (D).

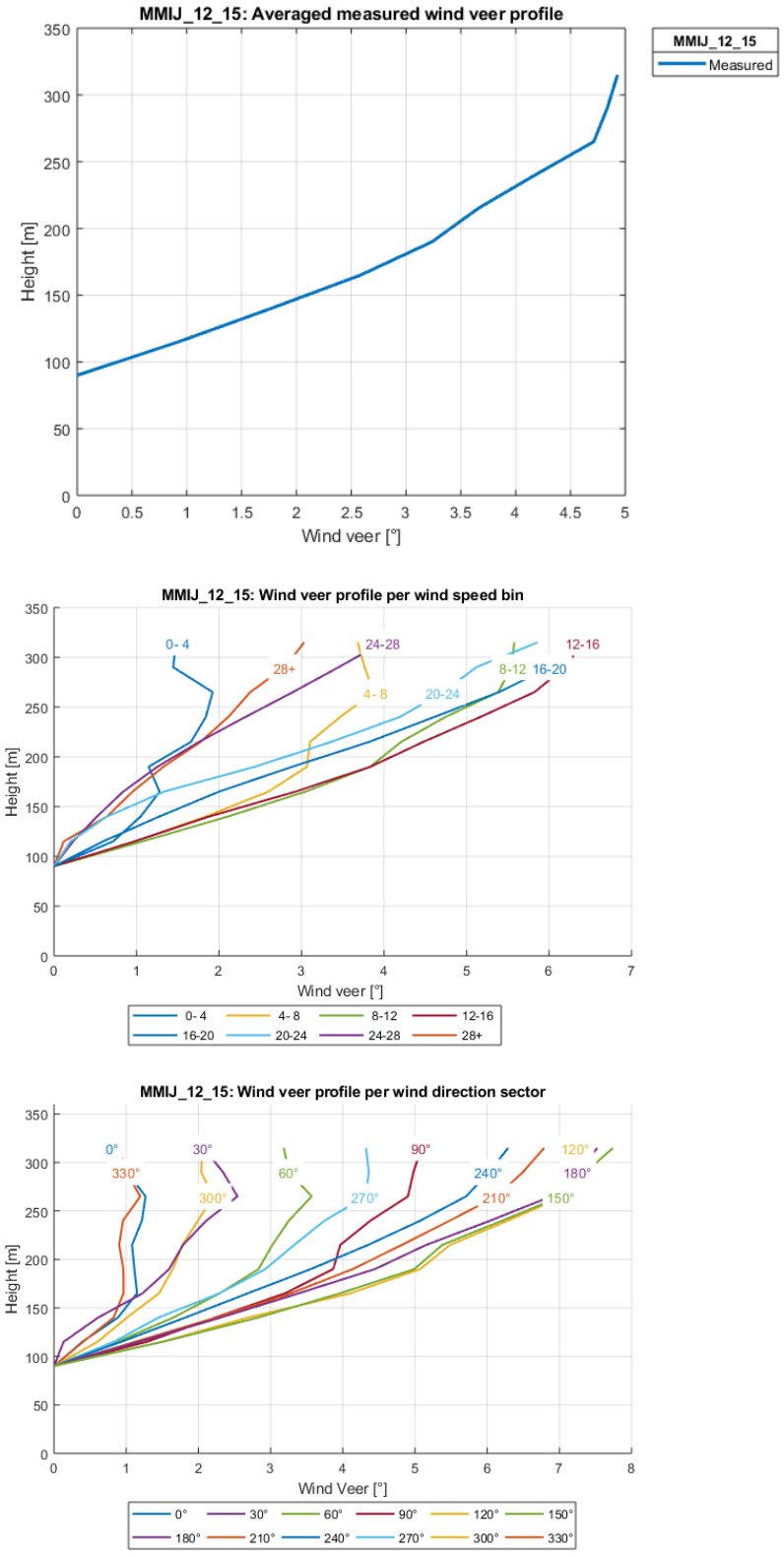

Figure B.12 (Top) Mean wind veer profile and the mean wind profile for different (Middle) wind speed and (Bottom) direction sectors.

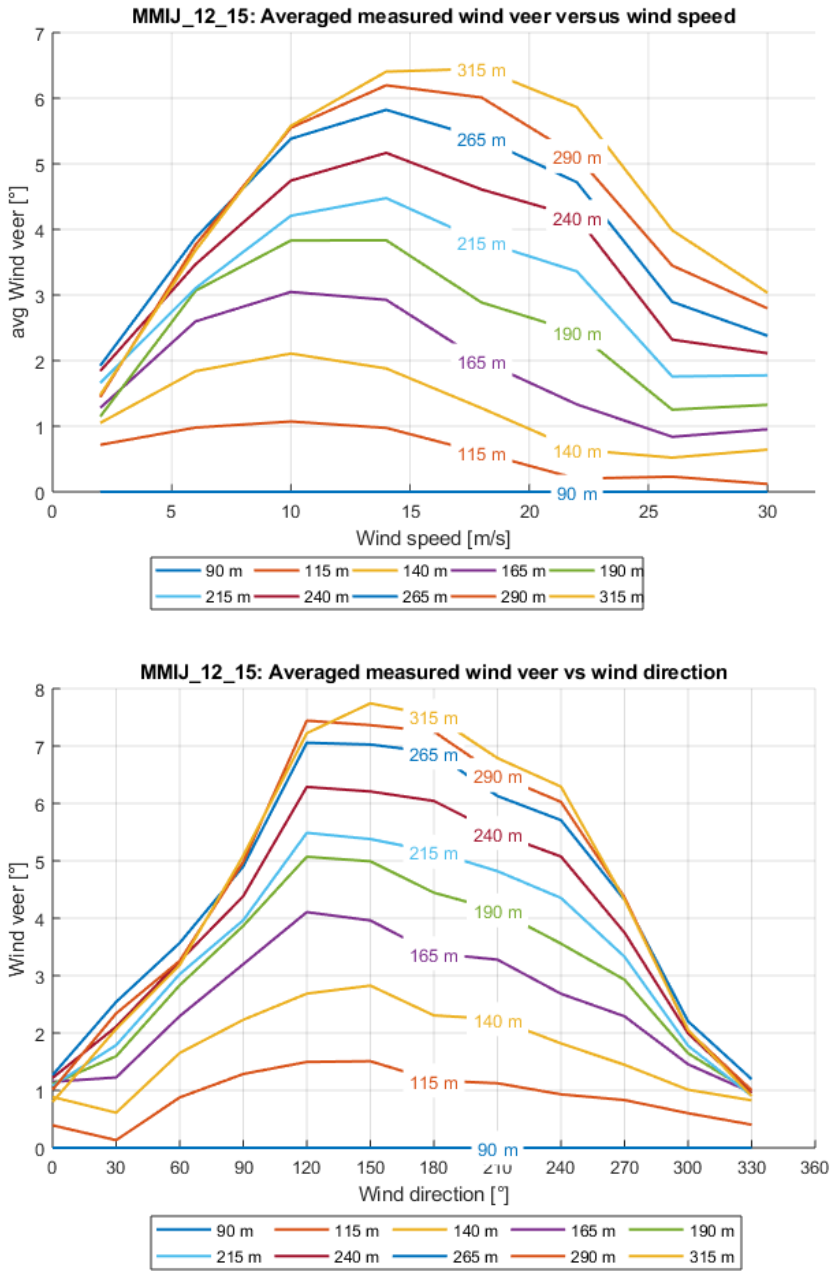

Figure B.13 (Top/Bottom) Mean wind veer as a function of measurement height for different (Top) wind speed and (Bottom) direction sectors.

C LEG wind resource summary

LEG_2015C Dataset

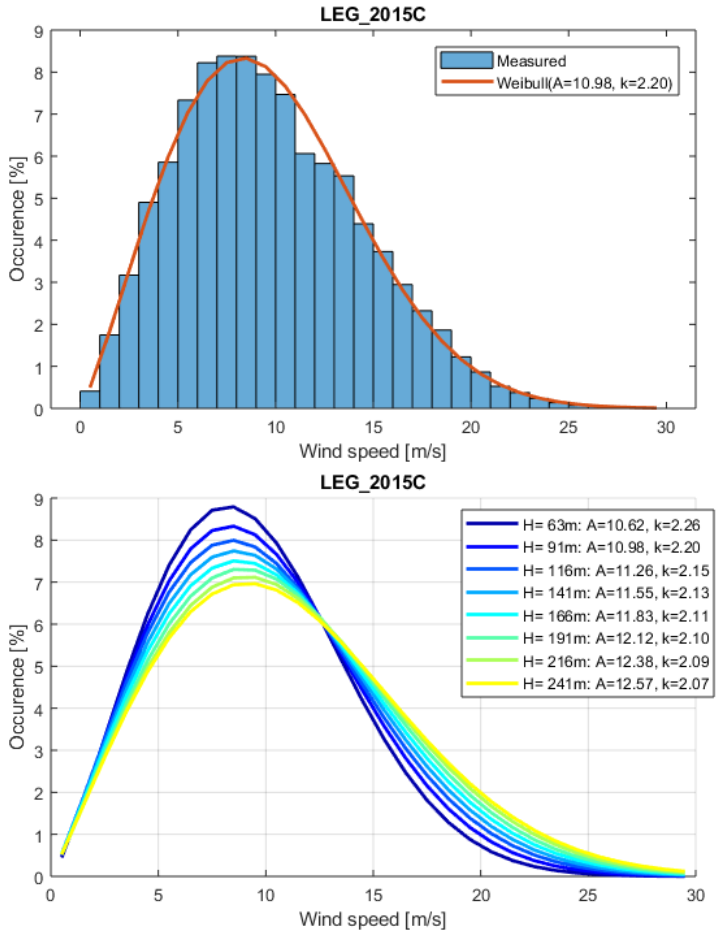

Figure C.1 (Top) Histogram (1 m s^{-1} bins) of the 10-min mean wind speeds at 91 m overlaid by the fitted Weibull distribution. (Bottom) The fitted Weibull distribution at each available measurement level from 63 m through 241 m.

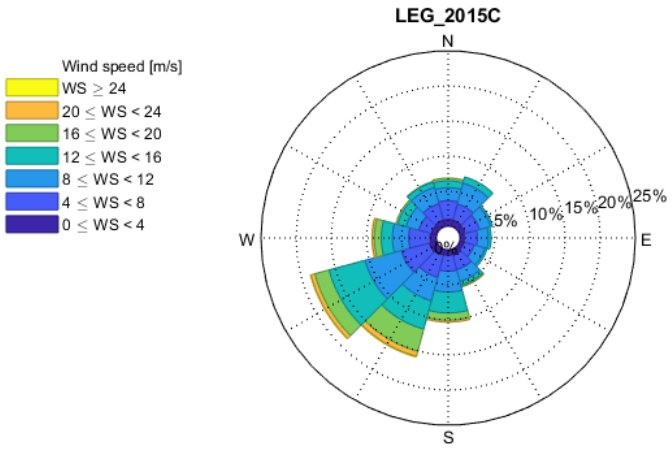

Figure C.2 Wind rose (30º wind direction bins) at 91 m.

LEG_2016C Dataset

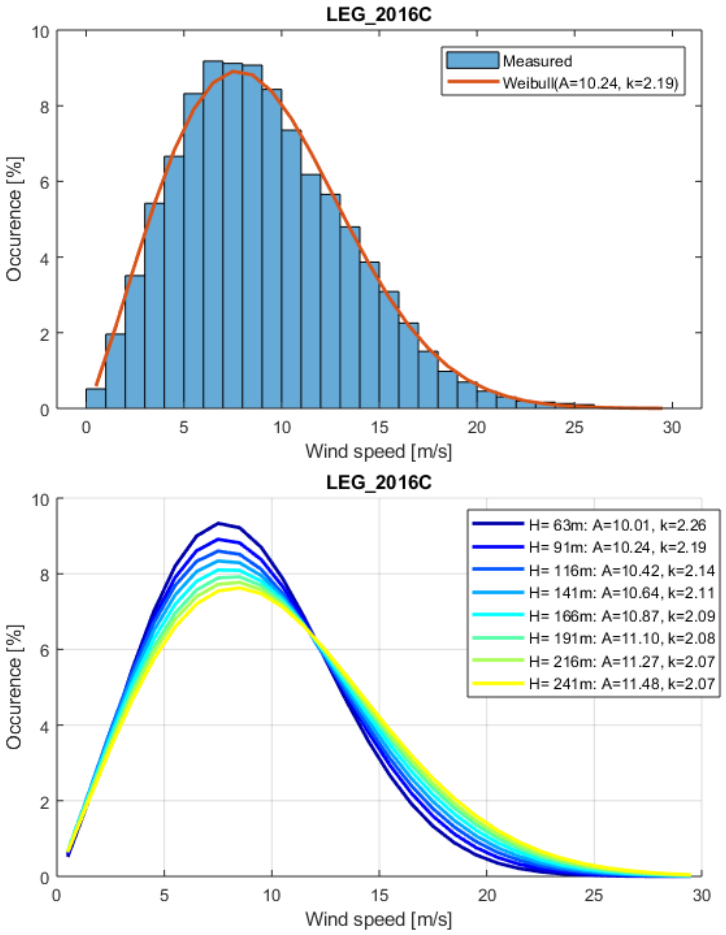

Figure C.3 (Top) Histogram (1 m s^{-1} bins) of the 10-min mean wind speeds at 91 m overlaid by the fitted Weibull distribution. (Bottom) The fitted Weibull distribution at each available measurement level from 63 m through 241 m.

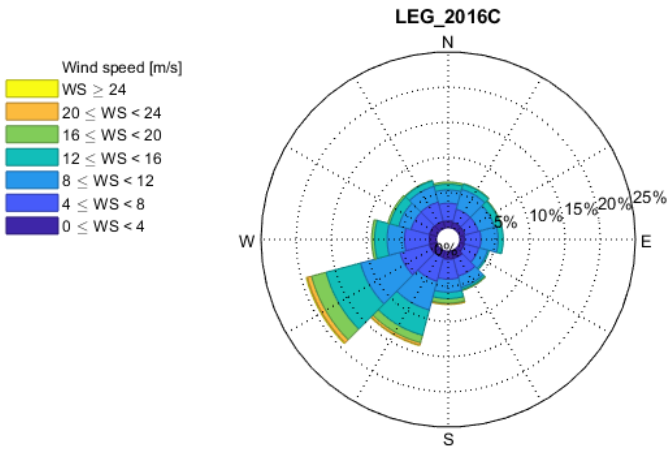

Figure C.4 Wind rose (30º wind direction bins) at 91 m.

LEG_2017C Dataset

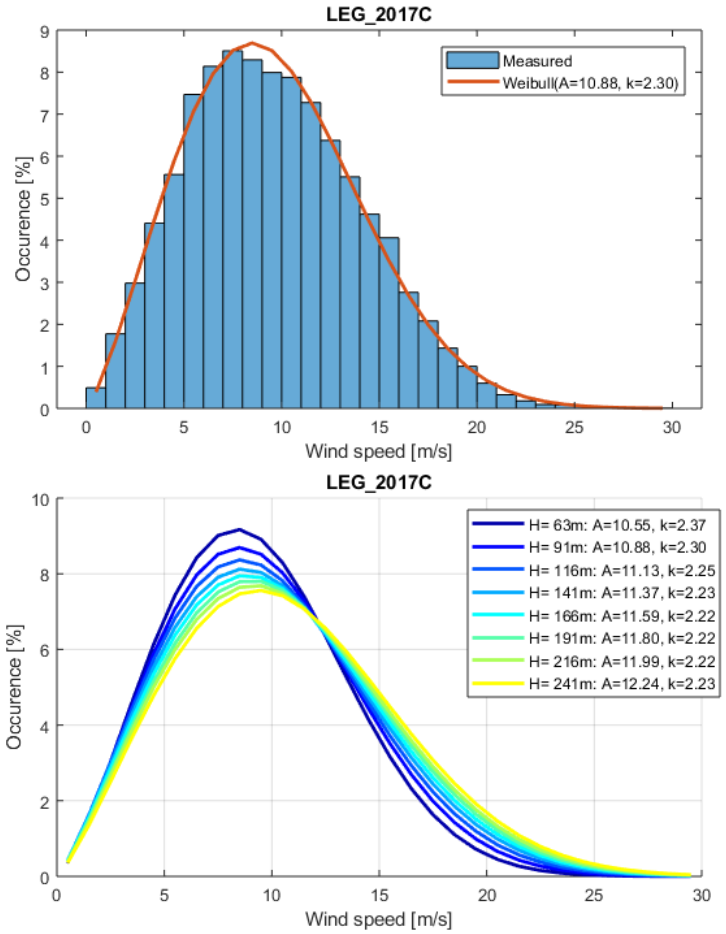

Figure C.5 (Top) Histogram (1 m s^{-1} bins) of the 10-min mean wind speeds at 91 m overlaid by the fitted Weibull distribution. (Bottom) The fitted Weibull distribution at each available measurement level from 63 m through 241 m.

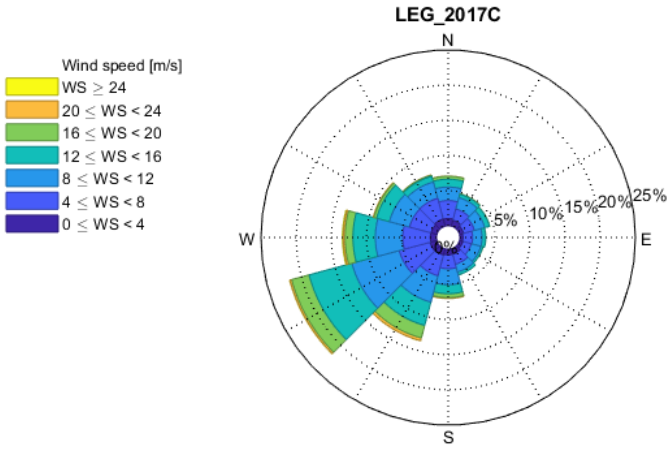

Figure C.6 Wind rose (30º wind direction bins) at 91 m.

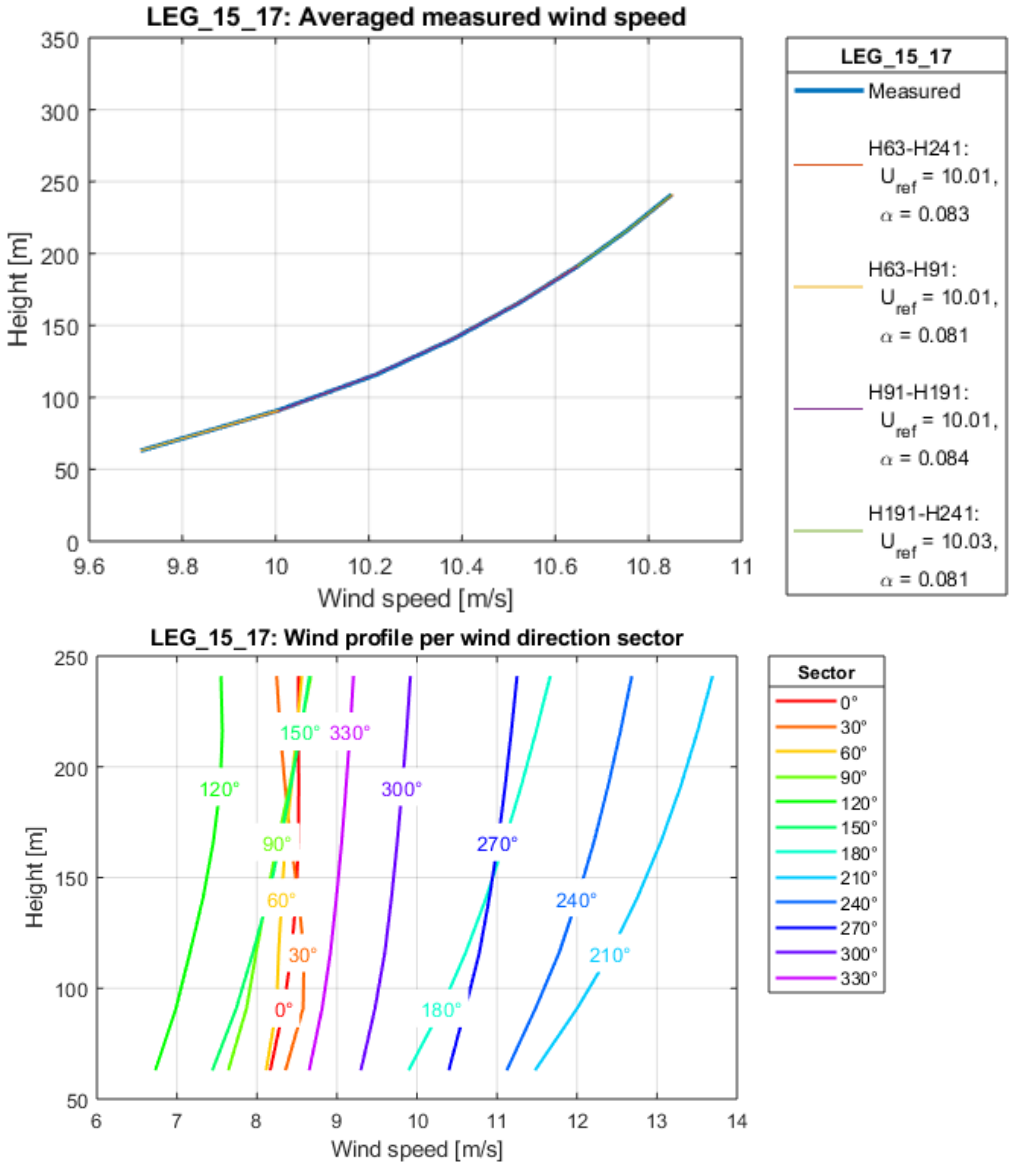

Figure C.7 (Top) Mean wind profile overlaid by varying power-law fits that depend upon which measurements levels (or layers) were considered. (Bottom) Mean wind profile as a function of wind direction.

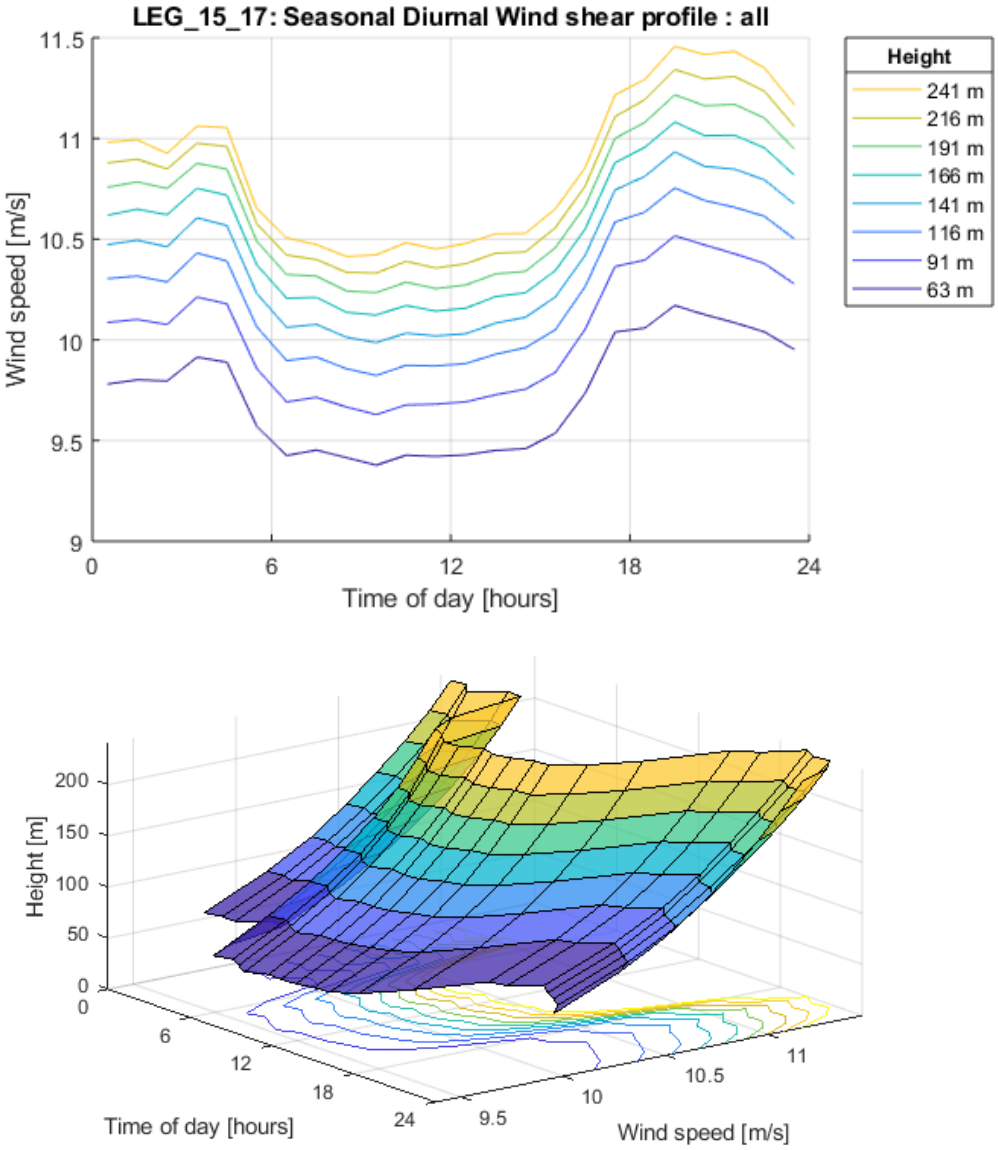

Figure C.8 (Top/Bottom) Different visual representations of variability in mean wind speed with height and the diurnal cycle.

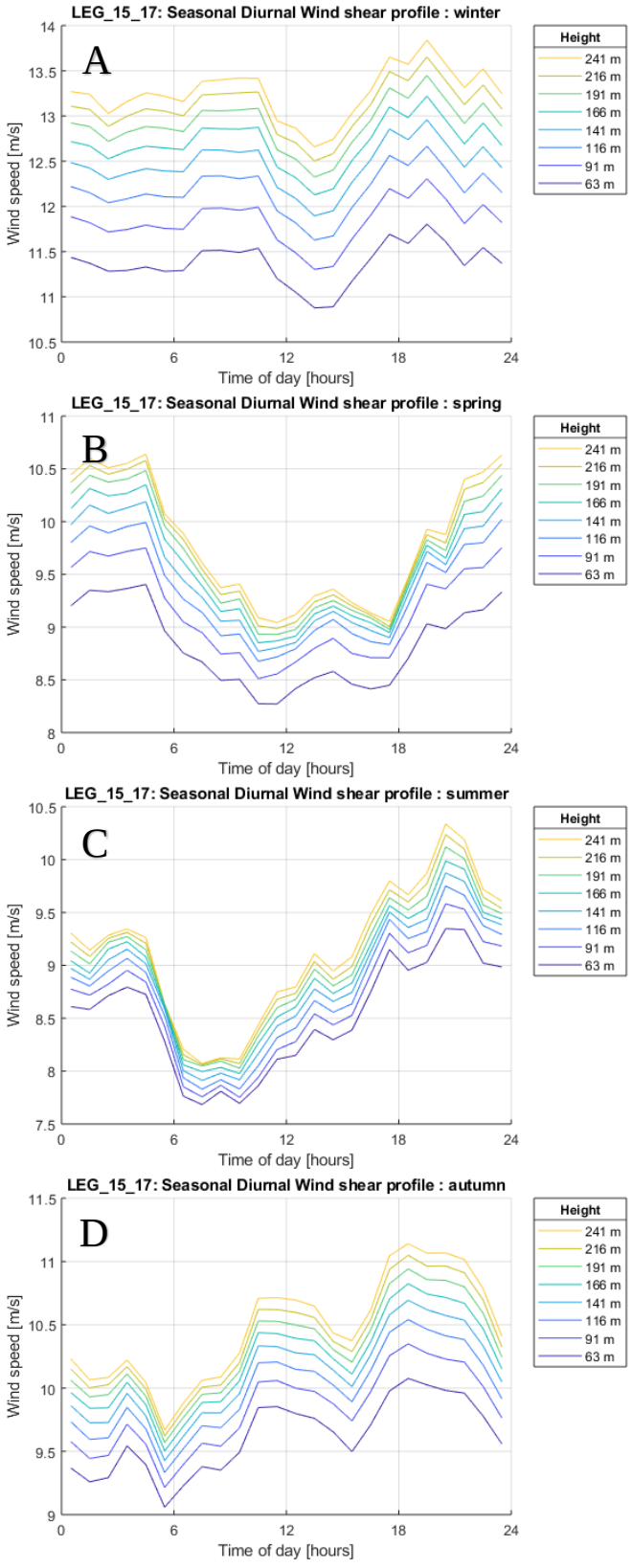

Figure C.9 Same as C.8 (Top) except that the mean wind speed data is parsed according to seasonal cycle – i.e. Winter (A), Spring (B), Summer (C), Autumn (D).

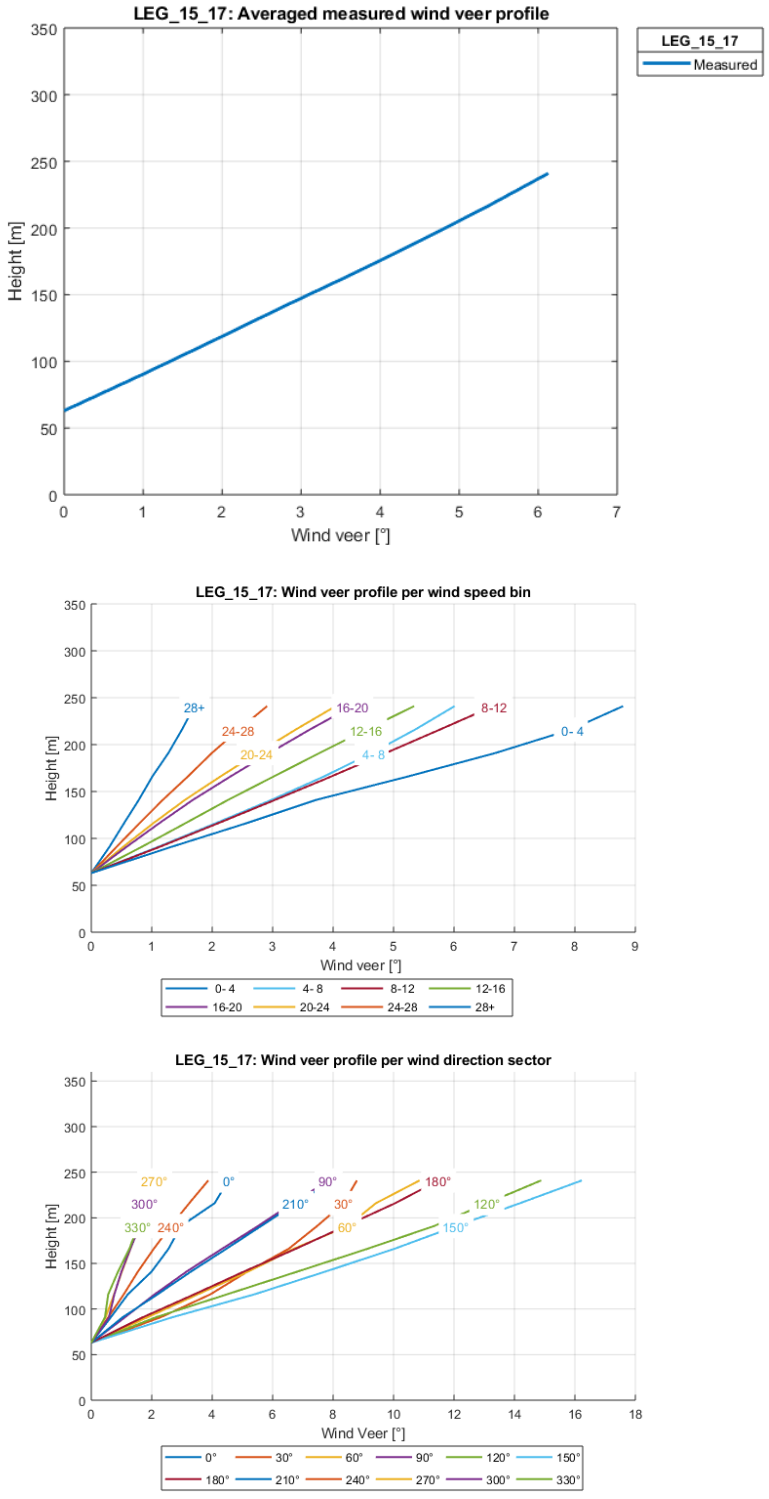

Figure C.10 (Top) Mean wind veer profile and the mean wind profile for different (Middle) wind speed and (Bottom) direction sectors.

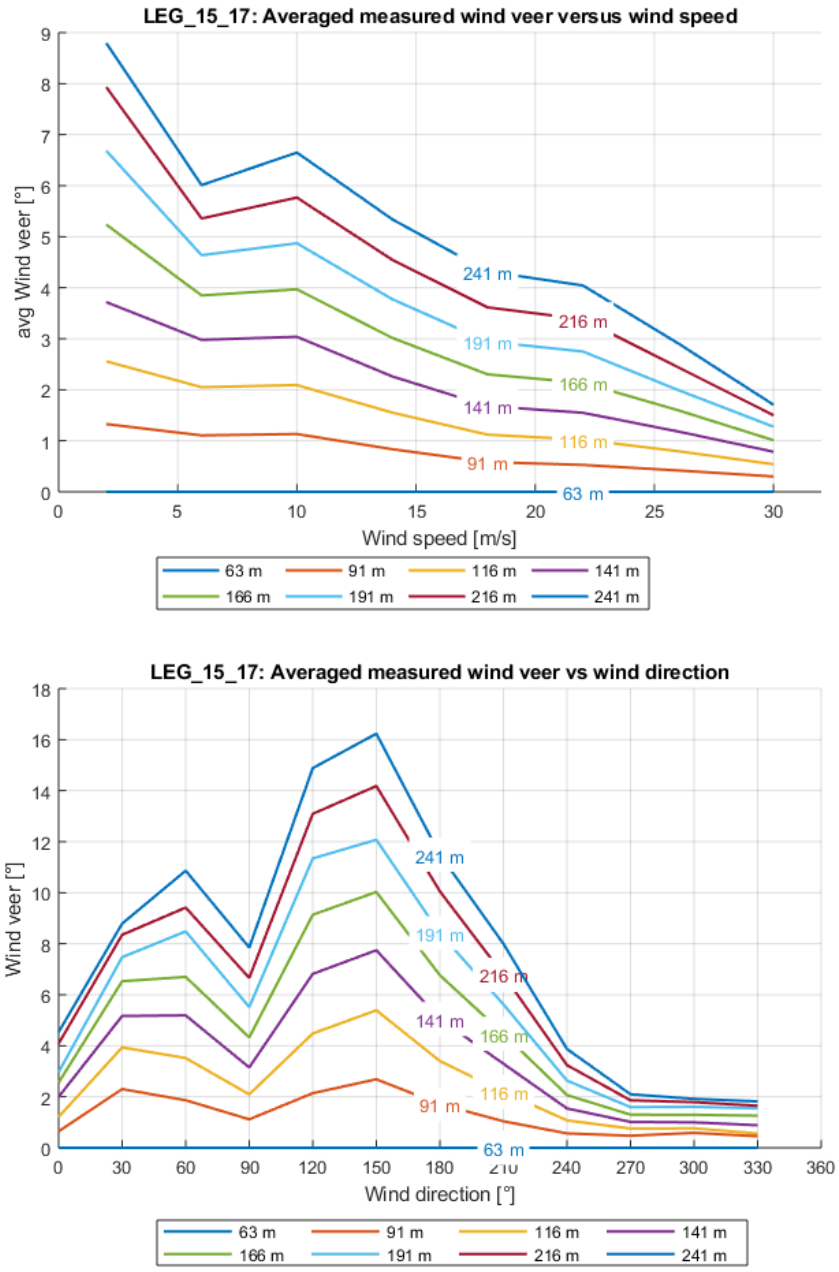

Figure C.11 (Top/Bottom) Mean wind veer as a function of measurement height for different (Top) wind speed and (Bottom) direction sectors.

D EPL wind resource summary

EPL_2016A Dataset

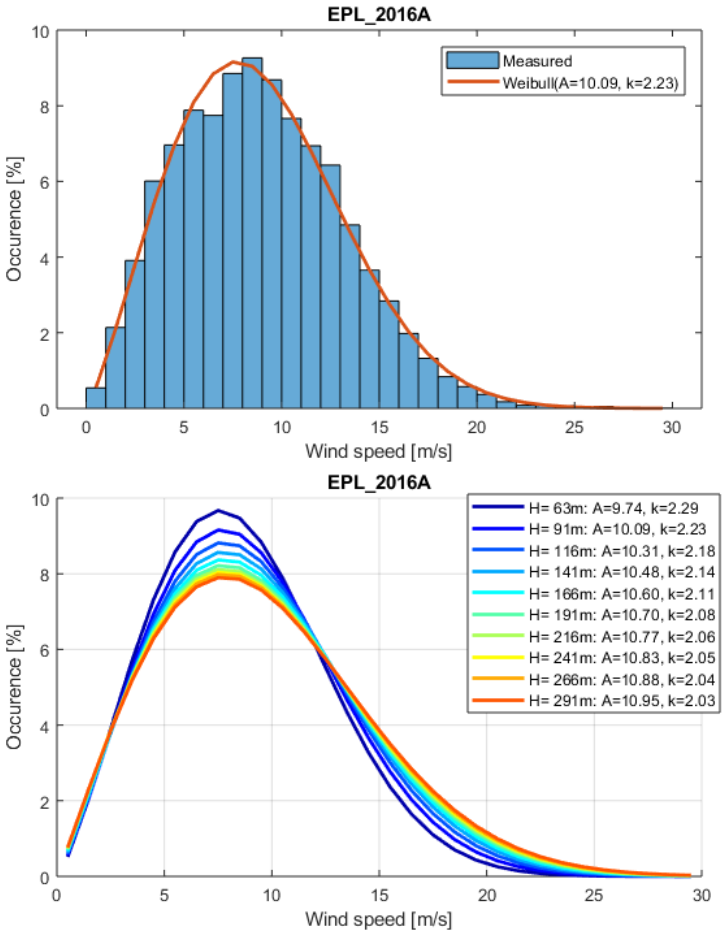

Figure D.3 (Top) Histogram (1 m s^{-1} bins) of the 10-min mean wind speeds at 91 m overlaid by the fitted Weibull distribution. (Bottom) The fitted Weibull distribution at each available measurement level from 63 m through 291 m.

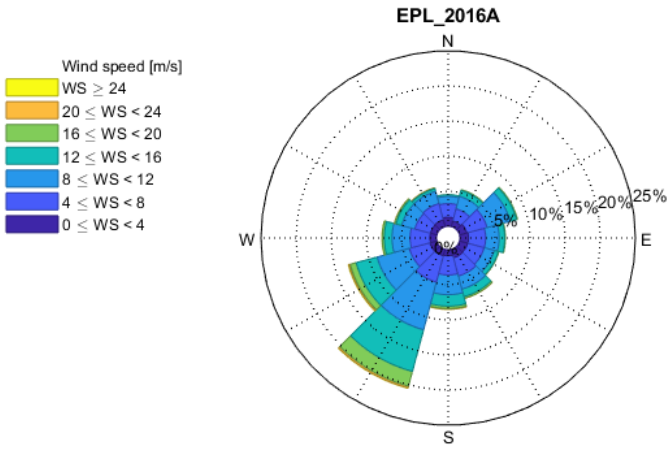

Figure D.4 Wind rose (30º wind direction bins) at 91 m.

EPL_2017 Dataset

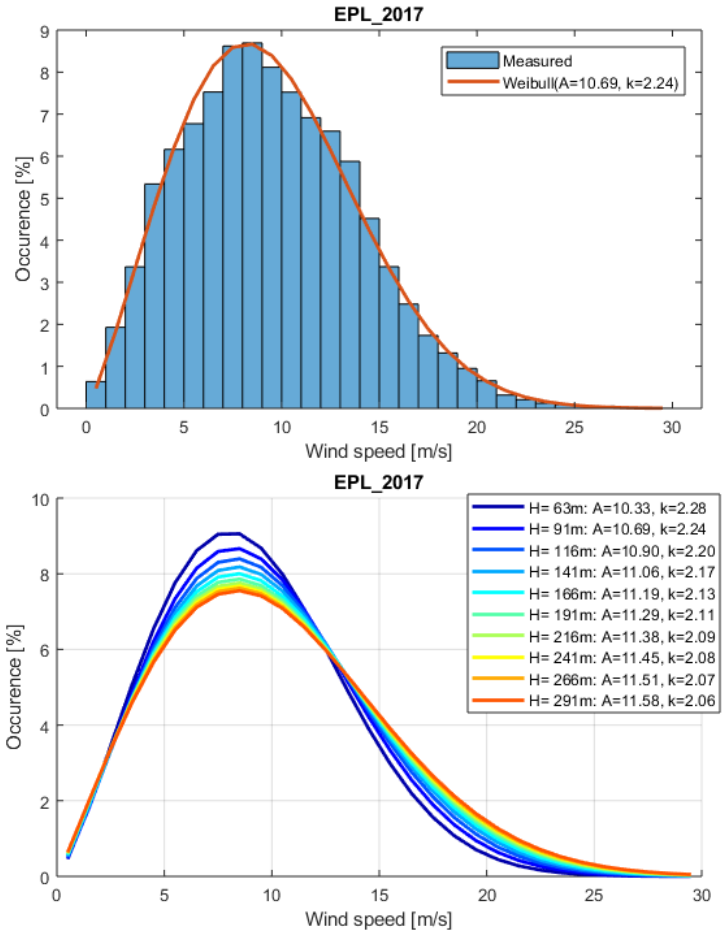

Figure D.3 (Top) Histogram (1 m s^{-1} bins) of the 10-min mean wind speeds at 91 m overlaid by the fitted Weibull distribution. (Bottom) The fitted Weibull distribution at each available measurement level from 63 m through 291 m.

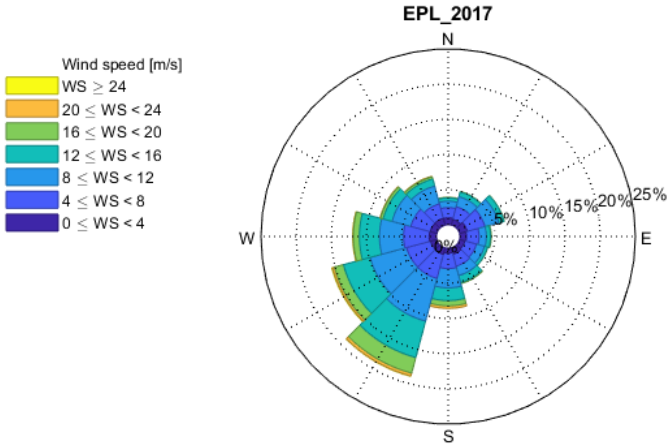

Figure D.4 Wind rose (30º wind direction bins) at 91 m.

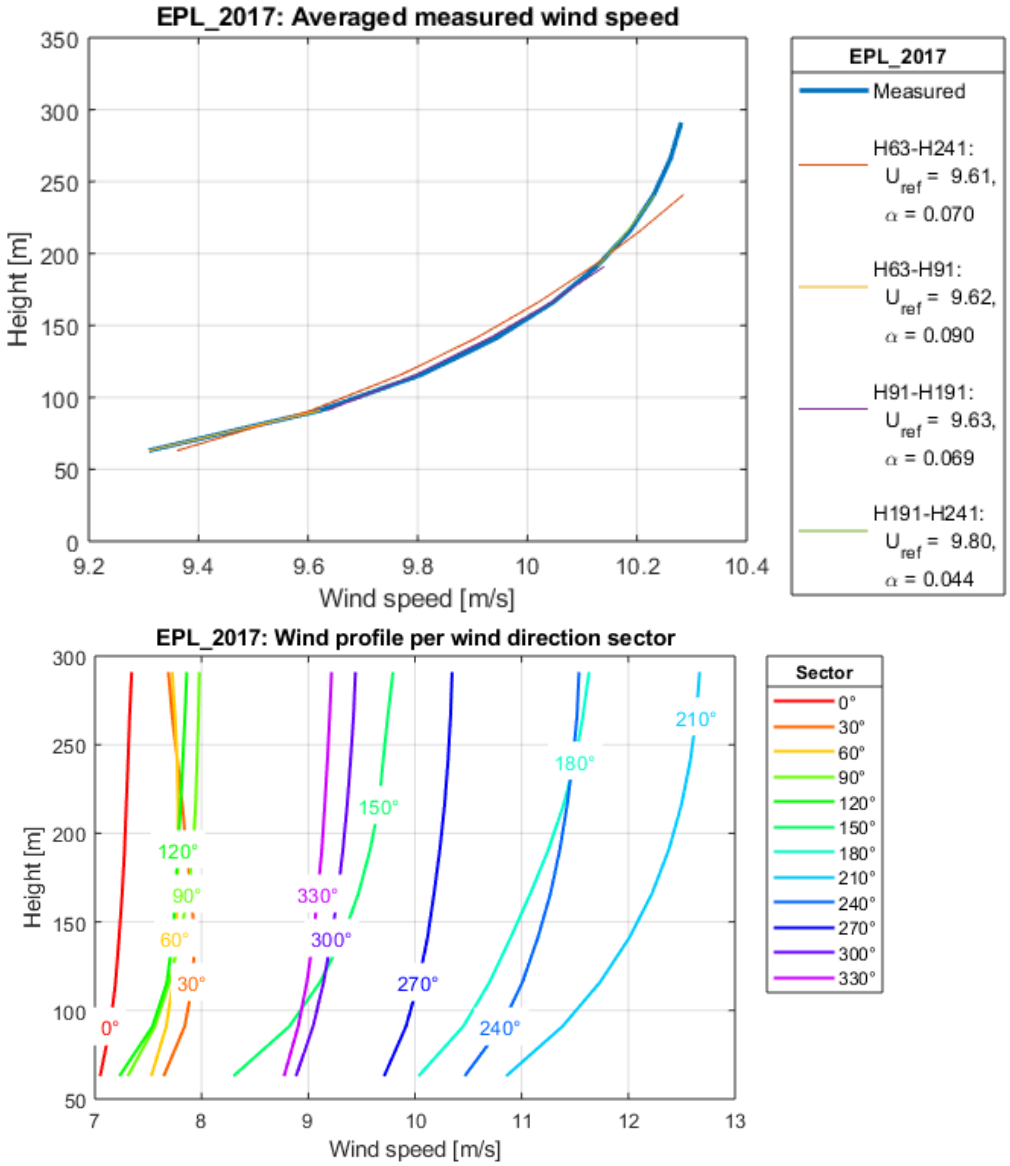

Figure D.5 (Top) Mean wind profile overlaid by varying power-law fits that depend upon which measurements levels (or layers) were considered. (Bottom) Mean wind profile as a function of wind direction.

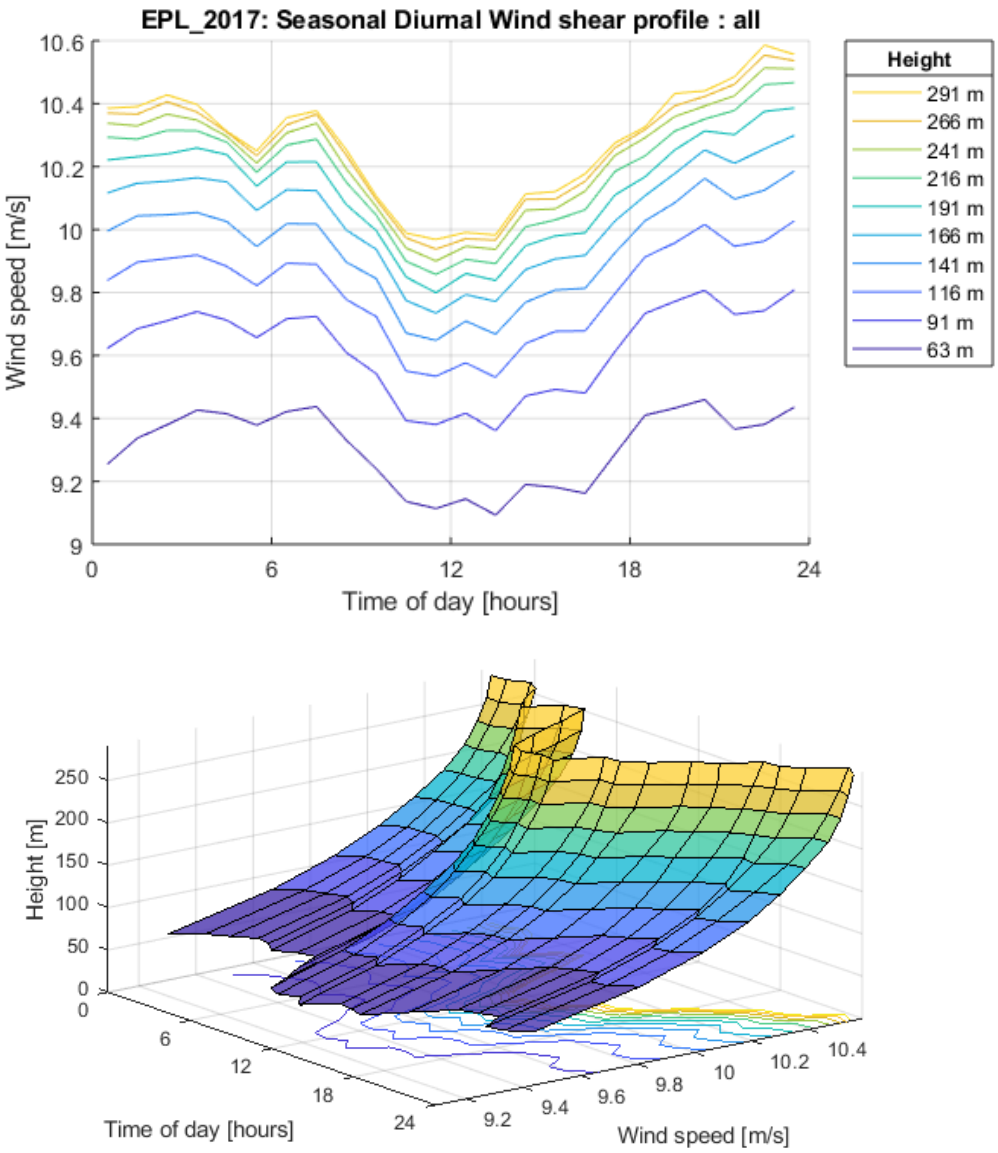

Figure D.6 (Top/Bottom) Different visual representations of variability in mean wind speed with height and the diurnal cycle.

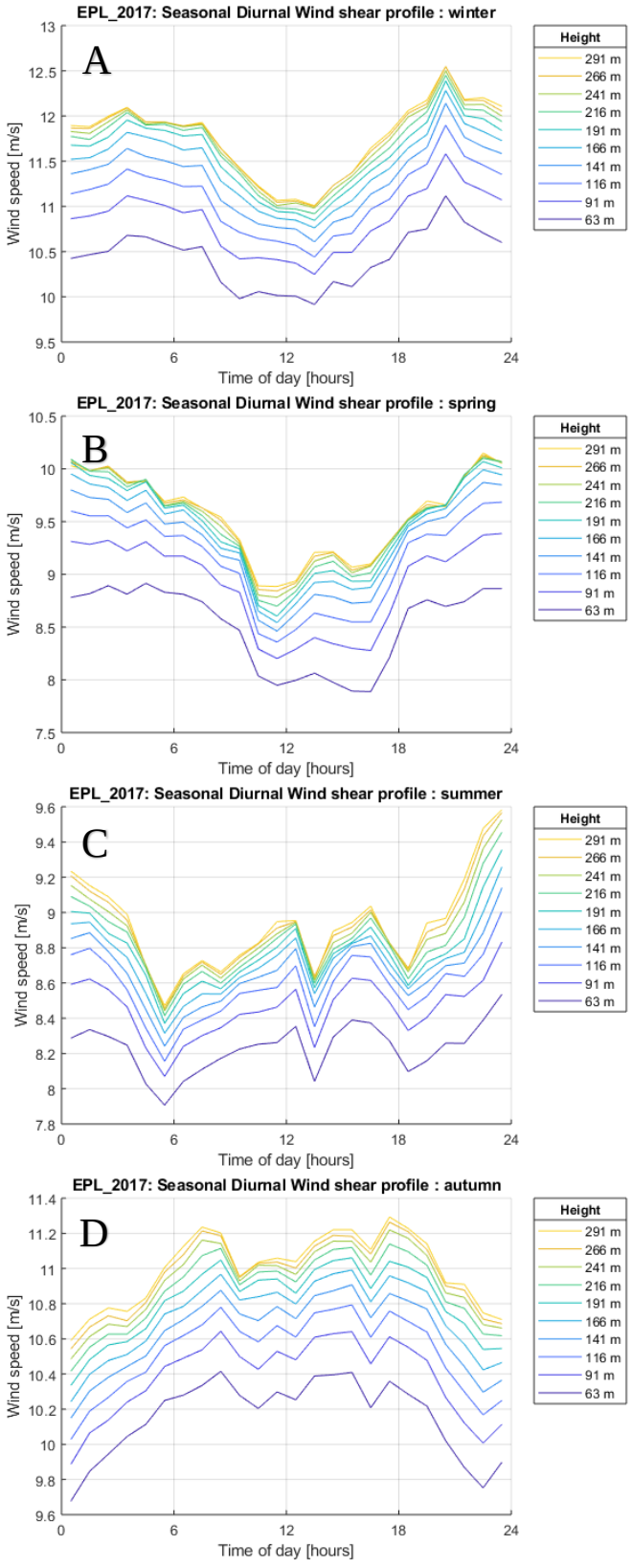

Figure D.7 Same as D.6 (Top) except that the mean wind speed data is parsed according to seasonal cycle – i.e. Winter (A), Spring (B), Summer (C), Autumn (D).

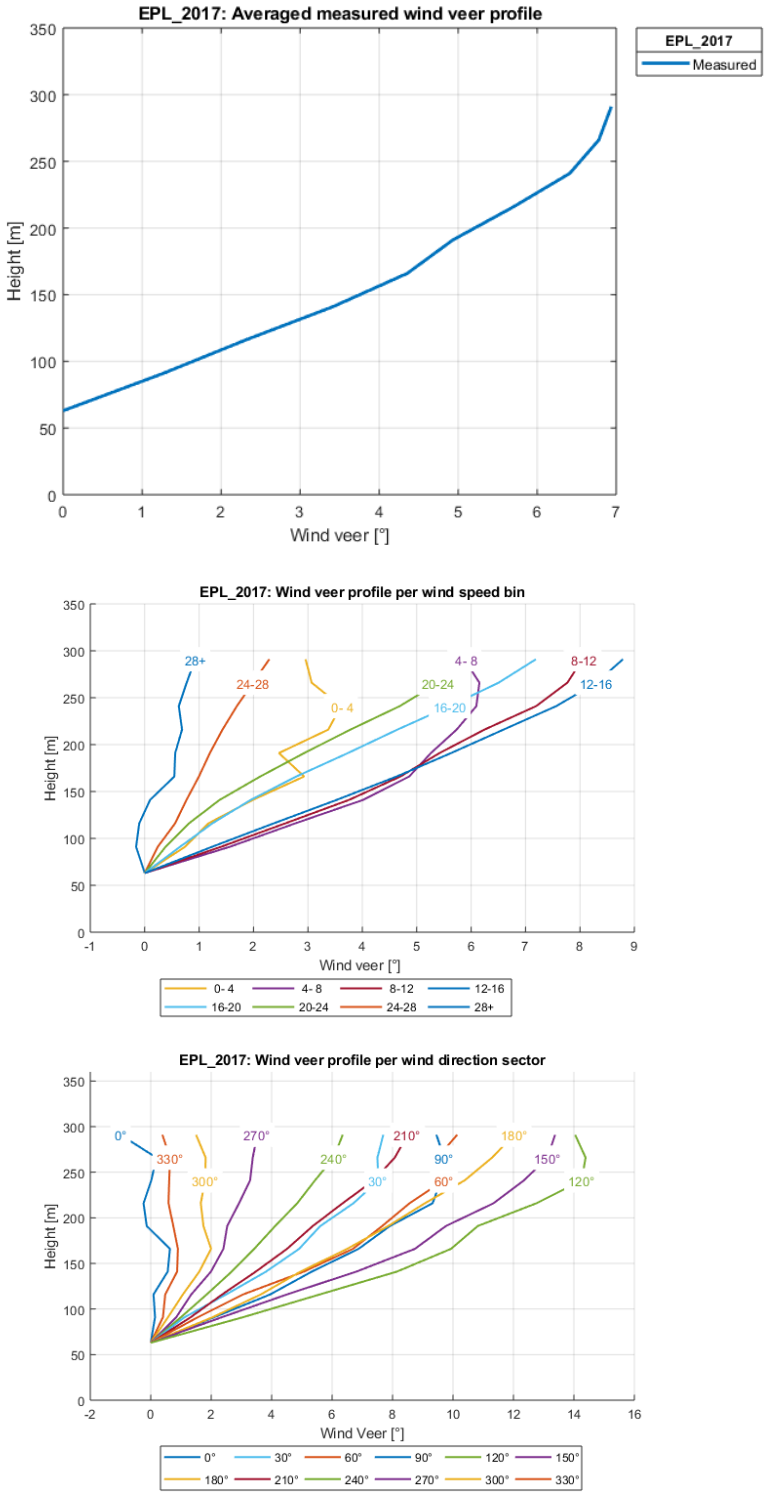

Figure D.8 (Top) Mean wind veer profile and the mean wind profile for different (Middle) wind speed and (Bottom) direction sectors.

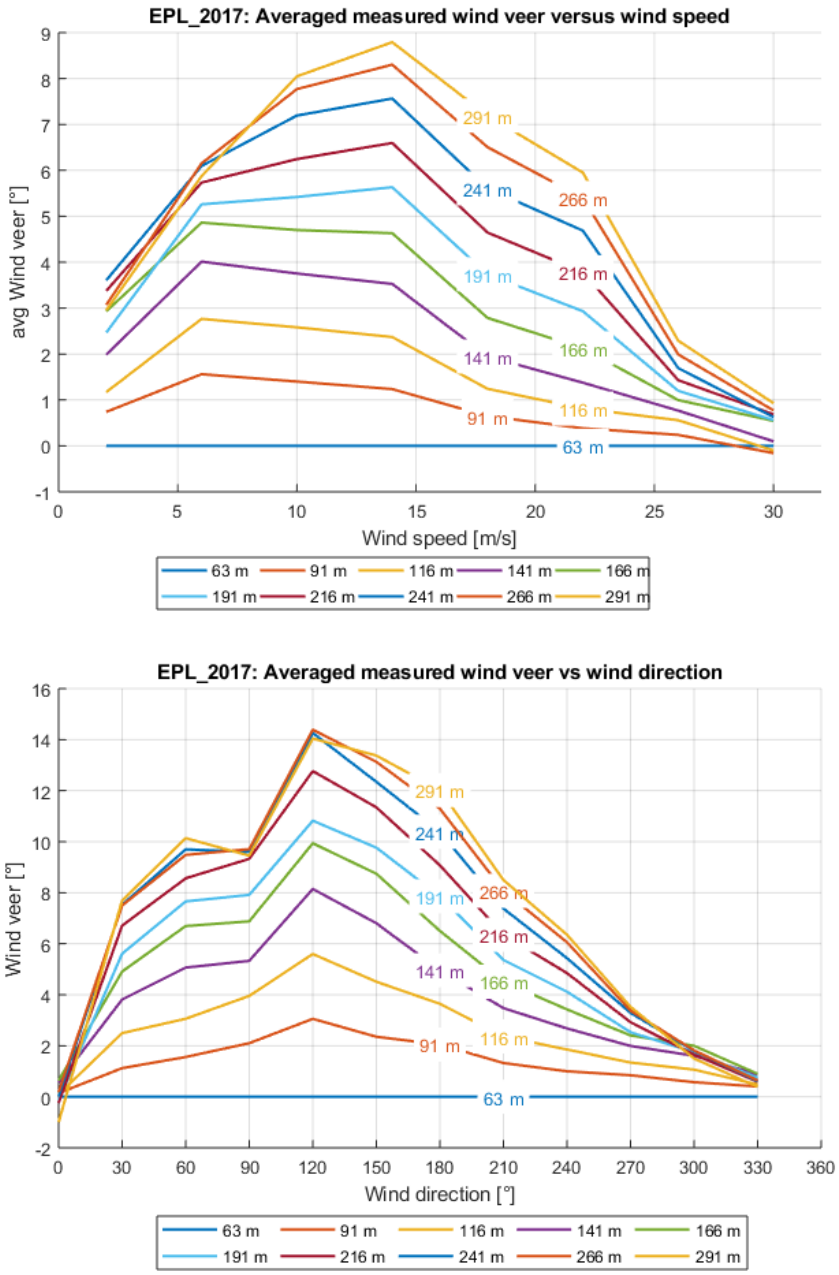

Figure D.9 (Top/Bottom) Mean wind veer as a function of measurement height for different (Top) wind speed and (Bottom) direction sectors.

E K13a wind resource summary

K13A_2017 Dataset

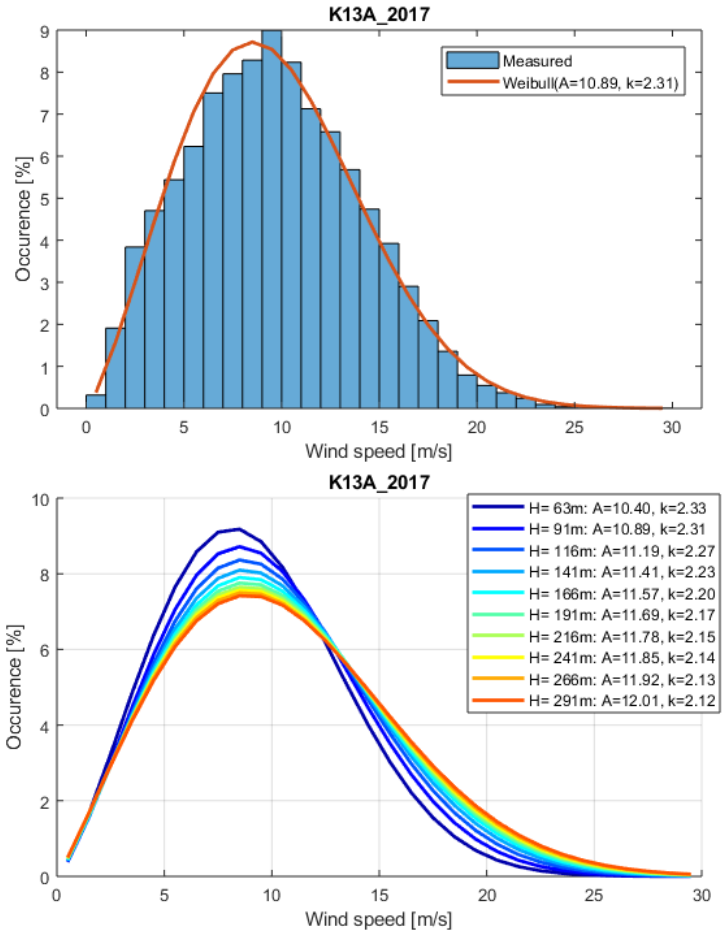

Figure E.1 (Top) Histogram (1 m s^{-1} bins) of the 10-min mean wind speeds at 91 m overlaid by the fitted Weibull distribution. (Bottom) The fitted Weibull distribution at each available measurement level from 63 m through 291 m.

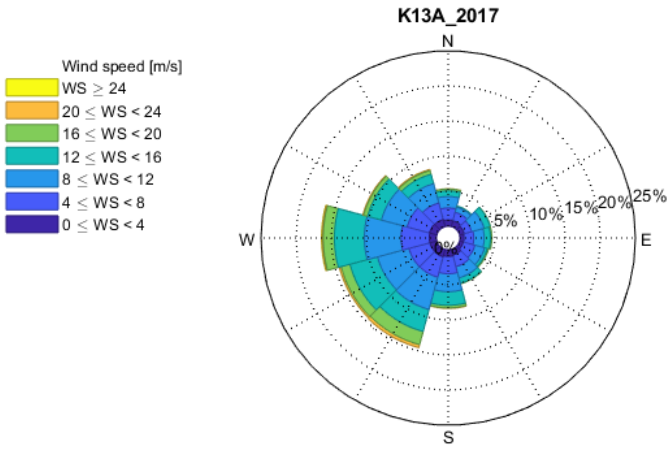

Figure E.2 Wind rose (30º wind direction bins) at 91 m.

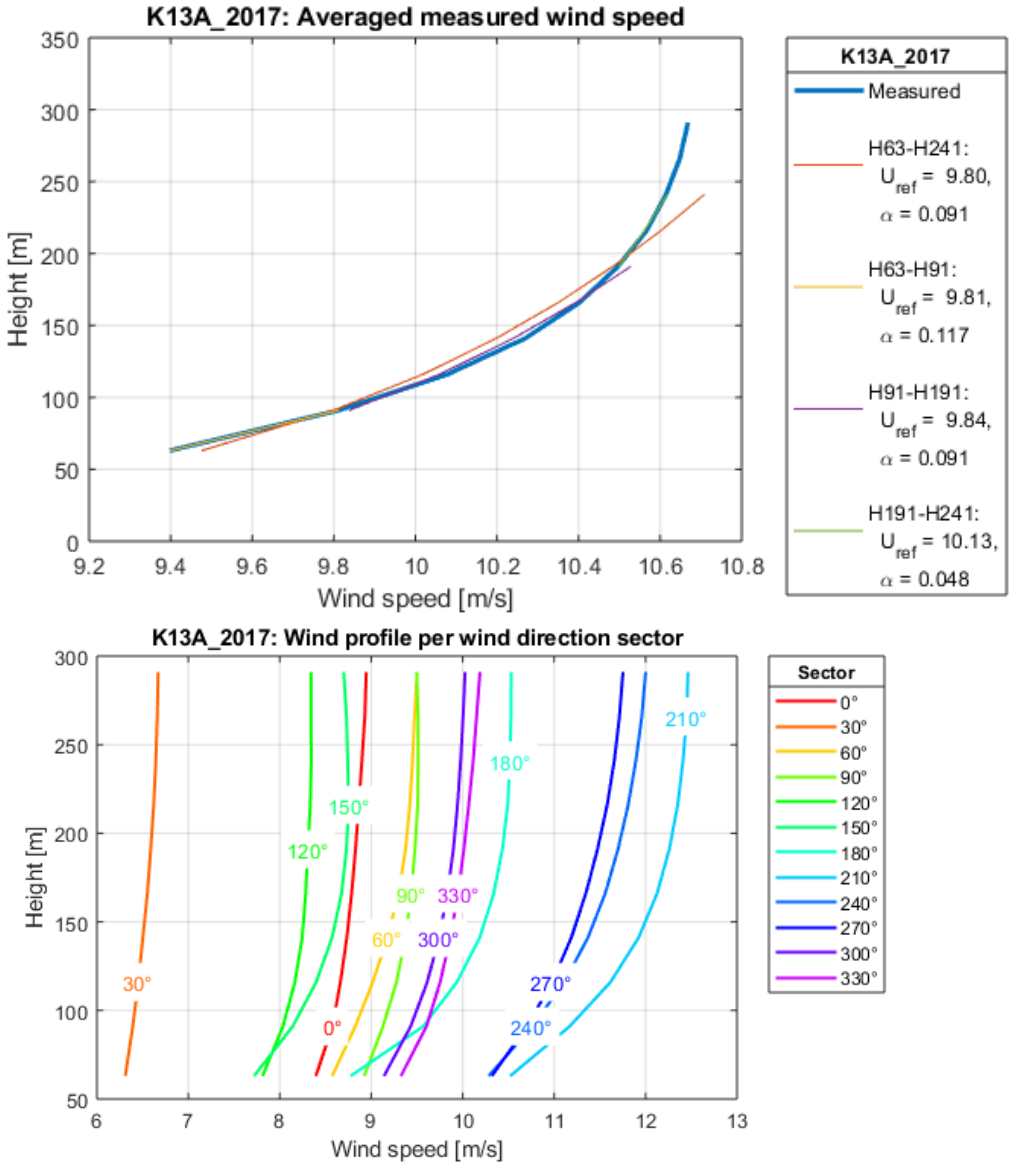

Figure E.3 (Top) Mean wind profile overlaid by varying power-law fits that depend upon which measurements levels (or layers) were considered. (Bottom) Mean wind profile as a function of wind direction.

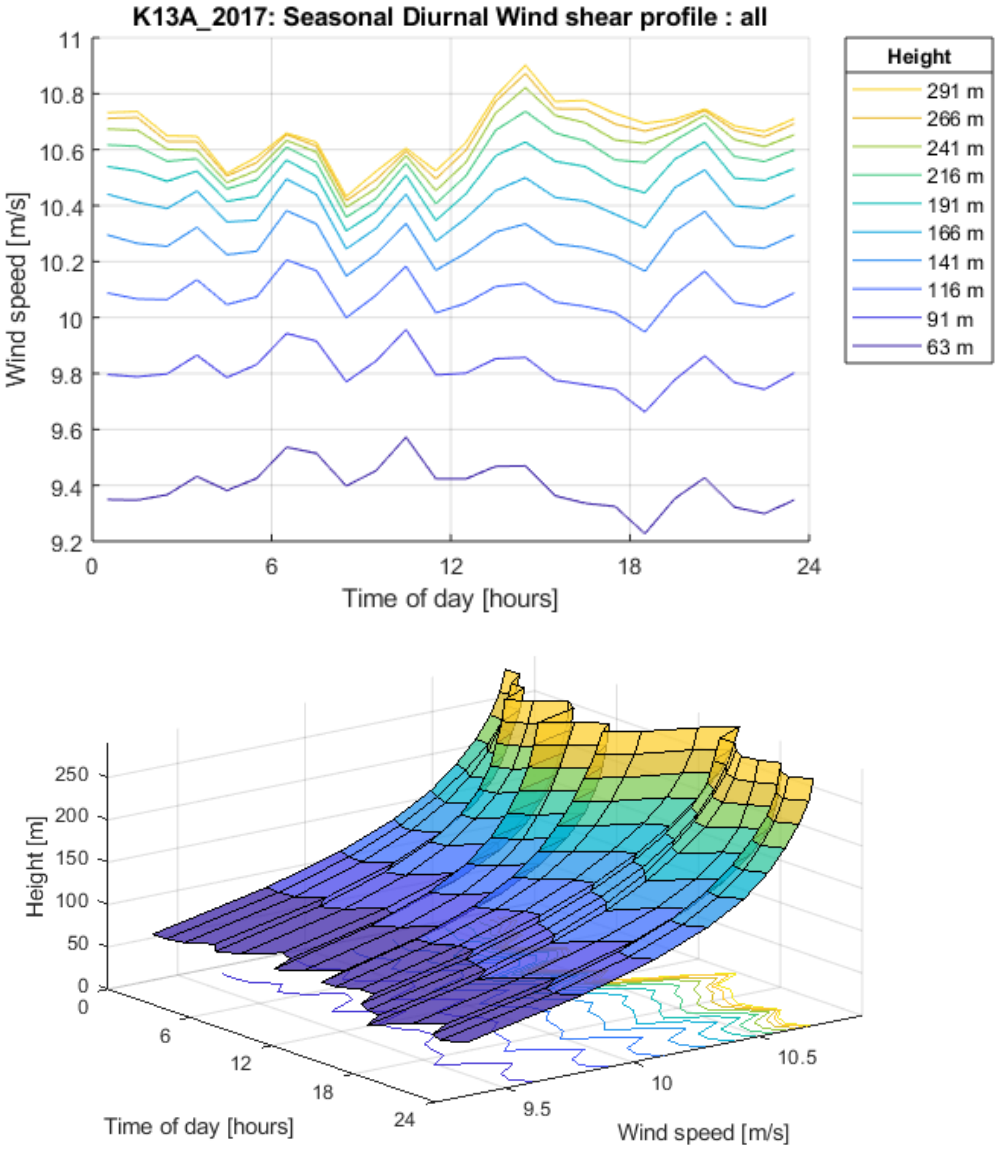

Figure E.4 (Top/Bottom) Different visual representations of variability in mean wind speed with height and the diurnal cycle.

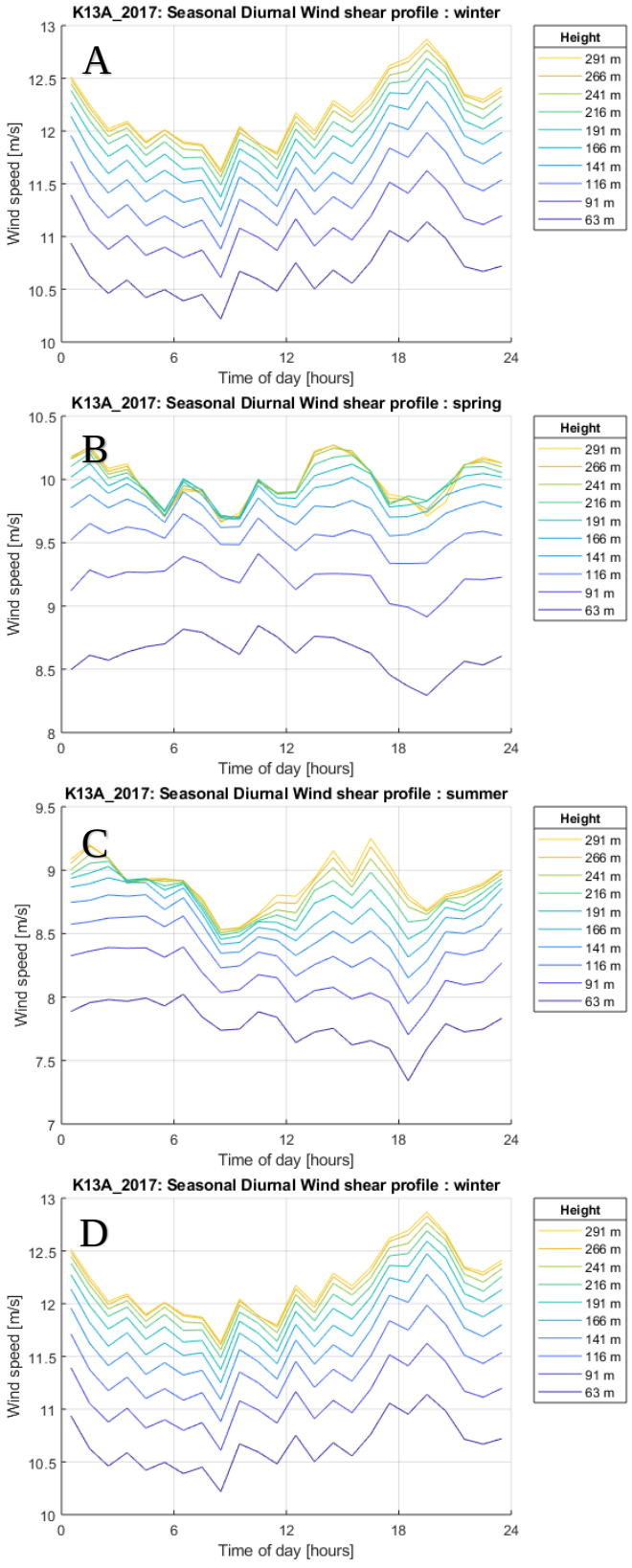

Figure E.5 Same as E.4 (Top) except that the mean wind speed data is parsed according to seasonal cycle – i.e. Winter (A), Spring (B), Summer (C), Autumn (D).

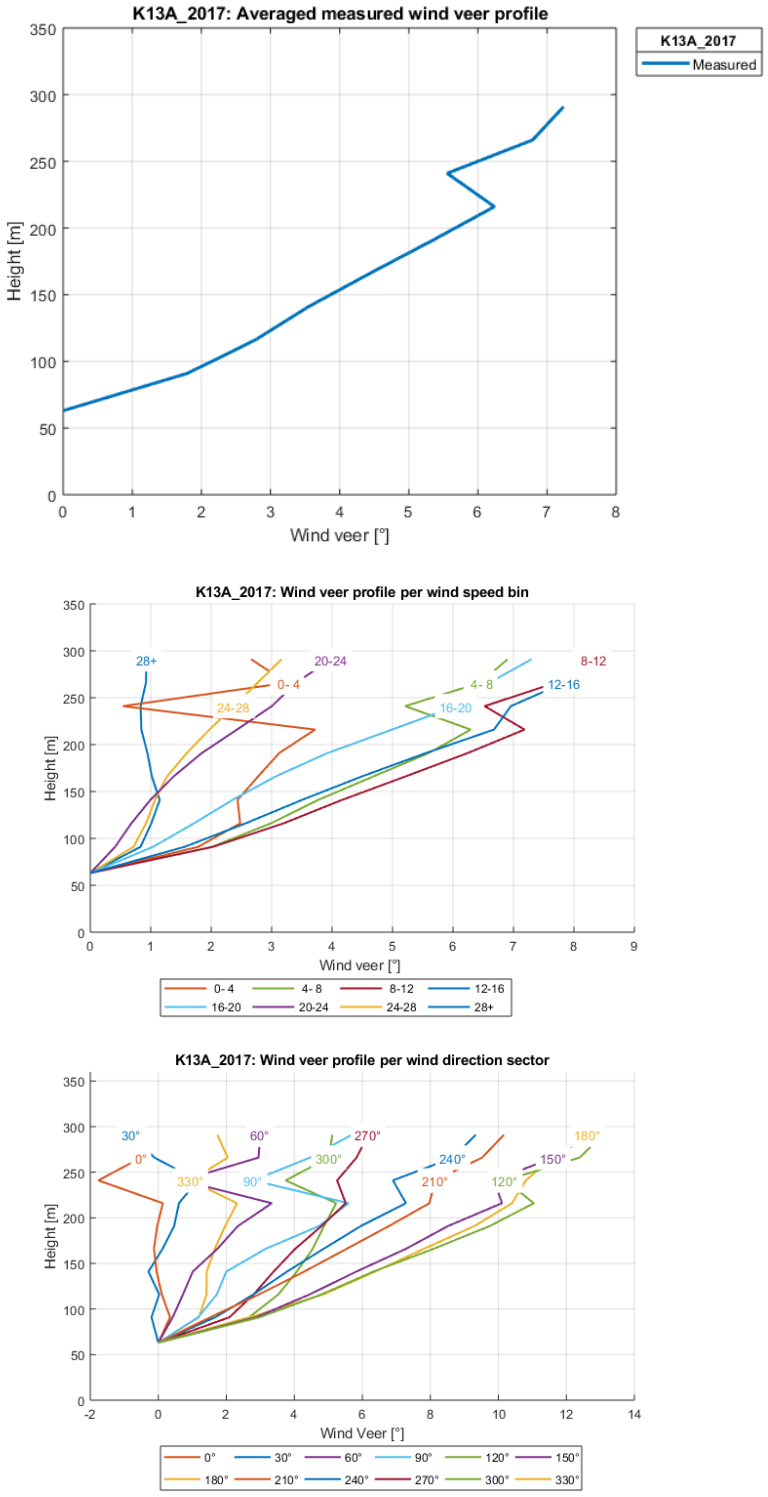

Figure E.6 (Top) Mean wind veer profile and the mean wind profile for different (Middle) wind speed and (Bottom) direction sectors.

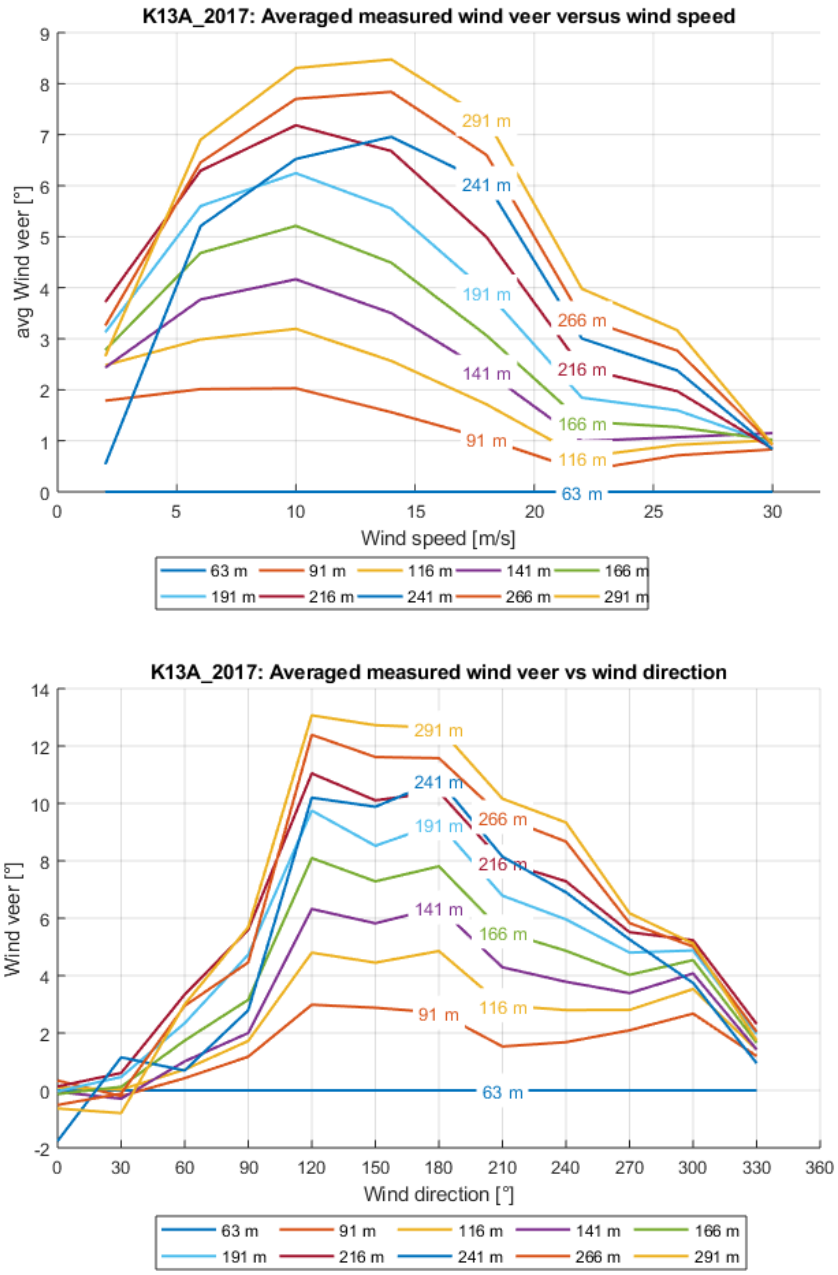

Figure E.7 (Top/Bottom) Mean wind veer as a function of measurement height for different (Top) wind speed and (Bottom) direction sectors.

F HKZ wind resource summary

HKZA_2016A Dataset

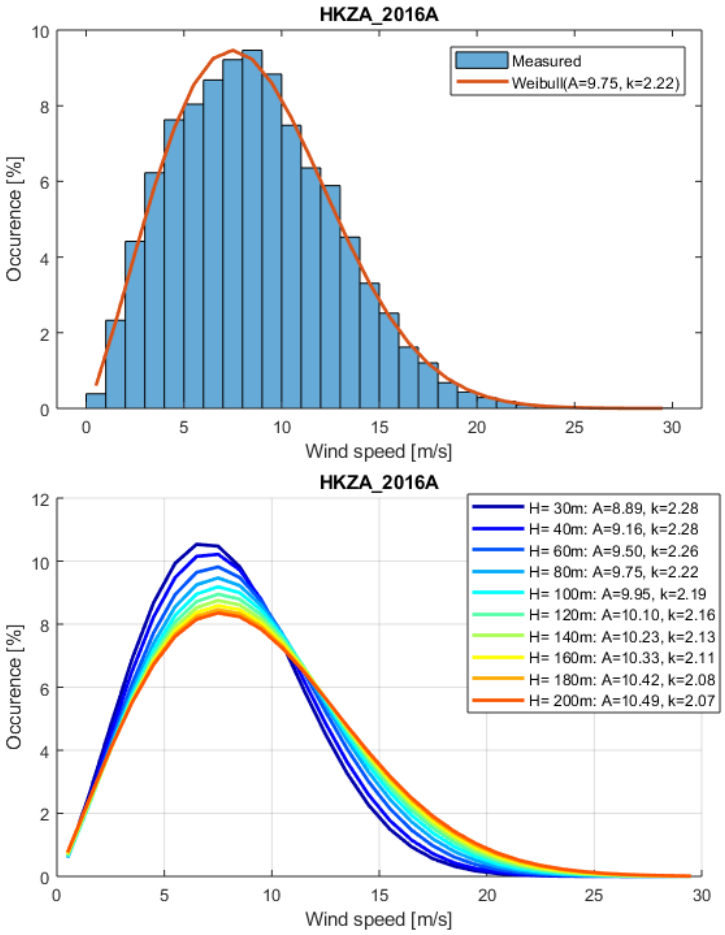

Figure F.1 (Top) Histogram (1 m s^{-1} bins) of the 10-min mean wind speeds at 80 m overlaid by the fitted Weibull distribution. (Bottom) The fitted Weibull distribution at each available measurement level from 30 m through 200 m.

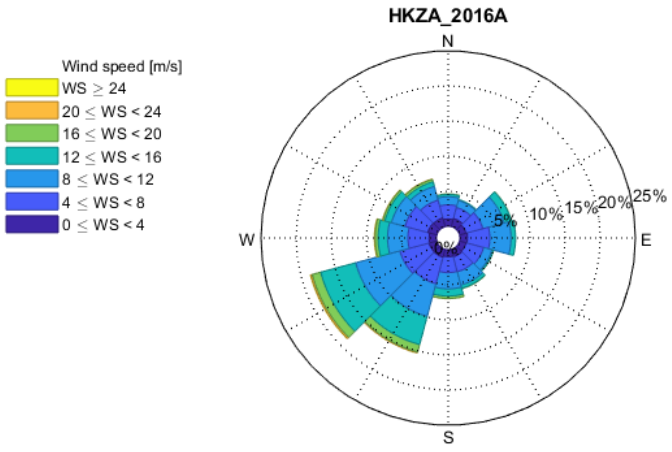

Figure F.2 Wind rose (30º wind direction bins) at 80 m.

HKZB_2016A Dataset

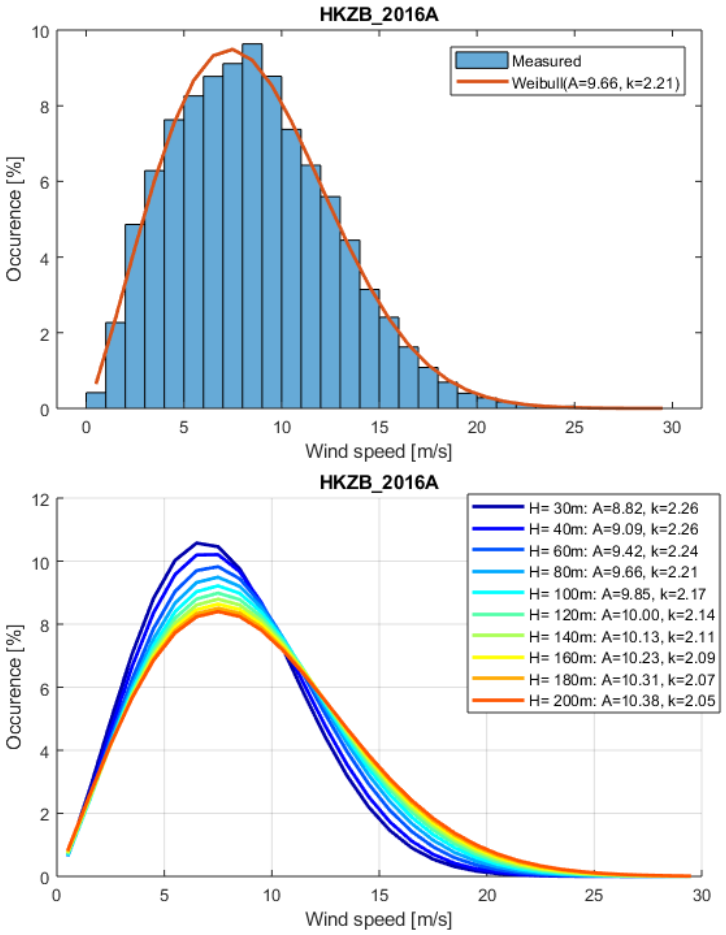

Figure F.3 (Top) Histogram (1 m s^{-1} bins) of the 10-min mean wind speeds at 80 m overlaid by the fitted Weibull distribution. (Bottom) The fitted Weibull distribution at each available measurement level from 30 m through 200 m.

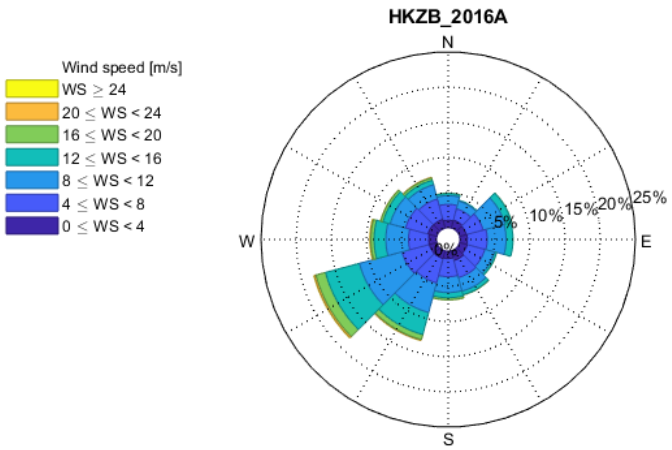

Figure F.4 Wind rose (30º wind direction bins) at 80 m.

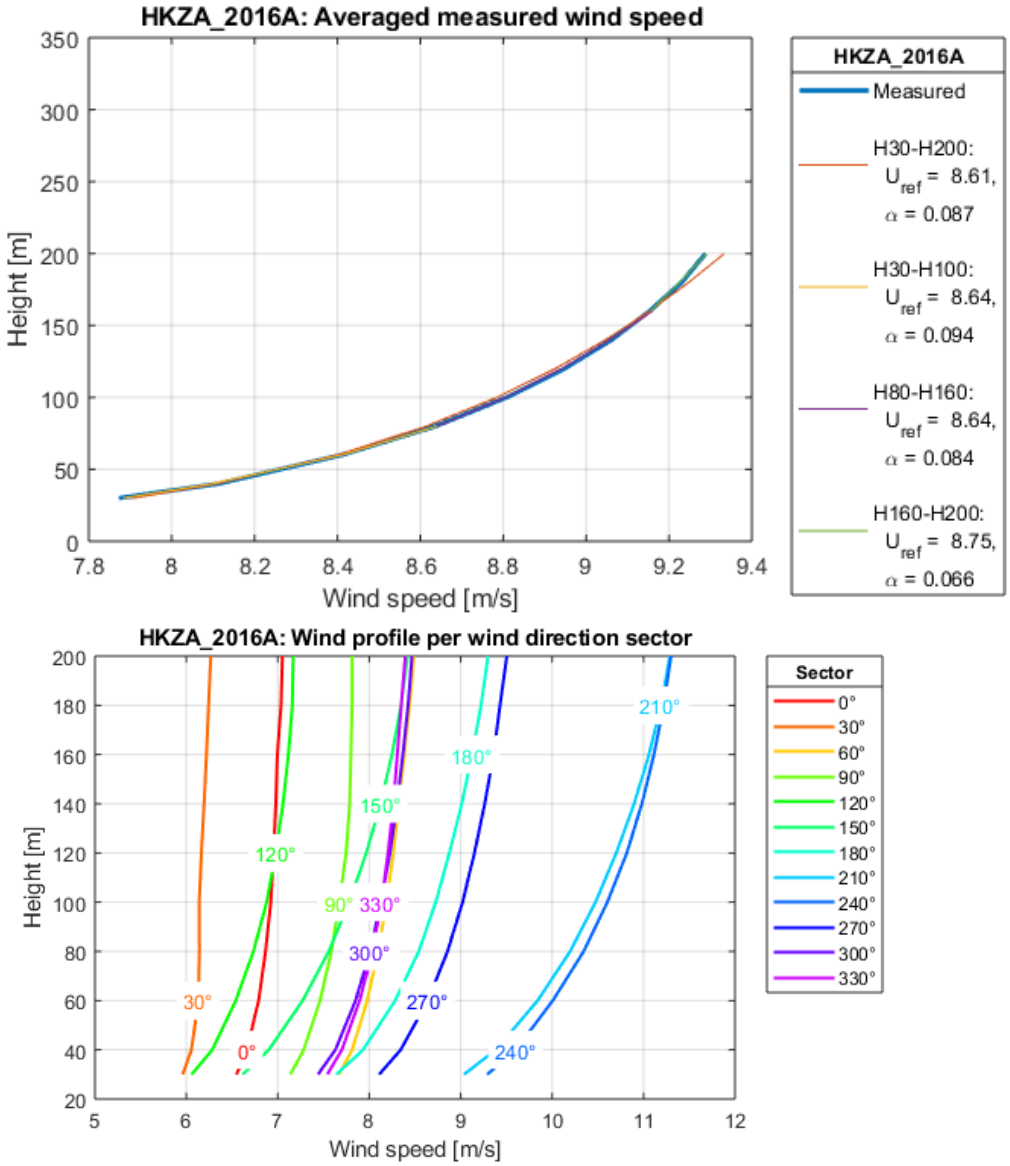

Figure F.5 (Top) Mean wind profile overlaid by varying power-law fits that depend upon which measurements levels (or layers) were considered. (Bottom) Mean wind profile as a function of wind direction.

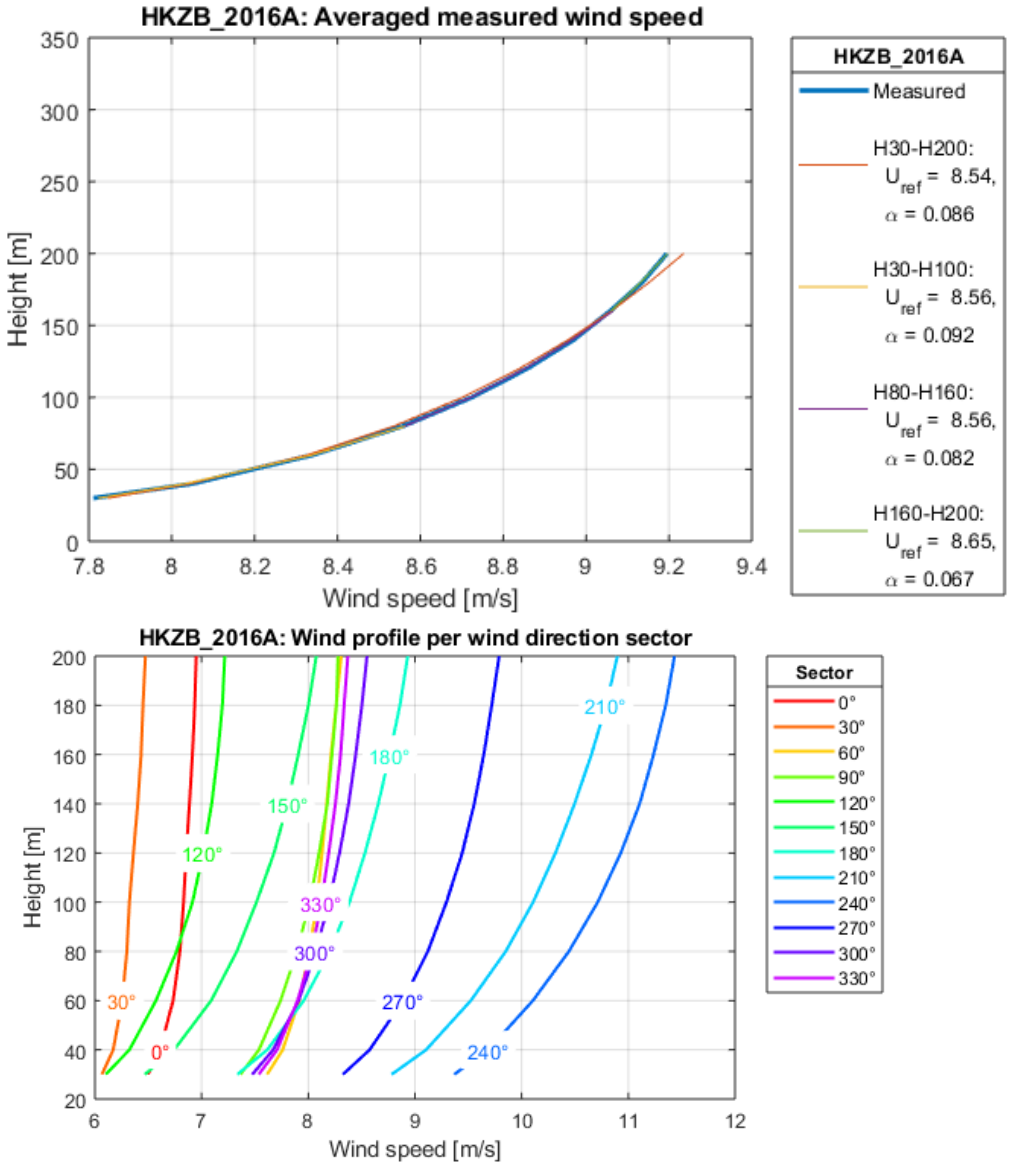

Figure F.6 (Top) Mean wind profile overlaid by varying power-law fits that depend upon which measurements levels (or layers) were considered. (Bottom) Mean wind profile as a function of wind direction.

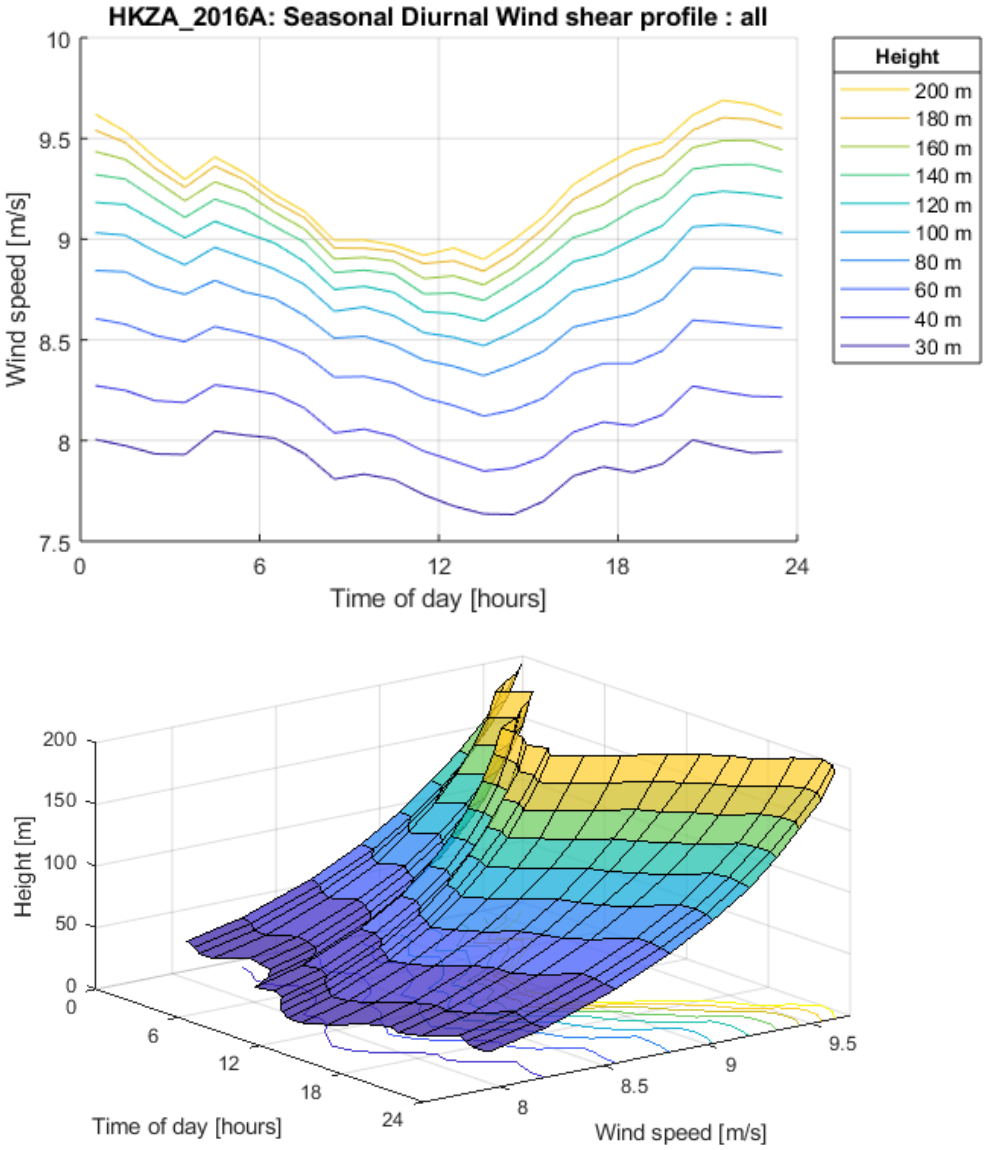

Figure F.7 (Top/Bottom) Different visual representations of variability in mean wind speed with height and the diurnal cycle.

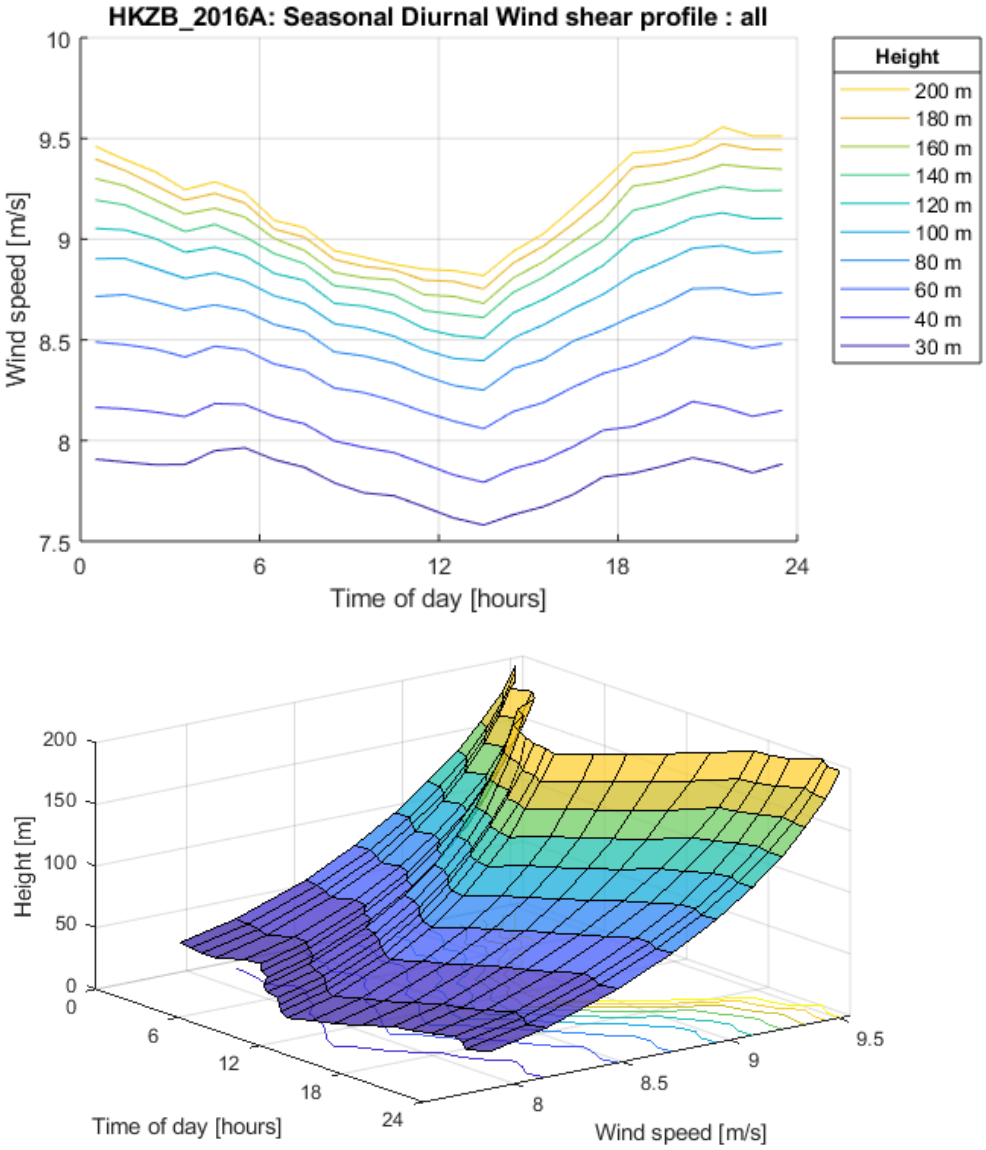

Figure F.8 (Top/Bottom) Different visual representations of variability in mean wind speed with height and the diurnal cycle.

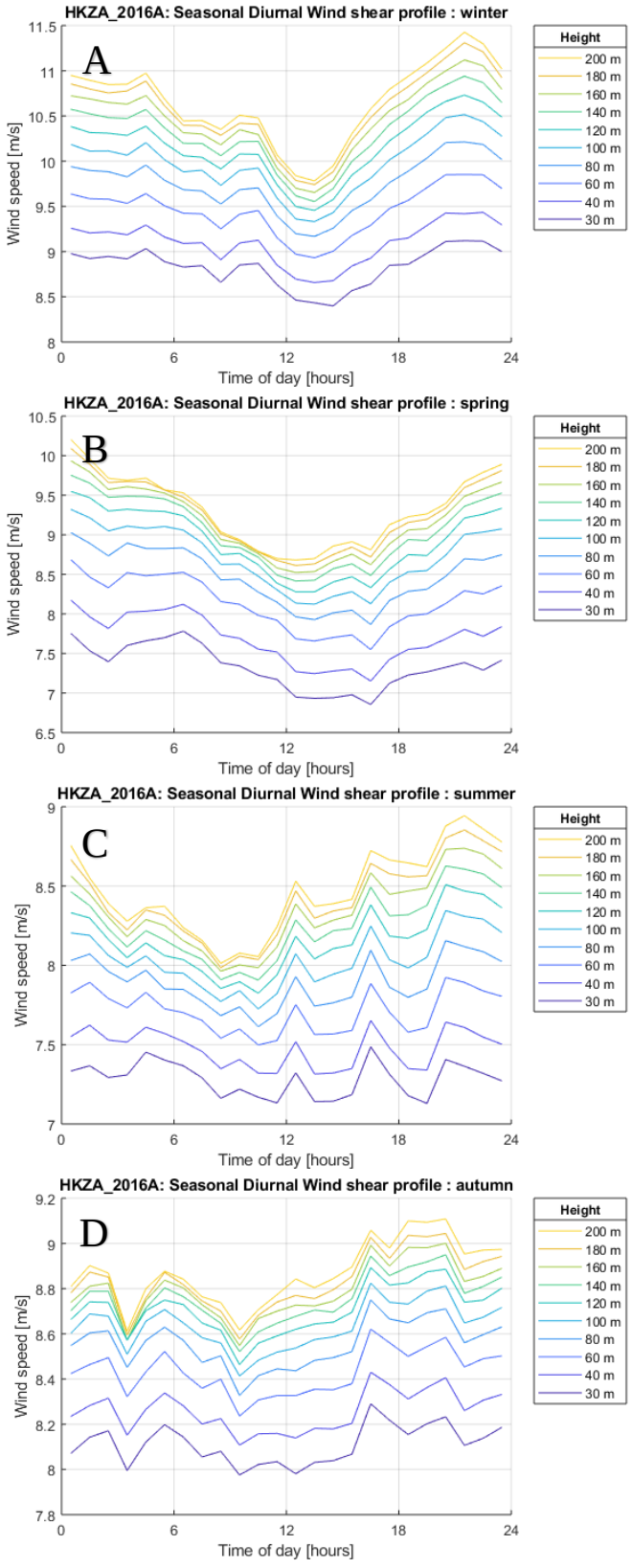

Figure F.9 Same as F.7 (Top) except that the mean wind speed data is parsed according to seasonal cycle – i.e. Winter (A), Spring (B), Summer (C), Autumn (D).

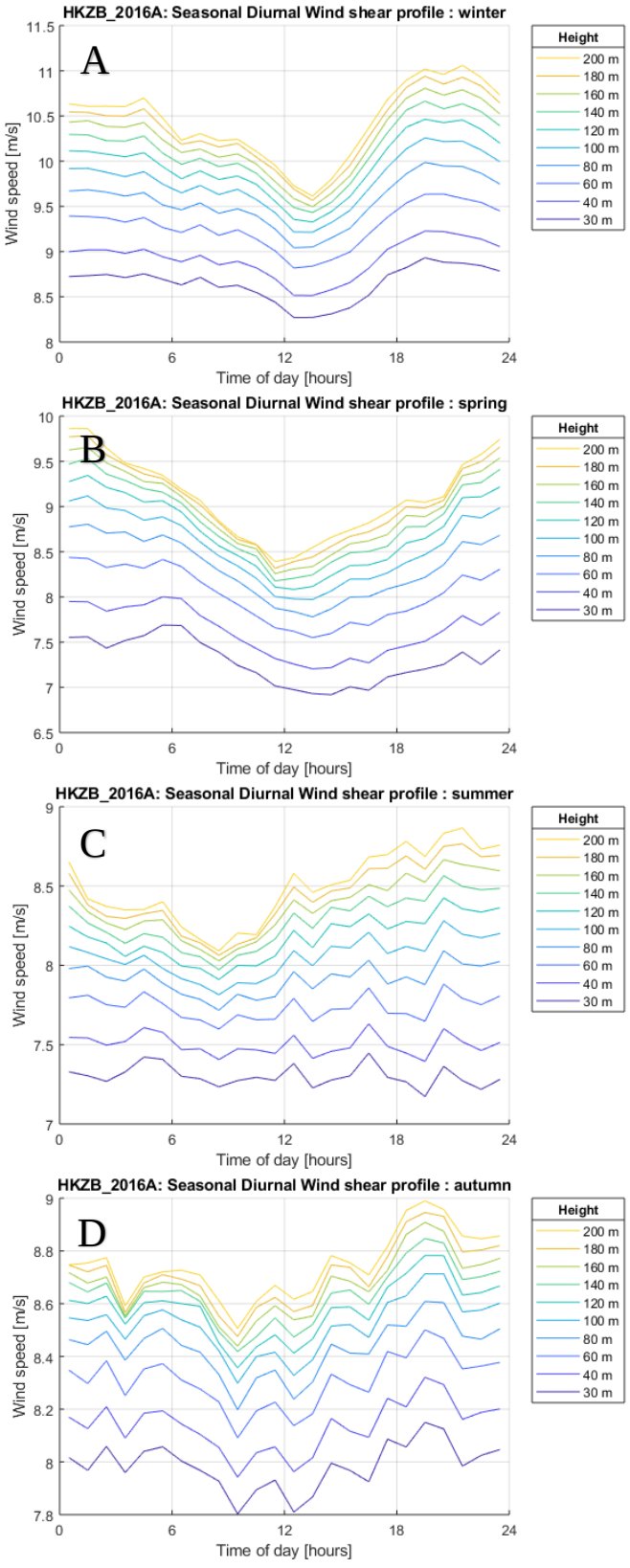

Figure F.10 Same as F.8 (Top) except that the mean wind speed data is parsed according to seasonal cycle – i.e. Winter (A), Spring (B), Summer (C), Autumn (D).

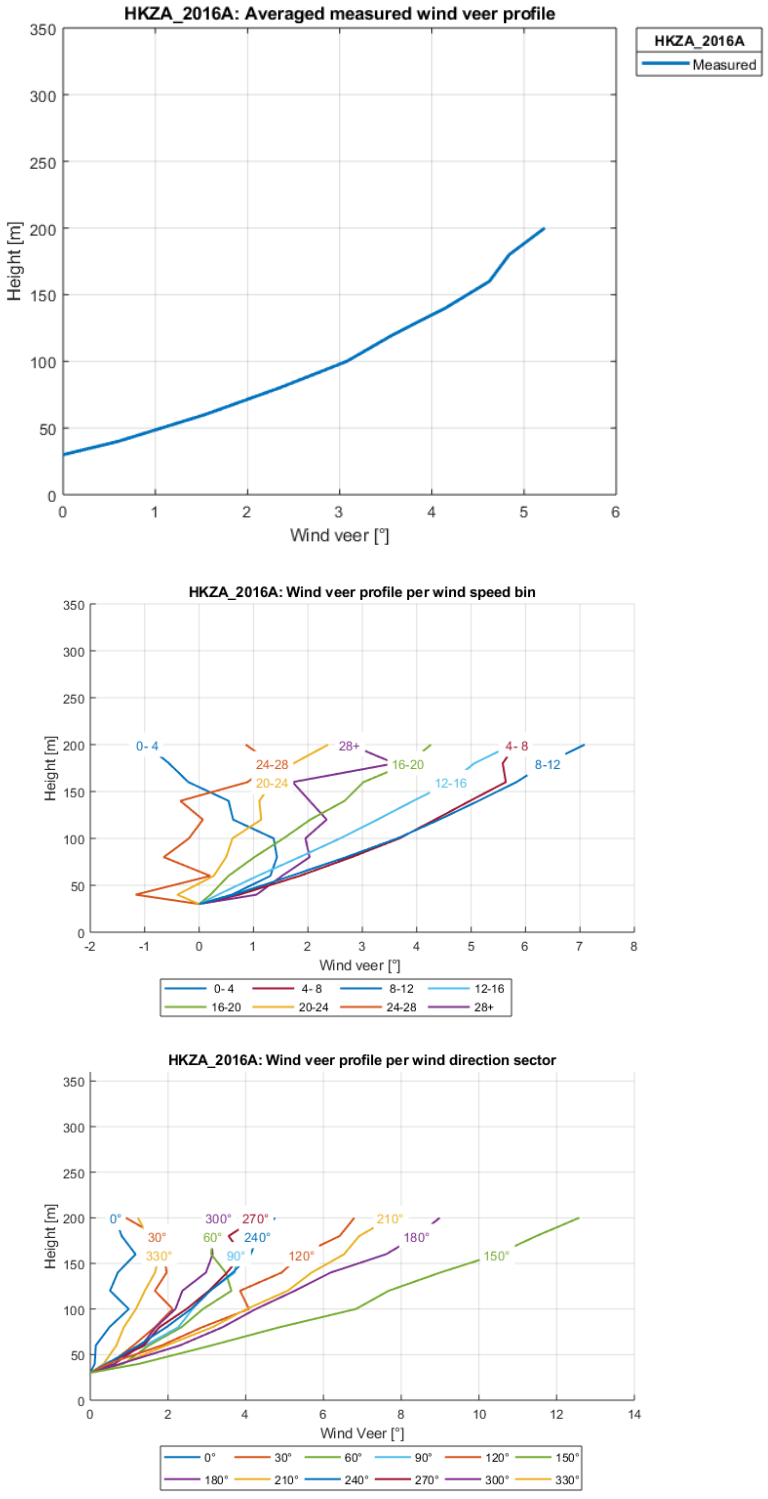

Figure F.11 (Top) Mean wind veer profile and the mean wind profile for different (Middle) wind speed and (Bottom) direction sectors.

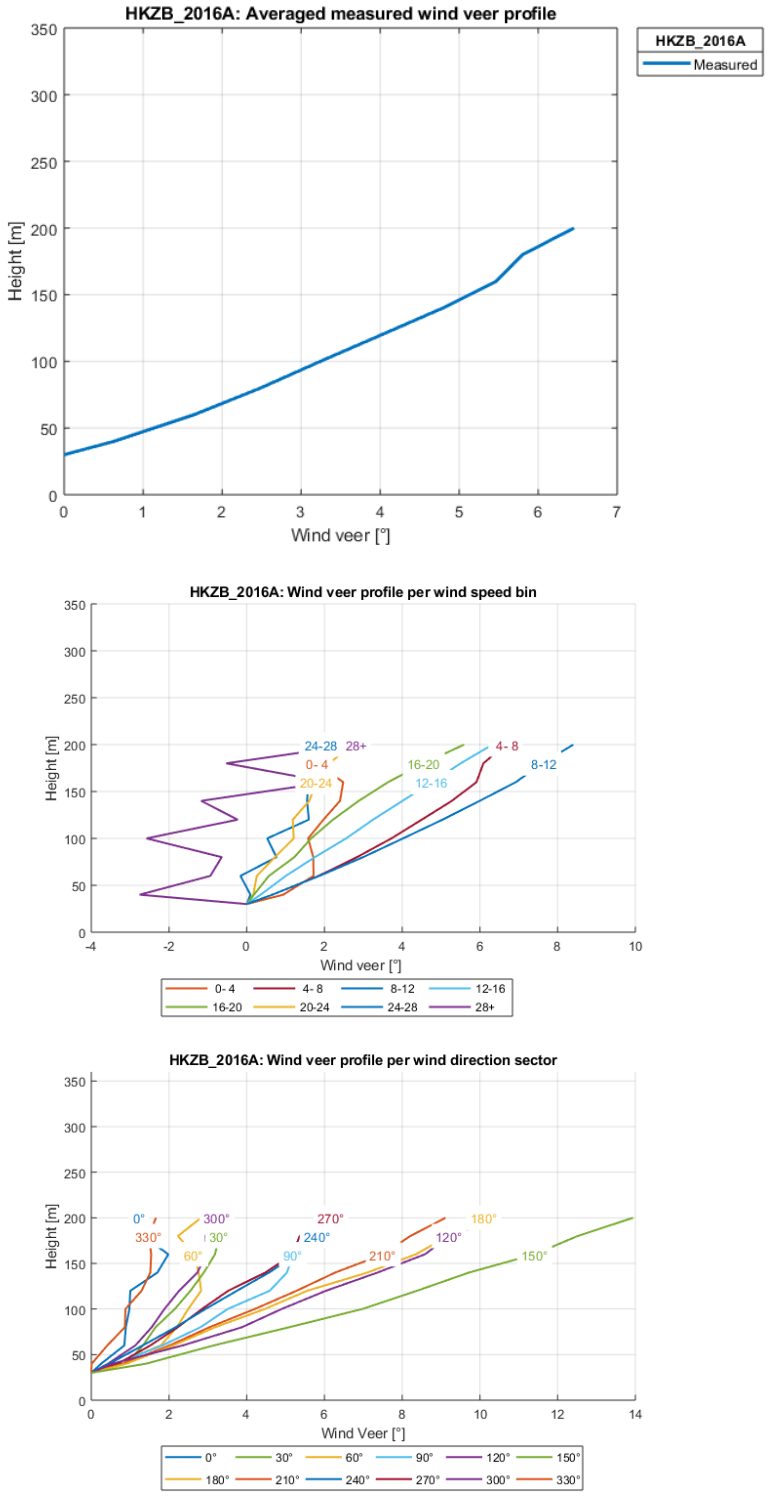

Figure F.12 (Top) Mean wind veer profile and the mean wind profile for different (Middle) wind speed and (Bottom) direction sectors.

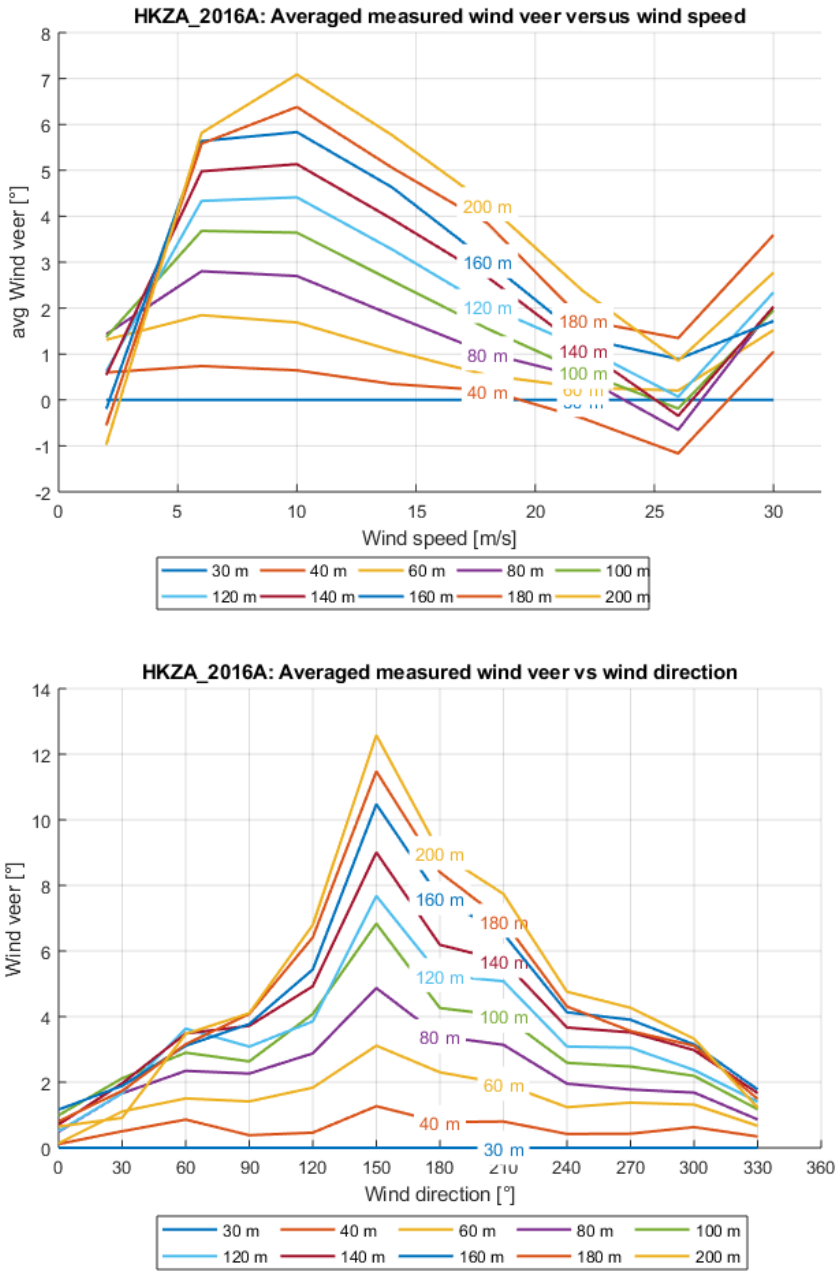

Figure F.13 (Top/Bottom) Mean wind veer as a function of measurement height for different (Top) wind speed and (Bottom) direction sectors.

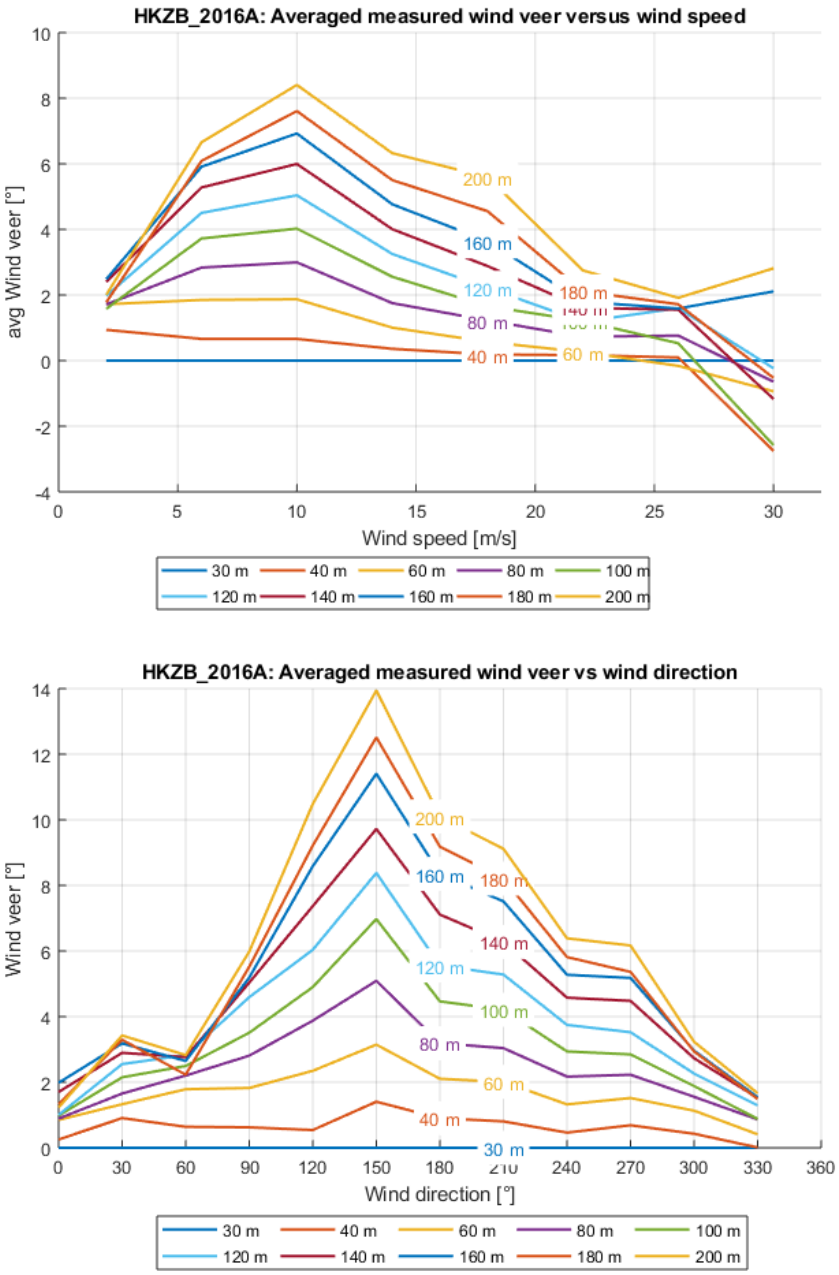

Figure F.14 (Top/Bottom) Mean wind veer as a function of measurement height for different (Top) wind speed and (Bottom) direction sectors.

G BWFZ wind resource summary

BWFZ_2016C Dataset

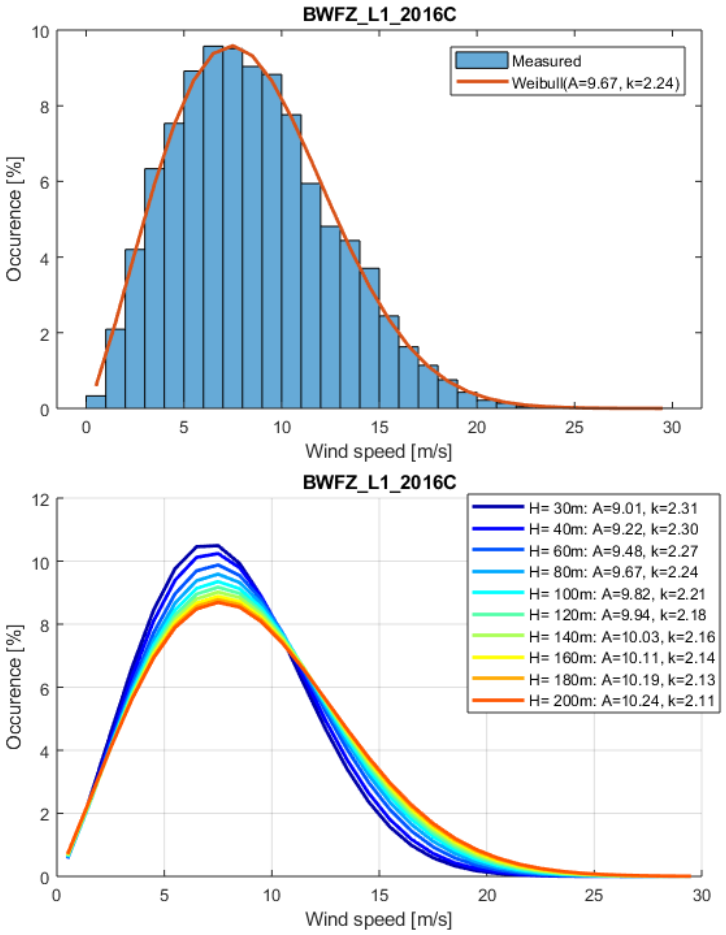

Figure G.1 (Top) Histogram (1 m s^{-1} bins) of the 10-min mean wind speeds at 80 m overlaid by the fitted Weibull distribution. (Bottom) The fitted Weibull distribution at each available measurement level from 30 m through 200 m.

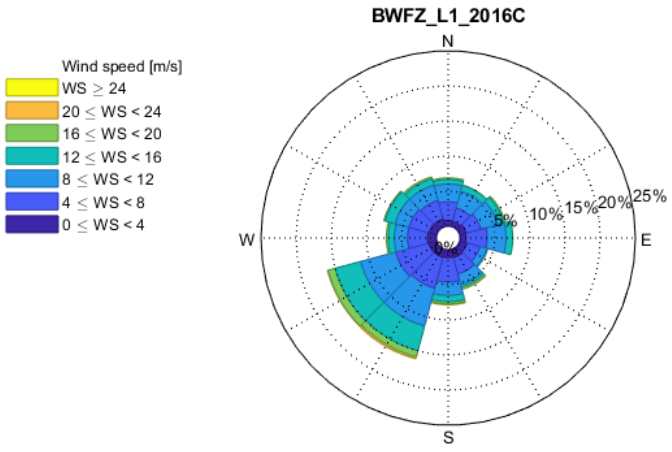

Figure G.2 Wind rose (30º wind direction bins) at 80 m.

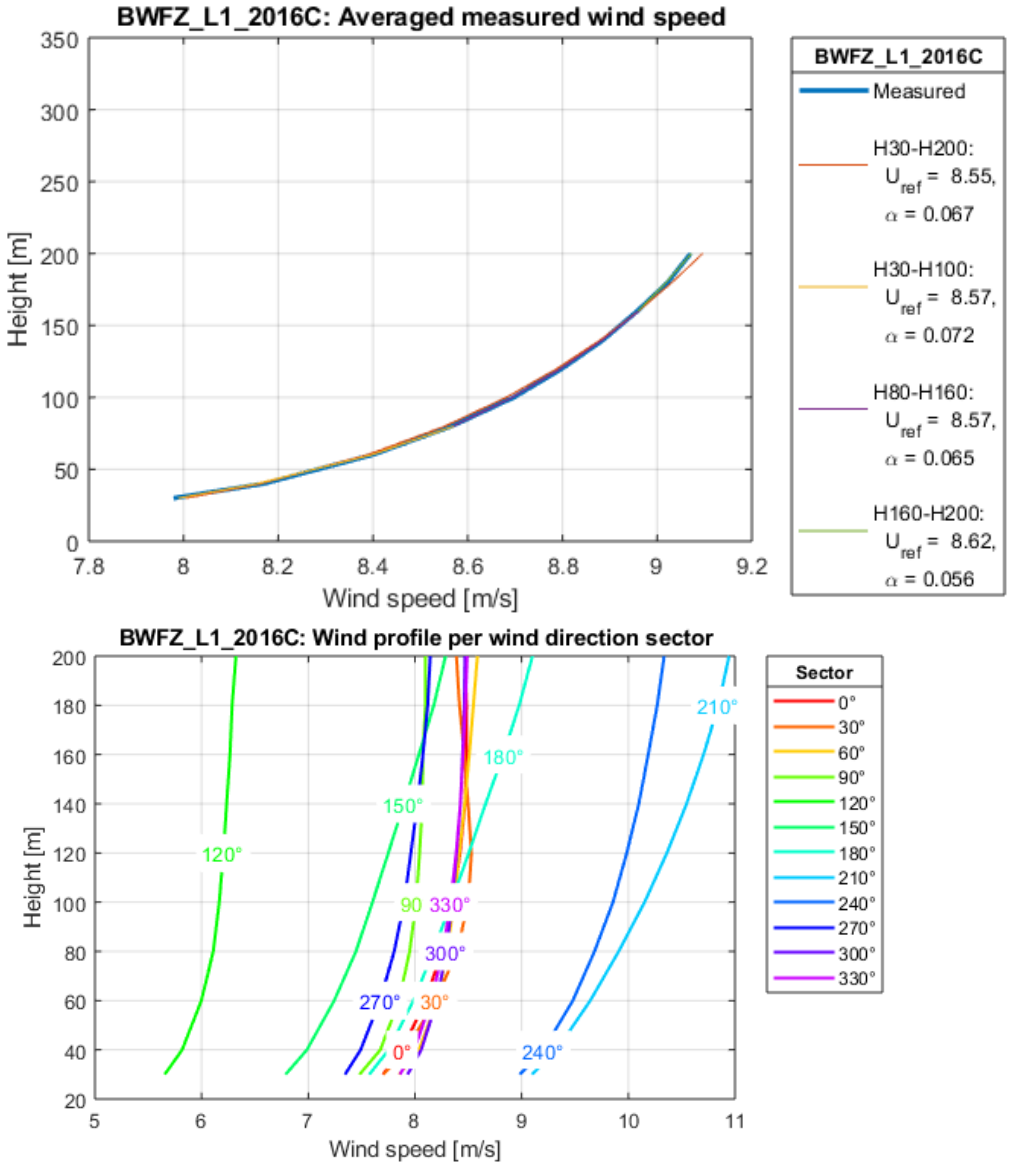

Figure G.3 (Top) Mean wind profile overlaid by varying power-law fits that depend upon which measurements levels (or layers) were considered. (Bottom) Mean wind profile as a function of wind direction.

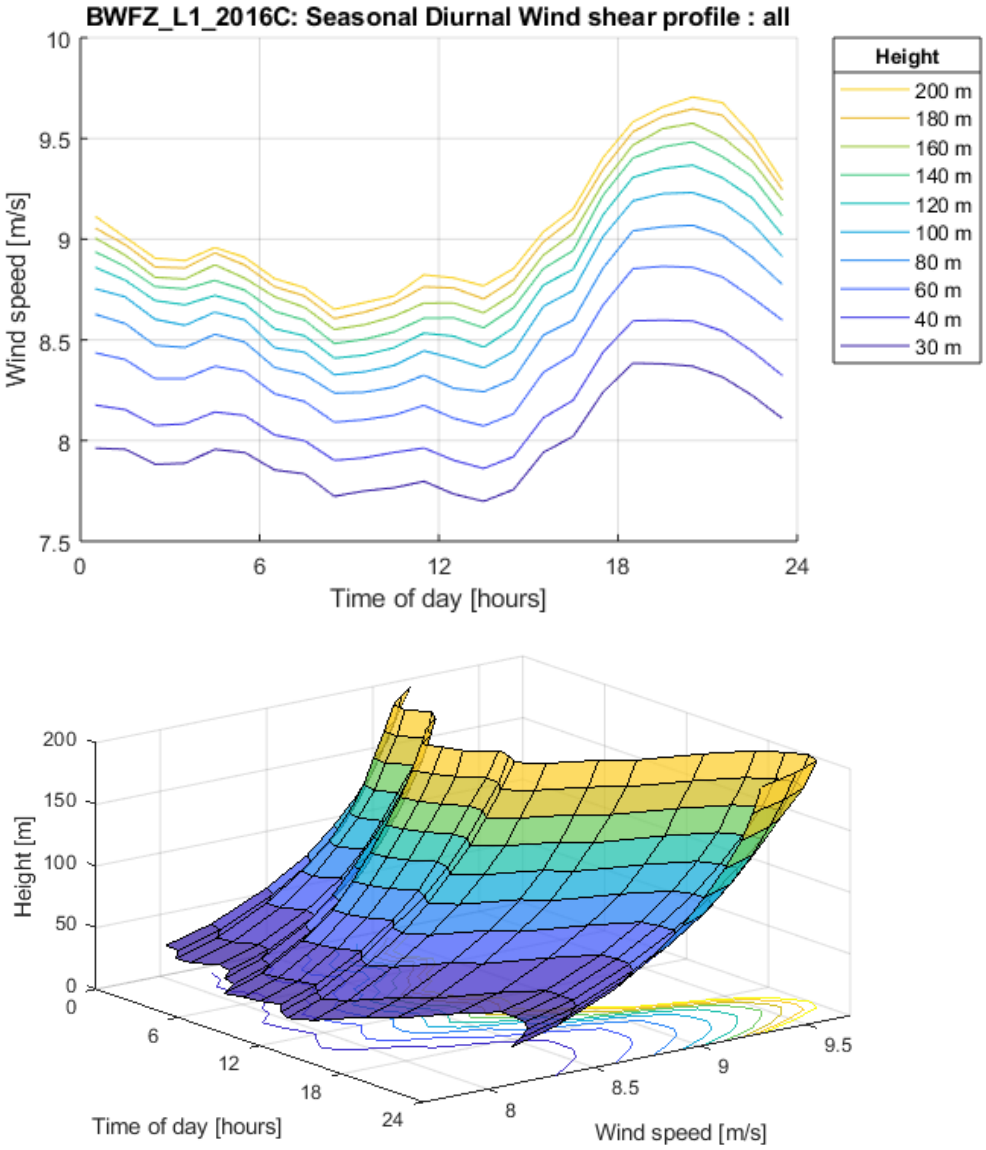

Figure G.4 (Top/Bottom) Different visual representations of variability in mean wind speed with height and the diurnal cycle.

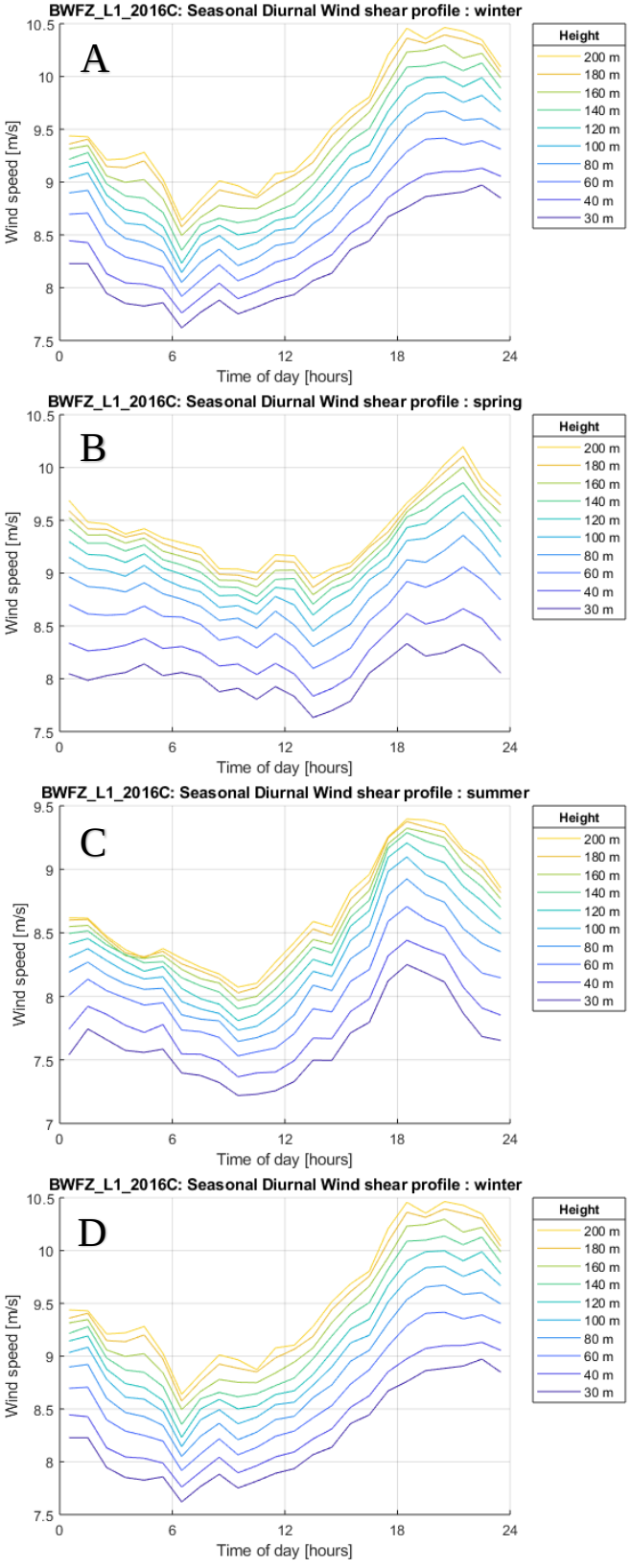

Figure G.5 Same as G.4 (Top) except that the mean wind speed data is parsed according to seasonal cycle – i.e. Winter (A), Spring (B), Summer (C), Autumn (D).

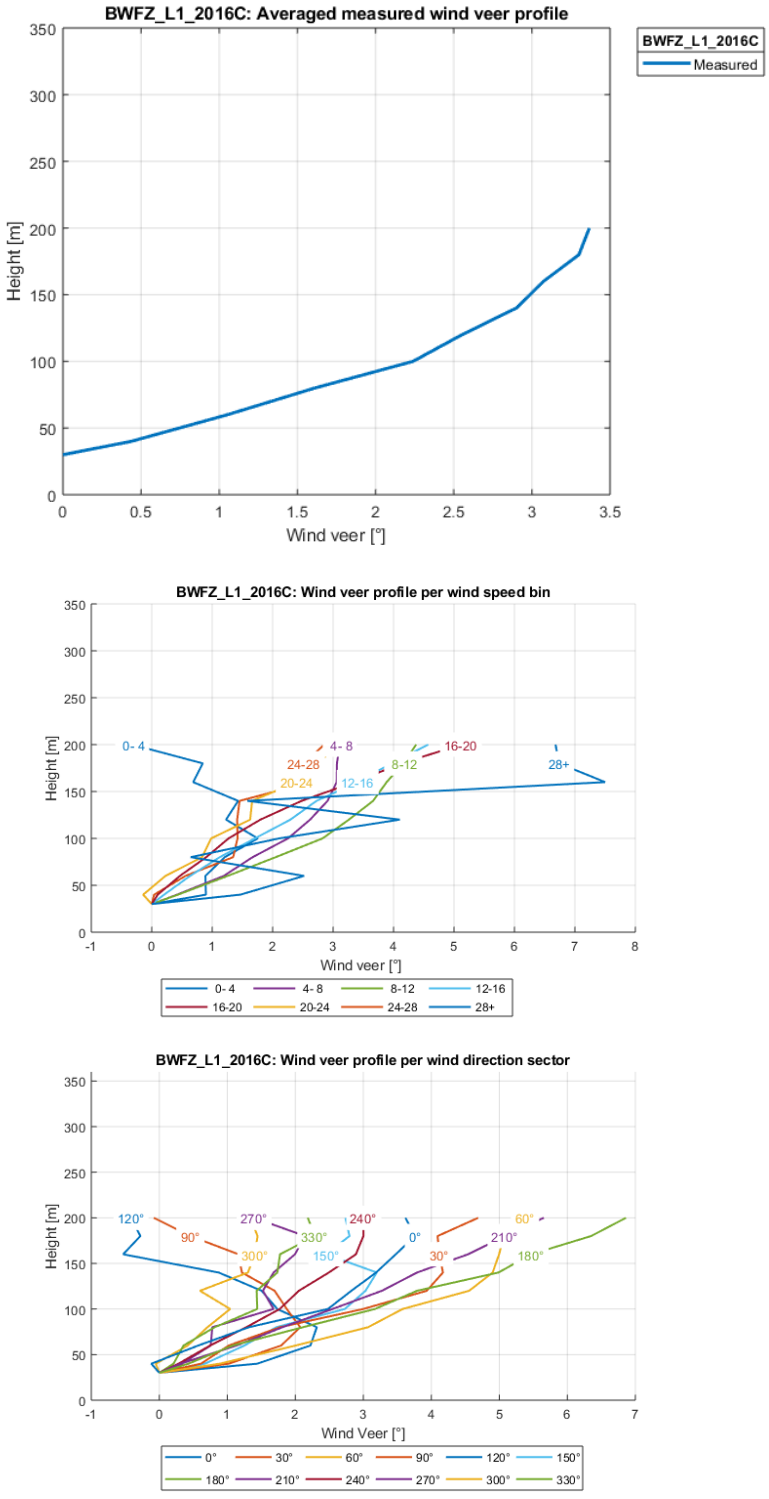

Figure G.6 (Top) Mean wind veer profile and the mean wind profile for different (Middle) wind speed and (Bottom) direction sectors.

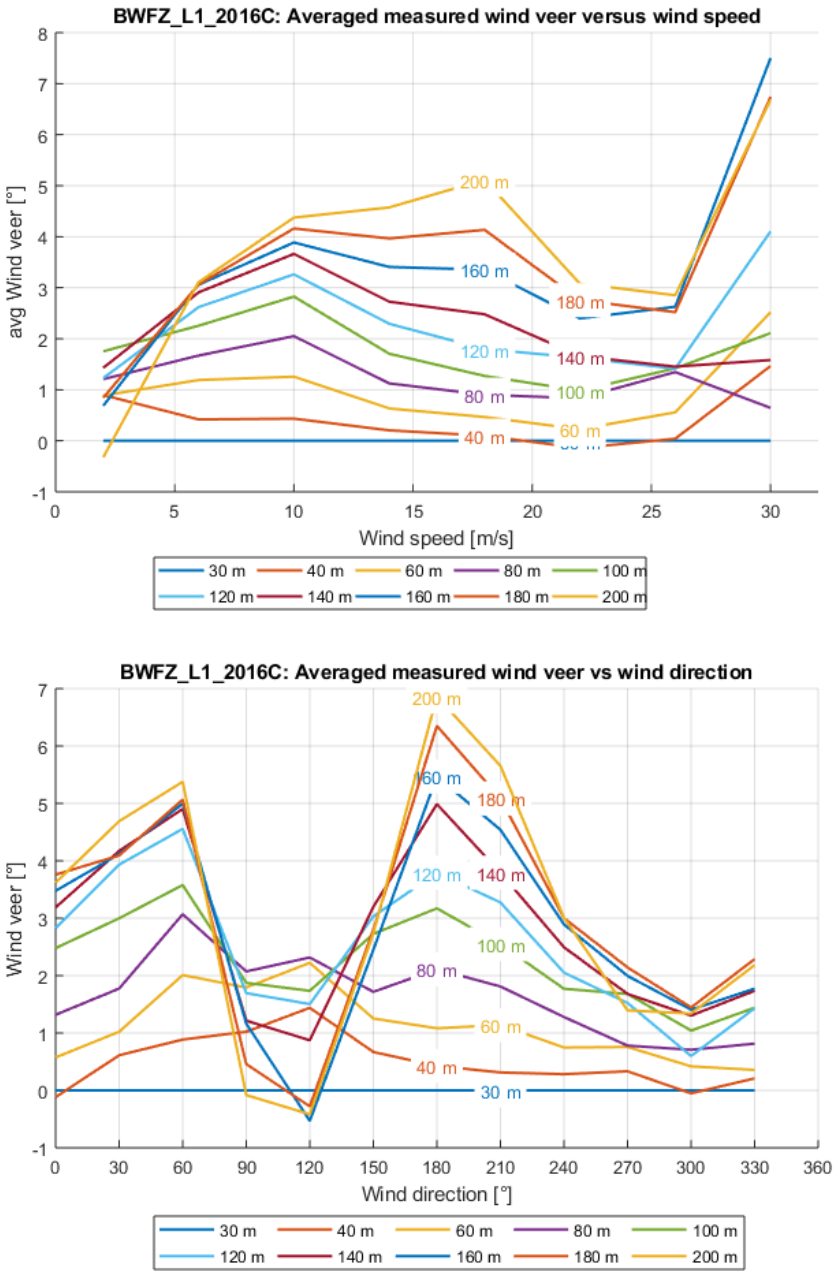

Figure G.7 (Top/Bottom) Mean wind veer as a function of measurement height for different (Top) wind speed and (Bottom) direction sectors.